Electrochemical characterization of the chlor-alkali membrane cell

Dissertation presented for the Doctor of Philosophy degree in Refining, Petrochemical and Chemical Engineering

by

Filipa Paulo Franco

Supervison: Professor Adélio Miguel Magalhães Mendes, LEPABE, FEUP

Doctor Svetlozar Gueorguiev Velizarov, LAQV, FCT-UNL

Doctor Jorge Miguel Velho Prior, Bondalti Chemicals S.A.

Porto, February 2020

This work was supported by FCT-Fundação para a Ciência e Tecnologia and Bondalti Chemical S.A. under the Doctoral Program in Refining, Petrochemical and Chemical Engineering (PD/BDE/114351/2016).

AGRADECIMENTOS

Mais uma etapa concluída no meu percurso académico. Não posso deixar de expressar o meu agradecimento a todos que partilharam comigo este percurso.

Em primeiro lugar agradecer à minha equipa de orientação: Professores Adélio Mendes e Svetlozar Velizarov e aos meus Coordenadores Empresariais Jorge Prior e Catarina Dias, que ainda me acompanhou nos primeiros passos. Ao longo destes quatro anos contei com o vosso apoio técnico, científico e partilha de conhecimento, mas, acima de tudo, obrigaram-me a desafiar-me constantemente e ultrapassar cada barreira que surgia. Obrigado pela vosso apoio, ânimo e paciência. Agradeço ainda ao Paulo Araújo, Coordenador do Departamento de Processos e Desenvolvimento da empresa Bondalti Chemicals S.A., por ter acreditado em mim para este projeto e proporcionar todas as condições e recursos necessário para o seu desenvolvimento. Não tem a menor dúvida que este contacto diário com o ambiente industrial foi uma mais valia no meu percurso profissional. Novos interesses surgiram e estou muito grata por continuarem a apostar em mim, agora apoiado a área das operações do processo de cloro-álcalis. É ainda de mencionar o apoio da Fundação para a Ciência e Tecnologia pelo apoio financeiro concedido através da bolsa de doutoramento em ambiente empresarial ao abrigo do Programa Doutoral em Engenharia da Refinação, Petroquímica e Química (PD/BDE/114351/2016).

O meu muito obrigado:

Aos colegas do DTEPD, Alejandro, Dulce, Fernando, Hugo, Rui e Ana Afonso, pelo bom ambiente que me proporcionaram e apoio nas alturas de maior dificuldade.

Aos “estagiários” do DTEPD, em especial, ao Pedro, Diogo, Rui, Clara, Liliana e Paula pelas inúmeras horas que partilhámos entre laboratório, discussão de resultados, escrita e desabafos. Muito obrigado ainda a todos os outros colegas que aqui se cruzaram comigo nestes últimos anos. Os vossos conselhos não foram em vão.

Ao João, pelo exemplo que foi e disponibilidade constante na procura de novas alternativas e/ou soluções.

À Bela e Joana que estão sempre lá para mais um conselho, força ou desafio.

À Susana, Vasco, Catarina, Diogo, Sousa e Sérgio pela nova motivação adicional.

Aos colegas do LEPABE, sobretudo o André, Tiago, Frederico, Paulo e Tânia, obrigado por ter sido tão bem recebida e acompanhada nos meus primeiros passos na área de eletroquímica e, mais tarde, sempre que precisei apoio na execução de ensaios laboratoriais ou discussão de resultado.

Por último, mas não menos importante, o meu muito obrigado a um grupo de pessoas que sempre acreditou em mim. Muito obrigado à minha família por todo o amparo, carinho e ajuda durante esta longa caminhada:

Aos meus pais pela educação e oportunidades que me proporcionaram.

Ao Tiago que, apesar das longas distâncias, não deixou de evitar uma força extra ou acompanhar todos os desenvolvimentos.

Ao André, que esteve lá do primeiro ao último minuto. Obrigado por estares sempre do meu lado, pela paciência inesgotável, apoio carinho e apoio ao longo deste percurso. Mais alegrias estão para chegar!

"It always seems impossible until it's done."

(Nelson Mandela)

ABSTRACT

The chlor-alkali is still today one of the most energy-intensive industrial process. Despite the significant improvements achieved in recent years, electrical energy continues to represent most of the production costs. Therefore, increasing the energy efficiency of the membrane cell process remains one of the greatest challenges proposed.

The determination of the optimal replacement time for the membrane cell elements is very important. If, on one hand, it is intended to maximize the service life of membranes and electrodes, on the other hand, the energy efficiency of the process cannot be compromised. Therefore, it is necessary to guarantee preventive maintenance, always with a focus on minimizing the operating energy costs. In this relation, the objectives of this work were both practical and fundamental: to develop a methodology that allows following the evolution of the energy-related performance but also to contribute to the existing knowledge about the impact of the operating conditions in the kinetics of the chlorine evolution reaction.

For the first part of the work, a case study was chosen and the electric current and cell potential histories for a set of industrial membrane cells (electrolyser) were collected and analysed during eight years of operation. The methodology developed for the data analysis was based in the normalized cell potential, using as a reference the first month of operation of a fresh group of elements (electrodes and membranes). Discounting the equilibrium potential of the chlorine and hydrogen evolution reactions for the operating conditions, it was isolated the ohmic contribution, mainly associated to the membranes performing and, the activation overpotential related to the kinetics of the reactions at the electrode's surfaces. The methodology also allowed to represent the evolution of the ohmic and activation overpotentials, only depending on the service time of the membranes and electrodes.

In the second part of this thesis, a dedicated laboratory unit was designed and built to investigate the anodic compartment reactions kinetics evolution under different operating conditions, using appropriate *in-situ* electrochemical characterization techniques. The effects of the electrolyte composition (concentration of sodium chloride and sodium chlorate and electrolyte pH) and temperature on the kinetics of the chlorine evolution reaction were systematically studied. The results obtained for the reference conditions showed that the

kinetic parameters determined agreed with those reported in the literature. The pH proved to be a critical parameter, as the cell must operate neither below pH 2, for preventing accelerated degrading of the electrode, nor above pH 4 - 5, which favours the formation of hypochlorite. Temperature not only affects the equilibrium potential of the chlorine evolution reaction but also defines the chloride ions' activity, which in turn impacts the formation of chlorine. As expected, the presence of sodium chlorate decreases the selectivity of the chlorine evolution reaction, but only for concentrations significantly higher than those usually encountered in the industrial process.

Overall, the methodology used for the analysis of industrial data proved to be a powerful tool in the electrochemical characterization of the membrane cell process, especially for obtaining membrane performance as a function of the operating period. At the same time, the knowledge acquired in the kinetics studies of the chlorine evolution reaction can be used for process simulation and optimization purposes.

RESUMO

O processo cloro-álcalis continua a ser um dos consumidores industriais de energia com maior expressividade. Apesar das melhorias significativas alcançadas nos últimos anos, a energia elétrica ainda representa a maioria dos custos de produção. Portanto, aumentar a eficiência energética do processo das células da membrana continua sendo um dos maiores desafios propostos.

A determinação do tempo ideal de substituição para os elementos da célula de membrana é muito importante. Se, por um lado, se pretende maximizar a o tempo de serviço útil para as membranas e elétrodos, por outro lado, a eficiência energética do processo não pode ser comprometida. Portanto, é necessário garantir uma manutenção preventiva, sempre com o objetivo de minimizar os custos de energia operacionais. Nesta relação, os objetivos deste trabalho foram práticos e fundamentais: desenvolver uma metodologia que permita acompanhar a evolução do consumo energético, mas também contribuir para o conhecimento existente sobre o impacto das condições operacionais na cinética da reação de evolução do cloro.

Na primeira parte do trabalho, um estudo de caso foi selecionado e os perfis de corrente elétrica *versus* potencial elétrico de um conjunto de células de membrana industriais (eletrolisador) foram recolhidos e analisados para um período de oito anos de operação. A metodologia desenvolvida para a análise dos dados foi baseada no potencial elétrico normalizado, utilizando como referência o primeiro mês em operação de um novo grupo de elementos (elétrodos e membranas). Descontando o potencial de equilíbrio das reações de evolução do cloro e hidrogénio nas condições operacionais praticadas, individualizou-se a contribuição óhmica, associada principalmente ao desempenho das membranas e, o sobrepotencial de ativação relacionado com a cinética das reações na superfície dos elétrodos. A metodologia também permitiu representar a evolução do sobrepotencial óhmico e do sobrepotencial de ativação, dependendo apenas do tempo de serviço das membranas e elétrodos.

Na segunda parte, foi projetada e construída uma unidade de testes laboratoriais para investigar a cinética das reações que ocorrem no compartimento anódico sob diferentes

condições operacionais, utilizando técnicas apropriadas de caracterização eletroquímica *in-situ*. Os efeitos da composição eletrolítica (concentração de cloreto de sódio, concentração de clorato de sódio e pH do eletrólito) e temperatura na cinética da reação de evolução do cloro foram sistematicamente estudados. Os resultados obtidos para as condições de referência mostraram que os parâmetros cinéticos determinados estavam de acordo com os que são reportados na literatura. O pH mostrou-se um parâmetro crítico, pois a célula não deve operar em faixas muito baixas, pH < 2, por degradarem os elétrodos, ou acima de 4-5 que favorece a formação de hipoclorito. A temperatura não apenas afeta diretamente o potencial de equilíbrio da reação de evolução do cloro, como também define a atividade dos iões cloretos, que por sua vez afeta a formação de cloro. Como era expectável, a presença de clorato de sódio diminui a seletividade da reação de evolução do cloro, mas apenas para concentrações significativamente mais altas do que as usualmente encontradas no eletrólito industrial.

No geral, a metodologia utilizada para a análise de dados industriais provou ser uma ferramenta poderosa na caracterização eletroquímica do processo das células da membrana, especialmente para obter o desempenho da membrana em função do período de tempo decorrido. Ao mesmo tempo, o conhecimento adquirido nos estudos cinéticos da reação de evolução do cloro pode ser usado para simulação e otimização dos processos.

TABLE OF CONTENTS

LIST OF FIGURES

LIST OF TABLES

1 INTRODUCTION

The term chlor-alkali refers to two chemical commodities required by industry, chlorine, and alkali, which are simultaneously produced because of the electrolysis of a saltwater, in this case, a sodium chloride solution (brine). The chemicals produced are chlorine and sodium hydroxide (caustic soda), moreover, hydrogen is also obtained as a by-product of the electrolysis. The chlor-alkali process is one of the most important electrochemical processes and its industrial-scale production began in 1892. Until the middle of the 20th century, the mercury-cell process was the principal technology for producing chlorine and caustic, which was developed by Hamilton and Castner, an American, and Karl Kellner, an Austrian, in 1892 although the patent is prior to these dates [1]. Nowadays, there are two different technologies used in the production of chlor-alkali: the diaphragm cell process and the membrane cell process. Both technologies allow separating the main products, chlorine, and caustic soda, since the products are obtained in independent compartments.

Chlorine is one of the abundant and important chemicals produced by industry because it has a wide variety of uses. Initially, chlorine was used to produce bleaching products for the paper and textile industries and for the water treatment (cleaning and disinfecting) but, since 1950, chorine has become increasingly important as a raw material in the modern chemical industry. It is used in the nanomaterial formulation, for synthetic organic chemistry or as an essential component of solvents and construction materials. The electrochemical processes are the most important route to produce chlorine, representing more than 95 % of the total worldwide chlorine production and 99.5 % of the sodium hydroxide because its production is aggregated [2, 3]. Therefore, the chlorine and sodium hydroxide markets are interdependent, with annual production rates of 50 and 60 millions of tonnes, respectively [3].

Nevertheless, the chlor-alkali process has a high energy consumption. Brine electrolysis is energy-intensive: 50 - 70 % of the variable cost related to making chlorine is due to electricity and the increase in the energy efficiency of these processes is one of the most important challenges of the industry and academy in the last years [4]. Since the 1970s the development of the catalysts was driven by the need to reduce the energy consumption of the

process and to increase the stability of the electrodes used, especially for the membrane cell technology [5]. Another action, that has contributed to the reduction in energy consumption in recent years, was the closure and conversion of the process from mercury to membrane technology. Although this conversion was mainly driven by the need to minimize the environmental impact of the use of mercury, the membrane technology has a lower specific consumption because it requires fewer separation steps and the materials used are associated with a lower overvoltage [6].

Players in the chlor-alkali industry are increasingly concerned with using resistant and efficient materials for the electrodes and membranes but also with optimizing the operating conditions used. The main objective is to minimize the side reaction in the industrial cells related to the oxygen evolution. The increase in the oxygen evolution reaction can be associated with anode deactivation mechanisms and, consequently, with the increase in energy consumption of the membrane cell process over time [7, 8].

1.1 BONDALTI COMPANY

Bondalti company is one of the oldest companies in Portugal and the chemicals activity is located on the petrochemical site of Estarreja, focusing on the area of chemical commodities products, both organic and inorganic. It has performed some investments in the chlor-alkali sector with the aim of increasing its participation in the Iberian market. At the end of 2019, Bondalti Cantabria started operating in Torrelavega in the North of Spain. This unit resulted from the acquisition of an old installation that still used the mercury cell technology and its conversion to the membrane cell technology, following the best industrial practices of the chlor-alkali process. Bondalti company is an important supplier in the Iberian Peninsula chlor-alkali market and the only supplier in Portugal.

Currently, on Estarreja's site, the main products produced are aniline and chlorine, raw materials for diphenyl methylene diisocyanate, MDI, an intermediary in the polyurethane industry. MDI is produced by another player on the petrochemical plant. Bondalti also produces caustic soda, hydrogen, hydrochloric acid, and sodium hypochlorite in the chlor-alkali plant – represented in Figure 1.1. As for the aniline are the following by-products, are also produced mononitrobenzene, nitric acid, cyclohexylamine and sulphanilic acid –

represented in Figure 1.1. Most of these products are transported via a pipeline between different players of the Estarreja petrochemical site.

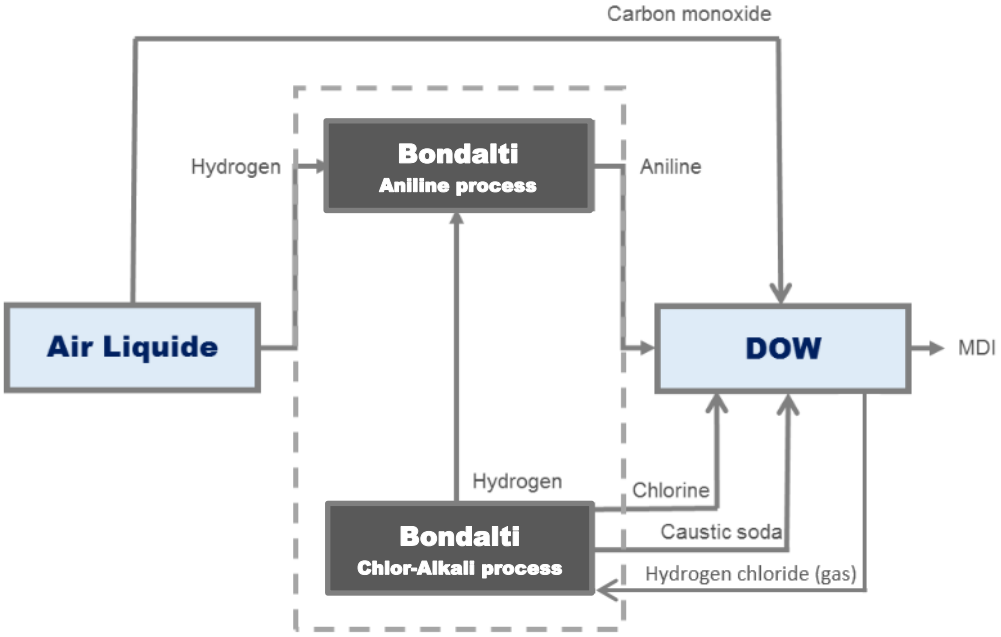

Figure 1.1 Links between Bondalti, Air Liquide and DOW in Estarreja petrochemical site.

The specification of the principal chlor-alkali products of Bondalti Chemicals S.A., caustic soda, and chlorine is expressed in Table 1.1.

Table 1.1 Specification datasheet by caustic soda and chlorine in Bondalti Chemicals S.A.

Properties	**Caustic soda [9]**	**Chlorine [10]**
Physical State (293 K)	Liquid	Gaseous
Boiling Temperature (1 bar)	416 K	259 K
Melting Temperature	283 K	-
Solidification Temperature (1bar)	-	171 K
Critical Temperature	-	417 K
Critical Pressure	-	77.1 bar
Vapour Pressure (293 K)	100 Pa	6.7 bar
Gas Density (air = 1)	-	2.49
NaOH concentration (mass fraction, %)	48.5 – 50.5	-
Liquid Density (293 K)	> 1.51 - 1.53	1.41
Viscosity (293 K)	0.075 Pa·s	-

1.1.1 Bondalti in a European context

The chlor-alkali production in Estarreja began in 1959 using mercury cell technology. In 1992, the first membrane cell electrolyser was installed, and ten years later, all the mercury cells were converted to membrane cell [11]. After the capacity expansion in 2017, the production of chlorine by the electrolysis of sodium chloride is around 94 000 tonnes per year and the production of sodium hydroxide or caustic soda is around 102 000 dry tonnes per year. There is also another technology that permitted to convert hydrochloric acid to chlorine using diaphragm cells, which contributed with more *ca.* 48 000 tonnes of chlorine per year.

Bondalti is a member of Eurochlor group. This association represents 39 producers of chlor-alkali in Europe that operate in 58 manufacturing locations in 19 European countries, representing 97 % of all European production capacity. According to the review of 2018/2019, the total of chlorine produced by these members was 11 693 000 tonnes, where 458 000 tonnes of chlorine was obtained in the Iberian Peninsula. In this period, Bondalti has already represented around 30 % of the chlorine produced from Portugal and Spain, and it is expected that its position will still be strengthened with the start-up of the Torrelavedra site [12].

1.2 CHLORINE AND SODIUM HYDROXIDE MARKETS

Sodium hydroxide is a strong base widely used in the industry as a raw material. regulators. Sodium hydroxide is also important for the manufacture of other products such as sodium salts, pH regulators, detergents and disinfectant agents and organic synthesis.

Chlorine is used in the manufacturing of chemical intermediates (e.g., polymers, pulp bleaching) and modern materials such as PVC, polyvinyl chloride, which amounts to about 33 % of chlorine total production. PVC production boosted after the Second World War and became a staple in the construction, automotive, electronics, and electrical industries [13]. Chlorine is also present in the pharmaceutic industry, water treatment and in the innovating materials, for example, in the nanomaterials composition [2].

United States of American and Canada, Western and Eastern of Europe, China, and Japan dominate the chlorine production. Usually, the sodium hydroxide, or so-called caustic soda, and chlorine are produced simultaneously, with a mass ratio of 1:0.88 [14]. The

independent production of sodium hydroxide is practically inexistent, but the chlorine can be produced by alternative routes, which represent about 5 % of its total production.

The fluctuations of chlorine and sodium hydroxide production and their supply and demand are critical to the profitability of the industrial sector [14]. It is easy to understand why its prices are interdependent.

1.3 CHLOR-ALKALI MANUFACTURING TECHNOLOGIES

Over time there have been three industrial electrochemical processes: diaphragm, mercury, and membranes.

In 1851, Charles Watt invented the first chlor-alkali technology, the diaphragm cell, and after thirty-seven years, the first commercial set was built [2]. In the diaphragm cell technology, a physical barrier is used to separate the anode and cathode sides, more specifically a permeable diaphragm usually asbestos-based, which present some issues for public health and the environment. Although the diaphragm technology is relatively inexpensive, the use of steam for the extra steps required for the sodium hydroxide concentration and its secondary environmental impacts led manufacturers to replace this technology, mainly in Europe [2, 15].

The mercury cell process was implemented in 1892 by Hamilton and Caster; during about 125 years, this chlor-alkali technology has been used throughout the world. A mercury cell is formed by two units: the electrolyser and the secondary electrochemical reactor or decomposer [16]. In the electrolyser, chlorine is produced at the anode and the cathode produces sodium metal in the form of an amalgam, NaHg. In the electrochemical reactor, water is used to decompose the sodium amalgam into sodium hydroxide, hydrogen, and mercury that returns to the electrolyser [2, 15]. For the mercury technology, the principal problems are the energy consumption required by the concentration of sodium hydroxide solution steps and the mercury emissions may involve serious environmental problems.

Since the 1950s the membrane cell technology appeared as an alternative to the electrolysis, where the physical barrier was replaced by a selectively permeable membrane, allowing only the cations to pass through the membrane [2, 15]. In 1975, Japan commissioned the first commercial plant with membrane cell [3]. The purity of the caustic soda solution in

membrane technology is greater than the other technologies. Moreover, energy consumption is the lowest of the three processes alternatives. However, a short membrane' service life and the erosion of the anodes became a problem for the industry.

The first anodes electrodes were made of carbon but, only in 1970s, there was a reduction in the maintenance cost with the development of dimensionally stable anodes, DSA®, which also allowed to reduce the energy consumption. These anodes were manufactured using titanium and a ruthenium-based oxide coating deposited on titanium support [5].

In the 1970s, the total installed capacity of chlorine in the world was about 20 million tonnes per year, with North America accounting for 50 % of the total chlorine production [2]. Between the 1970s and 2008, chlorine production increased by 2.8 % per year [15] and new markets were introduced to chlorine production, specifically, in Asia with China dominating. In 2008, the world's total capacity was 62.8 million tonnes of chlorine. China has become the world's largest producer, accounting for 26 %, and exceeded North America, with 23 %, and Europe, with 20 %, of the chlorine market. Nowadays the diaphragm process is still preferred in North America. The Asian market continues to grow, where the membrane technology is preferred. China is already the largest membrane technology producer in the world, with over 60 % of the installed capacity already using membrane technology [17].

In Europe, the distribution of the chlor-alkali technology in Europe, for 2001-2018, is demonstrated in Figure 1.2.

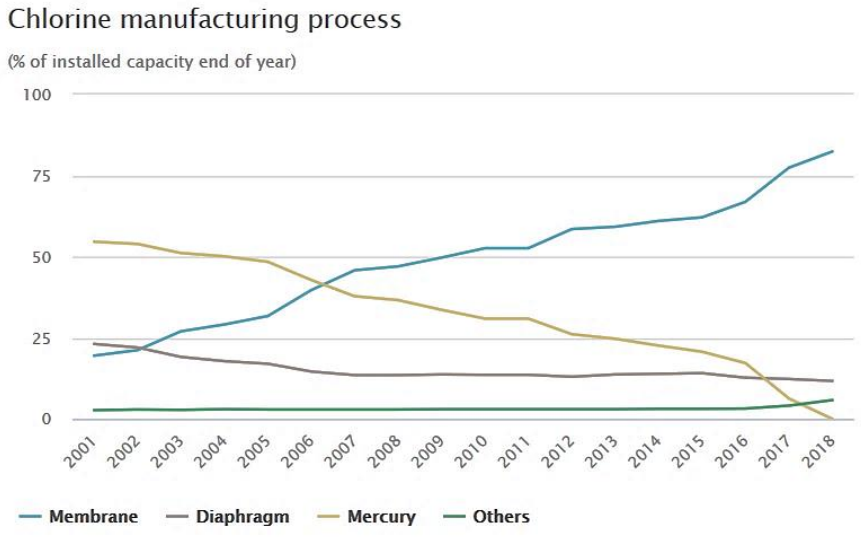

Figure 1.2 Total capacity of the chlorine manufacturing process installed in Europe (source: [12]).

Over the years the use of the mercury cells has decreased significantly, driven by strict governmental legislation in part influenced by raising social awareness about the health and environmental problems caused by pollutants emissions. In Western Europe alone, the natural and anthropogenic mercury emissions went down from 26.60 $g \cdot t_{chlorine}^{-1}$, in 1977, to 1.42 $g \cdot t_{chlorine}^{-1}$, in 2000, which was less than 0.1 % of the total emissions [18]. The value was reduced along of the years and, in 2014, the absolute level of European chlor-alkali industries remained stable at 2.07 tonnes, totalizing 0.74 $g \cdot t_{chlorine}^{-1}$, as shown in Figure 1.3 [18].

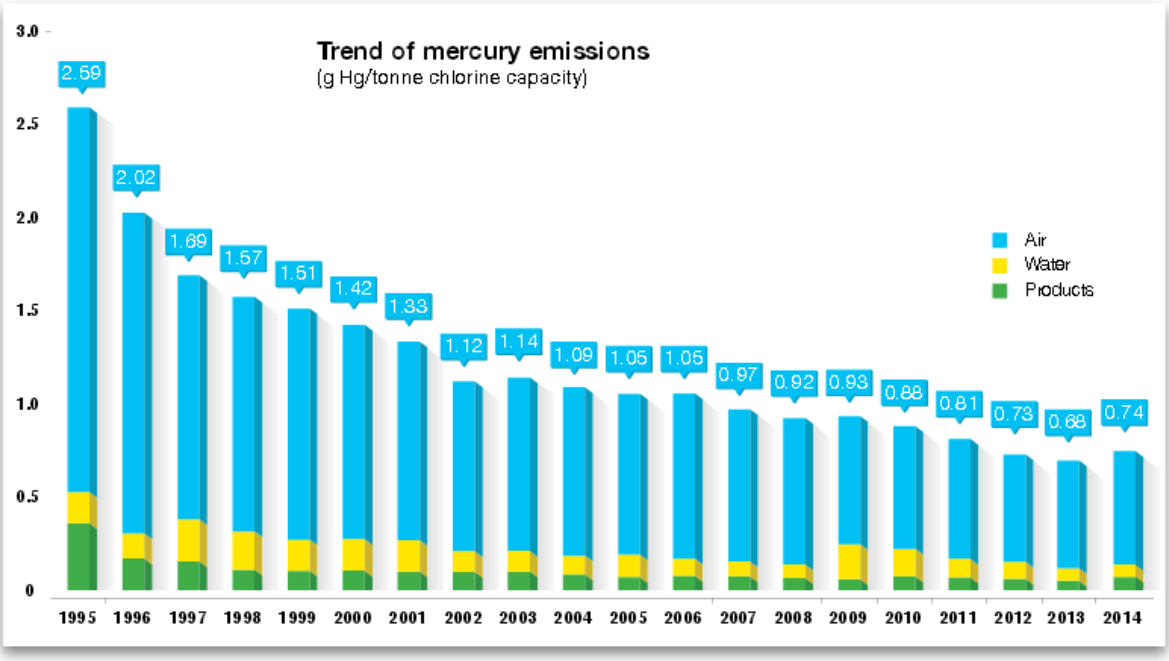

Figure 1.3 The contribution of the chlor-alkali industry to mercury emissions between 1995 and 2014 in Europe (source: [19])

European legislation dictated the mercury technology phase-out by the end of 2017 [13] and chlor-alkali manufacturers had to close or convert the mercury electrolysis to membrane technology, in the last decade, contributing to the reduction of the pollutants emissions.

1.4 TOPIC OVERVIEW – ENERGY CONSUMPTION

Energy consumption in chlor-alkali electrolysis is critical for the process of sustainability because it represents 50 % to 70 % of the variable costs related to making chlorine. In a chlorine plant, electric energy is required for the electrolysis operation and others, such as compressors, pumps, and refrigeration. Steam is used for heating fluids and particularly for the concentration of the caustic from a mass fraction of 32 % to 50 % [19]. According to Eurostat data, in 2015, the energy consumption of the European chlor-alkali industry was 27 446 GWh and, in addition, 6.7 million tons of steam were used for heating purposes (mainly in caustic soda evaporation). If it transforms the electricity and steam into gross energy terms, this would mean that the total energy consumption of the European chlor-alkali industry is, approximately, 4.1 million tons of oil equivalents or 0.25 % of the gross energy used in the Europe Union (28 countries) [20]. It clear that improvements in the energy efficiency of these processes could yield significant reductions in global energy consumption [3].

The development of dimensionally stable anodes, DSA®, is called “one of the greatest technological breakthroughs of the past 50 years of electrochemistry” [5]. The original DSA® coating composition for chlorine evolution reaction was a mixture of ruthenium and titanium oxide, typically a mass fraction of 30 % of RuO_2 and 70 % of TiO_2, deposited on a Ti-substrate. Since then, the DSA® introduction contributed to energy savings due to their lower potentials at industrial current densities [21]. Another improvement was the “zero-gap design”, which avoid the mass transport limitations because the electrodes remain in intimate contact with the ion-exchange membrane [3, 22, 23].

The principal undesired reaction occurs at the anode and involves oxygen evolution via water oxidation. The oxygen evolution is influenced by catalytic processes ongoing both in the electrolyte and on the anode surface, where oxygen might be involved both electrochemically and chemically through water or hypochlorite decomposition. This process is affected by some process parameters, with the compositions of the electrolyte and the anode also being. Furthermore, other process conditions, such as current density and temperature, affect reactions that take place in the bulk electrolyte and on the anode surface [3, 22, 23].

1.5 MOTIVATION AND OUTLINE

The electricity consumption in the chlor-alkali process has a great impact in the operating costs, which makes it clear that improvements in the energy efficiency of the process can yield significant reductions in the production costs of the chlorine. The anodes deactivation if not conveniently observed, it represents a high operational risk due to significant production losses in the exponential final stage. The project objective is to increase the knowledge about anode stability and the correlation between the mechanisms of deactivation and the operating conditions. The main questions that these thesis addresses are:

1. Which factors affect the mechanisms of anode deactivation? What is the contribution of each of them?

2. How can we do the electrochemical characterization of the chlor-alkali process?

3. What are the strategies for decreasing the operating costs and increasing the electrode coating service time?

In recent years, a lot of information about new types of membranes and electrodes was published in the literature but, a significant part of these do not have industrial applicability. **Chapter 2** presents a background of the chlor-alkali process. In the first part, the fundaments and components of membrane cell technology are mentioned, as well as the main developments that have occurred in recent years. Given the special interest in the evolution of energy consumption associated with the anode, the second part of this chapter focuses on the dimensionally stable anodes, DSA®, the most used type of anodes in this type of industry: its configuration, reactions that occur in the coating electrode and the degradation mechanism.

This work pretends to develop an evaluation toolbox can provide information about the energy consumption as a function of the service time of the electrode and of the membrane for an industrial case, to answer the questions 2 and 3. The history of the potential and electrical current of an industrial chlor-alkali membrane electrolyser is a powerful tool to track its operational efficiency progress over time and for deciding the required maintenance instants. The performance of a dedicated industrial NaCl electrolyser is analysed for a long period, and the different components of the system are individualized and analysed in **Chapter 3**.

Chapter 4 presents a laboratory study of the relationship between the kinetics of the chlorine evolution reaction and the operating conditions applied (sodium chloride concentration, sodium chlorate concentration, electrolyte pH and temperature), analyzing the questions 1 and 3 of the thesis motivation. Through the results of the electrochemical characterization of the system (cyclic voltammetry – CV and polarization curves – PC), it is intended to obtain trends that can help define actions of preventive maintenance of the chlor-alkali membrane cell process.

Finally, **Chapter 5** presents the general conclusions of this work and **Chapter 6** presents some suggestions for future works in the area.

1.6 REFERENCES

1. O'Brien, T., Bommaraju, T., Hine, F., *History of the chlor-alkali industry*, in *Handbook of Chlor-Alkali Technology*, Springer, Editor. 2005: New York. p. 17-36.
2. O'Brien, T., Bommaraju, T., Hine, F., *Handbook oh chlor-alkali technology*, ed. Springer. 2005, New York.
3. Schmittinger, P., Florkiewicz, T., Curlin, L., Luke, B., Scannell, R., Navir, T., Zelfer, E., Bartsch, R., *Ullmann's encyclopedia of industrial chemistry*. 2012, Weinheim.
4. EuroChlor, *Electricity is essential for the chlor-alkali industry*. (Available from: https://www.eurochlor.org/topics/energy/, accessed 19/01/2020).
5. Trasatti, S., *Electrocatalysis: understanding the success of DSA®.* Electrochimica Acta, 2000. 45: p. 2377-2385.
6. O'Brien, T., Bommaraju, T., Hine, F., *Chlor-alkali technologies*, in *Handbook of Chlor-Alkali Technology*, Springer, Editor. 2005: New York. p. 387-442.
7. Karlsson, R., *Theoretical and experimental studies of electrode and electrolyte processes in industrial electrosynthesis*, in *KTH Royal Institute of Technology*. 2015, KTH Royal Institute of Technology: Stockholm.
8. Silva, J. F., *Study of dimensionally stable anodes for chlor-alkali electrolysis*, in *Chemical Engineering Department*. 2016, University of Porto.
9. Bondalti, *Liquid caustic soda specification data sheet*. (Available from: https://www.bondalti.com/contents/pdflist/dt-203-005-portugues.pdf, accessed 05/02/2020).
10. Bondalti, *Chlorine specification data sheet*. (Available from: https://www.bondalti.com/contents/pdflist/dt-203-003-portugues_8738.pdf, accessed 05/02/2020).

11. Dias, A. C., *Chlor-alkali membrane cell process: study and characterization*, in *Chemical Engineering Department*. 2010, University of Porto.

12. EuroChlor, *Chlorine Industry Review: 2018/2019* (Available from: https://www.chlorineindustryreview.com/wp-content/uploads/2019/08/EUROCHLOR_CHLOR-ALKALI-IndustryReview2018-2019.pdf, accessed 11/02/2020).

13. EuroChlor, *The chlor-alkali industry in Europe*. (Available from: http://www.eurochlor.org/thechlorineuniverse/thechloralkaliindustryineurope.aspx, accessed 12/04/2018).

14. Bommaraju, T., Luke, B. , O'Brien, T., Blackburn, M., *Encyclopedia of chemical technology Kirt-Othmer*, ed. J.W. Sons. 1993.

15. Kurt, C., Bittner, J., *Ullmann's encyclopedia of industrial chemistry*, W.-V.V.G.C. KGaA, Editor. 2000.

16. Schmittinger, P., *Principles & industrial practice*. 2008, Weinheim: Wiley.

17. Brinkmann, T., Santonja, G., Schorcht, F., Roudier, S., Sancho, L., *Best available techniques (BAT) reference document for the production of chlor-alkali*, in *Industrial Emissions Directive 2010/75/EU (Integrated Pollution Prevention and Control)*, J.S.a.P.R.E. EN, Editor. 2014.

18. Worldchlorine, *Chlorine and caustic soda: chlor-alkali manufacturing processes*. 2002.

19. EuroChlor, *Chlorine Industry Review: 2014/2015* 2015.

20. EuroChlor, *The Energy Situation in Europe*. (Available from: https://www.eurochlor.org/wp-content/uploads/2019/04/the_energy_situation_in_europe_2018.pdf, accessed 17/12/2019).

21. Beer, H. B., *The invention and industrial development of metal anodes.* Journal of The Electrochemical Society, 1980. 127: p. 303-307.

22. Bommaraju, T., Chen, C., Birss, V., *Deactivation of thermally formed RuO2 + TiO2 coatings during chlorine evolution: mechanisms and reactivation measures*, in *Modern chlor-alkali technology*. 2000, International Chlorine Symposium - Blackwell Science: UK.

23. Karlsson, R., Cornell, A., *Selectivity between oxygen and chlorine evolution in the chlor-alkali and chlorate processes.* Chem Reviews, 2016. 116(5): p. 2982-3028.

2 STATE OF THE ART

The most common chlor-alkali technology involves the electrolysis of an aqueous sodium chloride solution (brine) in a membrane cell configuration. The membrane prevents the back-migration of the hydroxide anions to the anodic compartment and the respective reaction with the chlorine formed in this side, which form undesirable by-products.

A lot of chlor-alkali technologies licensing companies and the academy has been contributing to optimize the membrane cell components, reducing the energy consumption, and increasing the service time of the different components. There are three subjects that are continuously investigated: the electrode coating composition and respective deposition over the substrate; the membrane structure; and, the zero-gap cell design that permitted the minimization of gas bubbles accumulation on the electrode surface.

2.1 MEMBRANE CELL TECHNOLOGY

The membrane cell is composed of three components: an ion-selective perfluorinated membrane, sandwiched between a DSA® anode and a nickel cathode. A schematic membrane cell is represented in Figure 2.1.

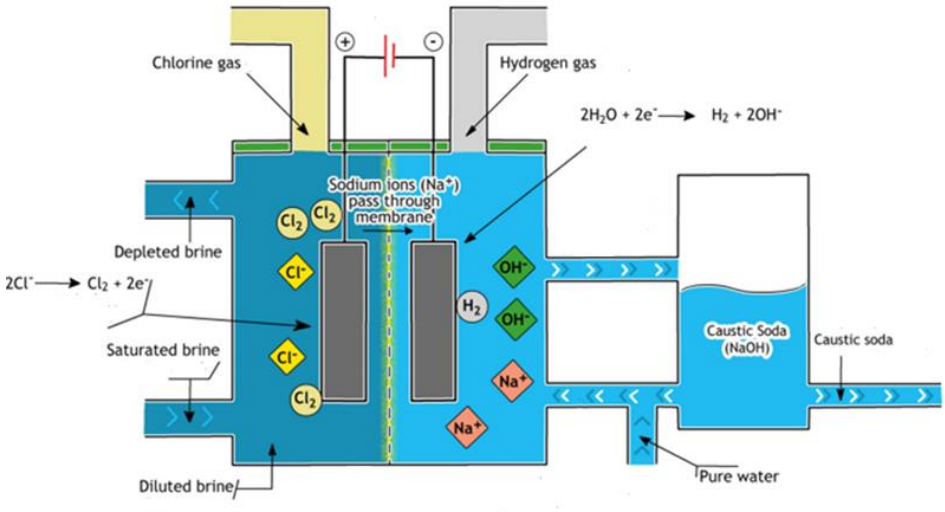

Figure 2.1 Schematic of ion-exchange membrane cell (source: [1]).

A concentrated brine, with a mass fraction of 26 %, is feed to the anode side where chlorine is formed from the oxidation of chloride ions; diluted brine, with a mass fraction of 20 %, leaves the anode side. Sodium ions and water migrate through the cation membrane to the cathode side. In the cathode side, the water is reduced to produce hydrogen and hydroxyl ions. These ions are combined with sodium ions generating highly concentrated sodium hydroxide, with a mass fraction of 32 %. A diluted sodium hydroxide solution is recycled to the cathode to avoid the water return by anode compartment [2, 3].

Table 2.1 shows the main reactions of the chlor-alkali membrane cell, the electrochemical half-reactions on each electrode, the chorine evolution reaction (CER) on the anode and the hydrogen evolution reaction (HER) on the cathode, and also the global equation of the process. In tspche same table, it is also presented the respective standard reduction potential relative to the standard hydrogen electrode, SHE [4].

Table 2.1 Main reactions of the chlor-alkali membrane cell process (source: [4]).

	Reactions	E^0/V *vs.* SHE	
Anode	$2NaCl\,(aq) \rightarrow 2Na^+(aq) + 2Cl^-(aq)$		(2.1)
	$2Cl^-\,(aq) \rightarrow Cl_2(g) + 2e^-$	1.36	(2.2)
Cathode	$2H_2O\,(l) + 2e^- \rightarrow H_2(g) + 2OH^-\,(aq)$	-0.83	(2.3)
	$2Na^+(aq) + 2OH^-\,(aq) \rightarrow 2NaOH\,(aq)$		(2.4)
Overall	$2NaCl\,(aq) + 2H_2O\,(l) \rightarrow Cl_2(g) + H_2(g) + 2NaOH\,(aq)$	-2.19	(2.5)

Typical operating conditions used in the membrane cell technology are summarized in the following Table 2.2.

Table 2.2 Operating conditions for the membrane cell (source: [4-6]).

Parameters of the membrane cell	**Values**
Cell potential (V)	2.4 - 2.7
Current density ($kA \cdot m^{-2}$)	1.5 - 7
Specific energy consumption ($kWh \cdot t_{chlorine}^{-1}$)	2500 - 2700
Temperature (K)	363
NaCl concentration in the anolyte feed (mass fraction, %)	26
Anolyte pH	2 - 4
NaOH concentration in the catholyte recirculation (mass fraction, %)	32

2.1.1 Membrane

The conventional physical barrier has the chemical structure as demonstrated in Figure 2.2.

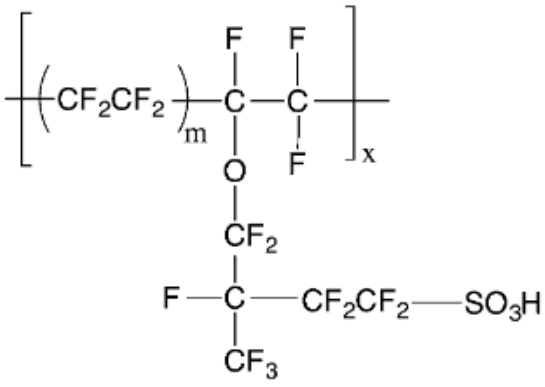

Figure 2.2 The primary chemical structure of Nafion Flemion® (source: [7]).

The membrane development allowed to improve and diversify the membranes mechanical, thermal, and chemical properties. The commercially available membranes in the chlor-alkali are bilayer membranes with a polymeric matrix made of tetrafluoroethylene. This type of membrane is composed of a thick layer of tetrafluoroethylene functionalised with sulfonic groups at the anode side, an excellent proton conductor, and a thinner layer of tetrafluoroethylene functionalised with carboxylic groups at the cathode side, high selectivity for the sodium cations and chloride anions. To avoid clogging and accumulation of encrustations from the membrane, a pre-treatment of brine is necessary to minimize the membrane current efficiency losses [8, 9].

2.1.2 Cathode

The primary materials for the electrodes used in the diaphragm cell were carbon steel for the hydrogen evolution reaction (HER). After the development and commercialization of ion-exchange membranes, nickel or ruthenium oxide-coated cathodes replaced the original carbon steel electrodes in chlor-alkali cells [2].

In the 1990s, nickel cathodes were implemented in most plants because of their excellent corrosion resistance when exposed to high concentrations of sodium hydroxide, and resistance to high temperatures that are required to increase the kinetics and maximize electrical conductivity within the electrolyte. Similarly, another factor to consider in choosing the material of the cathodes is its resistance against oxidation by chemical species like chlorine. During a plant shutdown, the chlorine species can migrate to the cathode and promote the cathode corrosion by chemical attack or by electrochemical dissolution. For typical operating conditions, nickel is a competitive material because it demonstrated a good electrocatalytic activity, corrosion resistance and reduces the overpotential to 100 mV [2, 10].

Improving the energy performance of the membrane cell is a crucial issue that drives the research of new high-performance materials. The overpotential can be further reduced by replacing nickel by a metal that presents a larger surface area, with the appropriate mechanical properties, or adopting technologies that increase the surface area of nickel electrode like the so-called Raney nickel cathodes, where a larger number of active sites are exposed [2, 11].

The most suitable metal in terms of electrocatalytic activity for HER is platinum, but its stability under alkaline conditions is limited. Nowadays, HER studies focus on the development of doping coating by different metals (e.g. Co, Cr, Ti, W, Fe or Mo) with greater catalytic activity and mechanical properties in alkaline solution [2].

2.1.3 Anode

The first metal used in the anode composition for the chlorine evolution reaction, CER, was graphite [2, 12]. However, the graphite was consumed during the process meaning that the service time of the electrode was quite short, and a frequent replacement was needed. A lot of solutions were studied by the suppliers, but the principal difficulty was to combine the electrochemical ability with the mechanical resistance and lower production cost of the

electrodes. For example, platinum has good resistance and it is a good electric conductor, but it is an expensive material. In the 1950s, a new type of electrodes was created, the titanium and ruthenium oxide-based electrodes, which later became an entire class, the dimensionally stable anode, DSA® in the 1970s. Today the composition used by the major of electrodes suppliers is still based on this material [4]. It can be said that this discovery was driven by a practical need of the industry [13]. Furthermore, the use of DSA® in other processes, such as electro galvanization or cathode protection, demonstrates the success of this type of electrodes, which ensure high activity and stability for a long period [14].

2.1.4 Monopolar and bipolar electrolysers

The membrane electrolysis has several single elements which are arranged to form an electrolyser. Each electrolyser module (stack) can have between 20 and 90 elements. Figure 2.3 demonstrates a scheme of the Asahi Kasei electrolyser in maintenance operation [15].

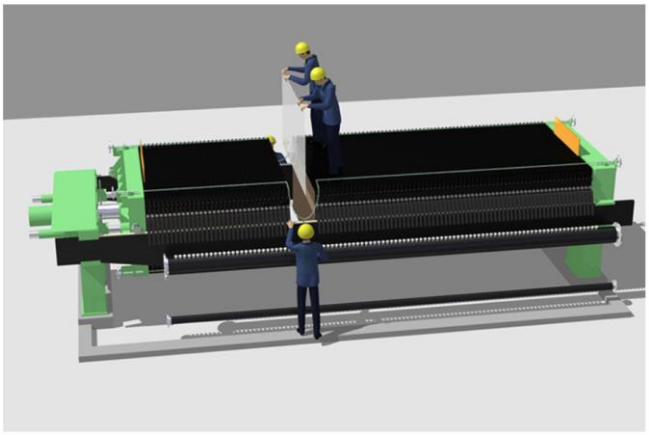

Figure 2.3 Bipolar membrane electrolyser in the maintenance operation (source: [15])

There are two categories of electrolysers: monopolar and bipolar, as represented in Figure 2.4. The configuration differences are related to the electrical supply system (rectifiers and transformers), which also influence the capital cost of the cell. In the first configuration, the electrolysers are connected in series and the individual elements are connected in parallel, with high current and low voltage. In the second configuration, the electrolysers are connected in parallel and the single elements in series, with low current and high voltage. Bipolar technology is most popular in the industry due to having has some appealing advantages such as a lower investment, lower energy consumption, and longer service time.

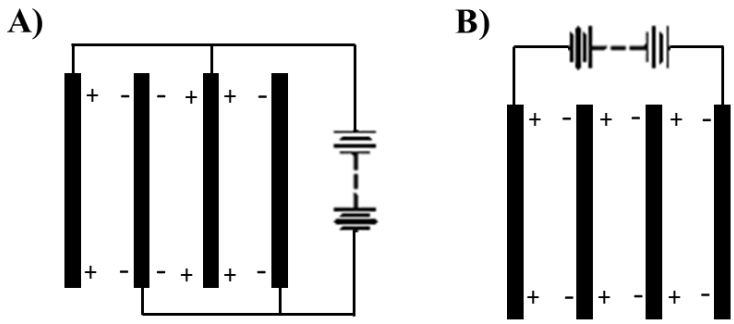

Figure 2.4 Scheme of an electric configuration: A) monopolar; B) bipolar.

2.2 DIMENSIONALLY STABLE ANODES

The dimensionally stable anodes, DSA®, were invented by Henry Beer in 1950-1960s and this discovery has improved the energetic performance of the chlor-alkali process [13].

The DSA® is the electrocatalyst of the chlorine evolution reaction and its composition has been modified in several steps to increase the resistance of the anode of the electrolyte and to increase the current efficiency associated with the chlorine production [4]. Initially, Henry Beer found titanium-based species were very resistant to corrosion in an alkaline solution such as the anolyte of the chlorine production [16, 17]. Due to its stability under typical operating conditions, in 1968, anodes with Ti-substrate coating with a layer of titanium dioxide, TiO_2, began to be used in an industrial plant. The excellent performance results obtained ignited scientific interest on its mechanical properties [17, 18].

After finding an alternative to graphite in the anodes manufacture that allowed fulfilled the desired mechanical resistance, the focus became the improvement of the catalytic properties of the anodes. It was looking for coating compositions including metal oxides because it had greater electrical conductivities, reducing the activation overpotential of the electrodes. Platinum and iridium solutions were shown to be the most promising. However, the high cost of these metals raised the research for alternative noble metals, cheaper but still with good electric conductivity, such as ruthenium in the 1960s [13, 19, 20]. The first Beer formulation was patented in 1965 as "Beer 1", honouring the inventor. In “Beer 1”, the ratio indicated for the coating was one part of ruthenium oxide, RuO_2, to one part of titanium oxide, TiO_2, which was deposited on Ti-support [21-23]. These anodes were then tested on the mercury technology, having increased durability of the anodes. The following years were dedicated to the optimization of the ratio of the noble metals, as had been detected that a large

amount of active phase of the electrode coating was not required to minimize the activation overpotential. Additionally, it was also important to have a good uniformity of distribution of the active sites (metal oxides) on the surface and adhesion between the coating layer and Ti-support to minimize the physical degradation of the electrode [24-26].

The "Beer 2" configuration did not take long to emerge. After two years, a mixture of 30 mol % RuO_2 and 70 mol % TiO_2 was proposed and its ratio remained for many years as the standard composition applied by manufacturers [18]. TiO_2 has a low electrical conductivity but when mixed with RuO_2, the conductivity of the mixture coating increases. The combination allowed to reduce the price of the electrode because TiO_2 is cheaper than RuO_2 but, at the same time, it permitted to increase the activity of the anode. Moreover, this mixture had higher selectivity to chlorine evolution than for the oxygen evolution, as intended [6].

Since "Beer 2", manufacturers made further modifications to the electrodes, with specific details kept undisclosed by electrode manufactures. The literature indicates that others noble metal oxides were tested in the mixture deposited on the electrode surface, marking as the most promising the introduction of iridium and tin in the coating, which are equally good electric conductors. The iridium oxides and tin oxides were not only tested as single only active species in the coating but also, in different proportions with RuO_2, TiO_2 or combinations of metal oxides in order to maintain and/or reinforce the mechanical and electrocatalytic properties of the anode and reducing the costs [27-31].

In terms of preparation, the most used method to coat the electrode support is the thermal decomposition. This method was based on coatings with a noble metal salt solution onto titanium at 400 - 500 °C in air, converting the salt to metallic form, following a methodology widely used in heterogeneous catalysis [32, 33]. However, other technics can be also applied, such as the sol-gel but, it can insert one or more dopant materials on the electrode surface, which is an undesirable situation as it can affect the chlorine evolution.

The compositions of the coating of the DSA® have a mixture of TiO_2-RuO_2-IrO_2, thermally deposited coating on the titanium substrate, as illustrated in Figure 2.5

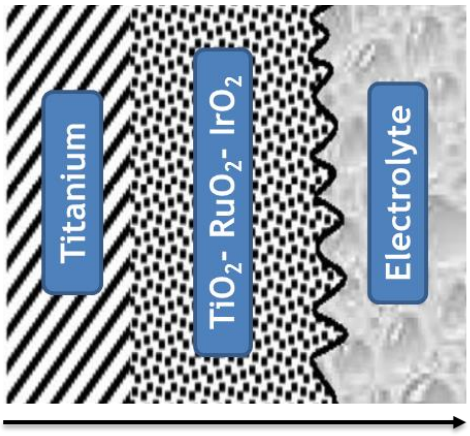

Figure 2.5 Scheme of an electroactive oxide coating on titanium-support designated for "Beer formulation" (adapted from [28]).

Nowadays, the coatings of the industrial electrodes have already a good electrocatalytic activity, which increased production of chlorine per tonne of brine feed; and, the electrode have high mechanical and chemical resistance, which allow to minimize the loss of active sites on the electrode surface and to maximize the service time of the electrode. Typically, the overpotential of standard anodes is 40 - 60 mV, for current densities of 200 - 250 $mA.cm^{-2}$ to 5.0 M NaCl solutions and temperatures of around 353 - 363 K. However, with prolonged use of anodes, the electrocatalytic activity decreases and the anode overpotential increases linearly for the first part and then exponentially to 300 - 400 mV. At this point, the anode is considered deactivated and the *ex-situ* recoating step is required with the electrodes manufacturers [34]. For a bipolar electrode, the cathode is also reactivated at the same time, although, in this case, the deactivation of the active site on the coating is linear along the service time and the increase of cathodic activation overpotential is only linear.

2.2.1 Thermodynamics and kinetics of the half-reaction

In electrochemical systems, the spontaneity of the half-cell reactions is provided by thermodynamic information, specifically the Gibbs free energy (ΔG). The chlor-alkali electrolysis uses an electrolytic cell ($\Delta G > 0$), where a chemical reaction is driven by a power supply. Equation (2.6) represents the minimum of the energy that the system requires, ΔG, at constant pressure and temperature, where, n is the number of electrons transferred between each species, F, is Faraday constant and E is the cell potential [35].

$$\Delta G = -n \cdot F \cdot E^0 \tag{2.6}$$

The equilibrium cell potential, E^0, results from the contribution of the potential of the half-cell reaction occurring in each electrode. By IUPAC convention, the cell potential is obtained by Equation (2.7), where $E_{0,c}$ is the reduction potential of the cathodic reaction and, $E_{0,a}$ is the reduction potential of the anodic reaction, corrected for the electrolytes concentration, temperature and pressure of the cell [35].

$$E^0 = E_{0,c} - E_{0,a} \tag{2.7}$$

A typical electrochemical reaction involves the transfer of charge between an electrode and a species in the electrolyte, as shown in Figure 2.6

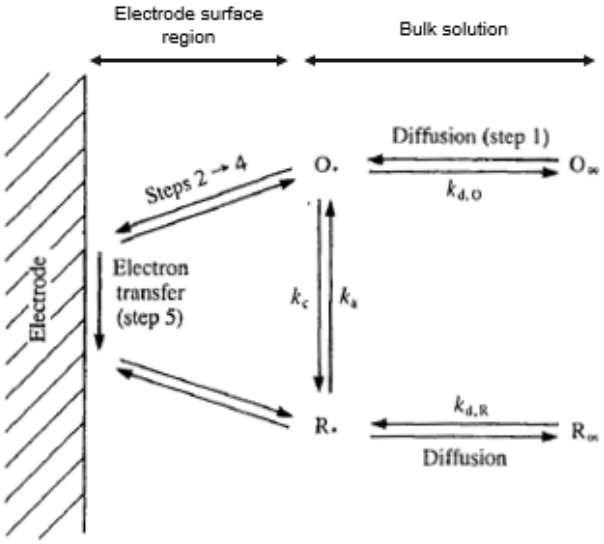

Figure 2.6 Scheme of electron transfer at an electrode (adapted from [35]).

The electron transfer rate is limited by an activation barrier that depends on the reaction mechanism. The activation barrier, corresponding to electrons energy at Fermi level, is influenced by the cell potential [35].

Current density is directly related to the rate of the electrochemical reaction and it is proportional to overpotential, which is given by the well-known Butler-Volmer equation, where n is the number of electron involved, η is activation overpotential, j_0 is the exchange current density, R is the universal gas constant, T is the absolute temperature, and α is the charge transfer coefficient [36, 37].

$$j = j_0 \cdot \left[e^{\left(\frac{\alpha \cdot F \cdot n \cdot \eta}{RT}\right)} - e^{\left(\frac{-(1-\alpha) \cdot F \cdot n \cdot \eta}{R \cdot T}\right)} \right] \tag{2.8}$$

Butler-Volmer equation has two limiting cases:

a) Small overpotential can be linearized by the first terms of a Taylor series expansion ($e^x \approx 1+x$).

$$j = j_0 \cdot \left(\frac{F \cdot n \cdot \eta}{R \cdot T}\right) \tag{2.9}$$

b) High positive or negative overpotential, where the forward rate of the reaction is predominant, and the backward reaction can be neglected, the current density is well-described by the Tafel equation.

$$j = j_0 \cdot e\left(\frac{\alpha \cdot F \cdot n \cdot \eta}{R \cdot T}\right) \tag{2.10}$$

Applying logarithms and rearranging Equation (2.10) it was obtained:

$$\eta = b \cdot [\ln(j_0) - \ln(|j|)] \tag{2.11}$$

where *b* is the Tafel slope or:

$$b = \left(\frac{R \cdot T}{\alpha \cdot F \cdot n}\right) \tag{2.12}$$

The activation overpotential of an electrochemical reaction represents the difference between the Fermi energy level of the metal and free energy of the electron in the redox system (electrolyte). That magnitude is determined by the interaction between the excess of charge on the metal and the ion on the electrolyte.

2.2.2 Charge and mass transport

The transport of the reactants from the bulk of the solution to the electrode surface and the removal of products from the surface are inherent steps in electrochemical reactions, as previously illustrated in Figure 2.6.

In an electrochemical system charges are present as ions, in the electrolyte, and as electrons, in the electrodes surface. The ions are transported to the electrodes and the electrons are transported through the external circuit from the anode (produced) to the cathode

(consumed). The accumulation/depletion of ions on the electrode surfaces creates a potential that drives the ion transport and a concentration gradient that through drives the electrolytes.

In metal electrodes, the driving force for charge transport is the electrical potential, while in electrolyte solutions, the motion of ions can occur due to different types of the transport mechanisms: migration, where the driving force is the electric potential gradient; diffusion, where the driving force is the concentration gradient and convection, where the driving force is the pressure gradient. The more relevant driving force of the charge transport in a membrane cell is the electrical potential gradient.

The electric field exists due to depletion/accumulations of the charges on the electrode surface. On the hand, in the brine electrolysis there is a depletion of anions, Cl^- and an accumulation of electrons on the anode surface and, on the other hand, it occurs the accumulation of anions, OH^-, and depletion of electrons, on the cathode surface. Moreover, in the membrane technology as the membrane type are permeable to the sodium cations, the Na^+ are transported from the anode to cathode side.

One important physical property for electrochemistry is the conductivity of a material, which measures it ability to transport electric current. The conductivity is affected by temperature and the composition of the material. It can be determinate by Equation (2.13), where R_c is the conductor resistance, σ is the conductor conductivity, l is the length of the conductor and A is the cross-sectional area of the current flow.

$$R_c = \frac{l}{\sigma \cdot A} \tag{2.13}$$

The charge transport due to current density (j) increases as the potential gradient increases. Ohm's law describes the relationship between the cell potential which is applied with the rate of electric charge flow, as represented by Equation (2.14):

$$E = j \cdot R_c \tag{2.14}$$

When the transport is slow and/or the electric field very high, the mass transport at the surface of the electrodes become rate controlling. This phenomenon is called concentration polarization and affects the rate of the electrochemical reaction. In the electrolysis process, this is often not considered, partially due to an excess of supply of raw materials to the process which minimizes the mass transport problems. Nevertheless, the presence of gas bubbles in

the electrolytes greatly affects the electrolyte conductivity and consequently the cell potential, by changing the electrolyte resistivity, according to the Bruggemann equation:

$$\frac{\rho}{\rho_0} = (1-\varepsilon)^{3/2} \tag{2.15}$$

where ρ is the resistivity of the electrolytes (inverse of conductivity), ρ_0 is the resistivity of pure electrolyte, or free of gas bubbles, and ε is the gas void fraction.

2.2.3 Mechanisms of the chlorine evolution reaction

The first mechanism studied for the chlorine evolution reaction, CER, on titanium coated with mixed oxides of noble metals backs to 1972. Faita and Fiori [38] proposed a two-step mechanism for the evolution of chlorine. The Tafel slope was 30 - 40 mV and the experiments carried out supported it where [S] is the active site.

$$[S] + Cl^- \rightarrow [S]Cl_{ads} + e^- \tag{2.16}$$

$$2[S]Cl_{ads} \rightarrow 2Cl_2 + 2[S] \tag{2.17}$$

In the same year, using a DSA® anode coating with a composition of 30 % RuO_2 and 70 % TiO_2, Erenburg [39, 40] presented a mechanism which considers three steps, similar to the Volmer-Heyrovsky-Tafel steps. Two parallel routes are possible: on the first route, the Volmer step is followed by the Heyrovsky step in which a chloride ion in solution reacts with the adsorbed species leading to the formation and desorption of chlorine; on the second route, two adsorbed chloride ions react with each other to form a desorbed molecule.

<u>Volmer or discharge step:</u> $[S] + Cl^- \rightleftharpoons [S]Cl_{ads} + e^-$ (2.18)

<u>Heyrovsky or electrochemical desorption step:</u> $[S]Cl_{ads} + Cl^- \rightarrow Cl_2 + e^- + [S]$ (2.19)

<u>Tafel or recombination step:</u> $2[S]Cl_{ads} \rightarrow Cl_2 + 2[S]$ (2.20)

The mechanism of Volmer-Heyrovsky-Tafel proved to be equally compatible with the Tafel slope. However, the experimental data comparison with the concentration of chloride anions came to show that the reaction speed is not of the first order, which goes against the mechanism proposed. To correct, the same group in 1975 suggested that the mechanism includes a chlorine intermediate positively charged, SCl_{ads}^{+} [39, 41-43].

Since 1977, mechanistic studies began strengthening the correlation between CER and electrolyte pH. Janssen tested two different DSA® coatings compositions, one similar to that suggested by Erenburg and, another mechanism for pure ruthenium, at an electrolyte pH range between 0 and 3 [44]. The results did not show pH influence, and the mechanism Volmer-Heyrovsky-Tafel proved to be again consistent with Tafel slope determined [39, 44].

Augustynski *et al.* [45] presented the first study with ex-situ characterizations for standard DSA® catalysts, using the X-Ray Photoelectron Spectroscopic (XPS) analysis, in 1978. This type of analysis allowed determining the existing amount of each metal species on the surface of a material, in this case, the anode coating. It was detected the presence of RuO_3, which was responsible for the stability of RuO_2 on the electrodes, which is the active site of the chorine evolution. The proposed mechanism included an oxidation step, a chloride surface adsorption, and the respective reaction between two adsorbed species or between an adsorbed specie and a chloride ion. Later, it occurs the chorine desorption [39, 45].

$$2Cl^- + [RuO_3] + 2H_3O^+ \rightarrow [RuO_2] + Cl_2 + 3H_2O \quad (2.21)$$

$$[RuO_2] + 3H_2O \rightarrow [RuO_3] + 2H_3O^+ + 2e^- \quad (2.22)$$

$$Cl^- + [RuO_3] \rightarrow [RuO_2]ClO_{ads}^- \quad (2.23)$$

$$[RuO_2]ClO_{ads}^- + [RuO_2]Cl_{ads}^- + 2H_3O^+ \rightarrow Cl_2 + 3H_2O + 2[RuO_2] \quad (2.24)$$

or,
$$[RuO_2]ClO_{ads}^- + Cl^- + 2H_3O^+ \rightarrow Cl_2 + 3H_2O + [RuO_2] \quad (2.25)$$

In 1984, Erenburg [46] suggested a correction to the effect of concentration of H^+ in CER mechanism proposed in 1975. This effect does not necessarily account for water formation but, it may be due to the equilibrium of acid-base processes on oxide electrodes.

$$[S]OH_2^+ \rightleftharpoons [S]OH + H^+ \quad (2.26)$$

$$[S]OH \rightleftharpoons [S]O + H^+ + e^- \quad (2.27)$$

$$[S]O + Cl^- \rightarrow [S]OCl_{ads} + e^- \quad (2.28)$$

$$[S]OCl_{ads} + Cl^- + H^+ \rightarrow [S]OH + Cl_2 \quad (2.29)$$

or, $$[S]OCl_{ads} + Cl^- \rightleftharpoons [S]O + Cl_2 + e^- \quad (2.30)$$

In the early 2000s, Fernandez *et al.* [47-49] published a series of three articles that discuss CER using a new methodology for the kinetic treatment of electrochemical reactions, based on the polarization resistance analysis. The anode was a titanium electrode coated with RuO_2 and it was confirmed that pH indirectly influences chlorine's formation, more specifically its inhibition at high concentrations of H^+. The experimental data stayed consistent with Volmer-Heyrovsky-Tafel reactions mentioned above [50]. The proposed model confirms the existence of a first independent CER step, which relates to the electrode of the acid-base equilibrium processes that showed a pH effect. It is followed by the electrochemical oxidation of the active sites, where chloride ions will be adsorbed. Finally, chlorine can be generated by two different ways: recombining two intermediate chlorides or reaction between adsorbed species and chloride ion in solution.

$$[S]^z + H^+ \rightleftharpoons [S]^{z+1} \quad (2.31)$$

$$[S]^z \rightleftharpoons [S]^{z+1} + e^- \quad (2.32)$$

$$[S]^{z+1} + Cl^- \rightleftharpoons [S]^{z+1}Cl_{ads} + e^- \quad (2.33)$$

$$[S]^{z+1}Cl_{ads} + Cl^- \rightleftharpoons Cl_2 + [S]^z \quad (2.34)$$

or, $$2[S]^{z+1}Cl_{ads} \rightleftharpoons Cl_2 + 2[S]^z \quad (2.35)$$

2.2.4 The selectivity of the chlorine evolution reaction

The chlorine production rate depends on the ratio between chlorine evolution, CER, and oxygen evolution, OER. The most used parameter to measure this balance is designated by the selectivity of the CER and its value is higher than 95 % for DSA® [6]. There are several factors that affect the selectivity of the chlorine evolution over DSA®: the process operating conditions (concentration of the solutions, temperature, current density or electrolyte pH), the effects of the presence of contaminants in the electrolyte (such as organics and impurities of the coating decomposition), and the effect of the structure and composition of the anode.

The oxygen production reduces the purity of the chlorine gas stream and, in addition, it also increases the energy required for the electrolysis of the brine. The oxygen evolution is a consequence of different undesirable electrochemical reactions that occurs in the anodic electrolyte [6]. In addition to contaminating the gas obtained, these reagents occupy some active sites on the coating surface, which are necessary for the chlorine evolution reaction, further affecting the selectivity of the chlorine.

The principal parasitic anodic reactions are represented in Table 2.3 with the respective equilibrium potential, which is compared with the value for the chlorine evolution. The reactions that contribute the most to reduce the chlorine selectivity are the water oxidation and the bulk hypochlorite decomposition because the equilibrium potential being very similar with the value for CER, as expressed in Table 2.3.

Table 2.3 Principals anodic reactions in the chlor-alkali membrane process (source: [6]).

Reactions	**Half-reactions**	E^0/ **V *vs.* SHE**	
Hydroxide oxidation	$4OH^- \rightarrow O_2 + 2H_2O + 4e^-$	0.40	(2.36)
Anodic chlorate evolution	$6ClO^- + 3H_2O \rightarrow 2ClO_3^- + 4Cl^- + 6H^+ + \frac{3}{2}O_2 + 6e^-$	1.14	(2.37)
Water oxidation	$O_2 + 4H^+ + 4e^- \rightarrow 2H_2O$	1.23	(2.38)
Chlorine evolution	$Cl_2 + 2e^- \rightarrow 2Cl^-$	1.36	(2.39)
Bulk hypochlorite decomposition	$2HCl + O_2 \rightarrow 2HClO$	1.48	(2.40)

Effect of the process operating conditions

For industrial chlor-alkali manufacturers, the effects of operating conditions are probably the most relevant because the parameters can be measured directly.

As mentioned before, the holders of anode manufacturing technologies electrodes suggest an electrolyte pH between 2 and 3 as the optimum range. The aim is to prevent some of the parasitic reactions, which are specially favoured for pH greater than 6. Because of the use preferably an acidic electrolyte, the chlorine selectivity is maximized, and the good conditions of the coating are preventing. Nevertheless, it should be taken into consideration that the membranes ability to handle this electrolyte acidic pH range. As it was previously referred, the oxygen formation mainly occurs according to two routes: direct water oxidation and bulk hypochlorite decomposition. The acidification of the electrolyte can be used to prevent oxygen formation because the chlorine evolution is preferable to water oxidation and the hypochlorite formation depends on the water and chlorine equilibrium, which is unfavourable for a pH < 6 [6, 51-53]. However, the optimization of these operating conditions is probably not enough for nullifying the oxygen presence in output gas current.

When representing the current *versus* the potential of the cell during the electrolysis of NaCl, the slope observed in the linear range can indicate if the chlorine selectivity is higher or not. This parameter is designated by Tafel slope. For the electrolysis of NaCl under a modern DSA® in an acidic electrolyte, if the value of the Tafel slope is about 40 mV, the chlorine evolution is preferable, whereas if the Tafel slope is about 60 mV, the dominating mechanism probably is the oxygen formation. As only the OER is directly affected by the pH of the electrolyte, for a basic solution the Tafel slope expected is 40 mV for the CER and 120 mV for the OER [54]. However, it is important to refer that this parameter also depends on the operating temperature. In terms of the current density, the values represent the flow of electrons transported between the electrodes. It is necessary for a high-value current density to increase the kinetics of the CER. Based on the previous information, the Tafel slope coefficient is repeatedly used for electrochemical characterization of the industrial processes as it allows to quantify and to distinguish the energy required for each reaction. As the current density increases, the overvoltage increases but the kinetics barrier to CER is lower so the CER kinetics is faster than the OER. The OER overvoltage will increase for more quickly [6, 51-53].

In terms of brine concentration, it is known that high chloride concentrations favour the chlorine evolution kinetics. Besides the oxidation reaction of the chloride anions to chlorine is a first-order reaction concerning the chloride concentration, [Cl^-], the production of chlorine is maximized when the brine concentration is enlarged [6, 12]. The higher the concentration of NaCl on the anode surface and the lower that of competing species, the higher the competitive adsorption of the same species on the metal active sites available by chloride anions. An increase in the concentration of by-products or other impurities can disrupt this balance if these species are able to adsorb in the same type of the active sites on the anode surface, namely when it bonds with a metal oxide as RuO_2, causing the chlorine activity to be reduced.

The temperature is also an important operating parameter for the efficiency of the current of the chlorine evolution because it directly affects the equilibrium potential of the CER but also the activity of the chloride ions. Nowadays, the technologies of the electrolysis of NaCl recommend a temperature range between 353 K and 363 K. The high temperatures allow to increase the conductivity of the electrolyte; however, it is necessary to prevent the water vaporization which occurs around 373 K. Nevertheless, it is not known assertive conclusions about the effect of the temperature on the selectivity between CER or OER. The temperature increase has the same type of effect for the oxygen evolution reaction and for the chlorine evolution reaction, so it is complex to determinate the optimal temperature to prevent the parasitic reaction-based only in this parameter [6, 53, 55].

Effect of the electrolyte contamination

The electrolyte contaminants besides having a negative effect on membrane performance, it also contributes to reducing the selectivity of chlorine formation at the anode. This is one of the reasons for the increasing number and relevance of the studies about the effects of the brine composition in the electrolysis performance under operating conditions like the industrial practices. The most important effect mentioned in the competitive adsorption between the chloride ions and the impurities of the brine on the active sites of the coating surface, as previously referred [6].

The phosphates, nitrates and sulphates ions (related with the membrane degradation) promote the parasitic oxygen formation due to the decomposition of hypochlorite [53, 56]. However, this is an effect that can be controlled if the electrolyte pH is kept lower. The presence of other metal species on electrolyte, such as Co, Cu, Ni, and Ir, should also be taken into account because its metals catalyse the hydroxide decomposition reaction, forming some oxygen gas and, consequently, contribute for the decrease in the selectivity of the chlorine evolution reaction [57].

Effect of the anode material

The effects of structure and composition of the electrode can be divided into effects due to changes in active surface area of the electrode, related to the number of active sites exposed; and effects related to the of the catalytic activity, expressed by the Tafel slope [13, 58].

An increase in the active surface area may be achieved by higher metal dispersion, doping with metal oxides, or reducing the particle size. The holders of DSA® technology reduced the amount of RuO_2 from the formulation "Beer 1" and "Beer 2" but the metallic dispersion and thermal deposition techniques have suffered great technological advances, enhancing the distribution and particle size to ensure a high surface area. [59, 60]. The higher active surface area corresponds to a smaller local current density and a greater selectivity for oxygen because the reaction involves fewer electron exchanges. The effect of this modification is similar to that discussed above for the current density but with local consequences [60].

The doping with metal oxides results in an increased exposed surface area, which modify the catalytic activity of the electrode. Burrows *et al.* [61] found a variation of the anode overpotential equal to 5 mV between two electrodes compositions, one having a mass fraction of 80 mol % of RuO_2 and another coating with 20 mol % of RuO_2 on the surface. This result is different from the 20 mV obtained directly by kinetic Tafel slope, suggested in 2015 by Karlsson [62]. During the last decade, a deeper understanding between the electronic effects and selectivity of chlorine was obtained from studies using the density functional theory. The objective is to decouple the effects of modification of the active surface area and the real electrocatalytic activity [62].

2.2.5 Mechanisms of the anode deactivation

The development of membrane cell technology has contributed to the performance improvement of the chlor-alkali process. However, there are some subjects that still require further studies given its importance for minimizing the operating costs of the process [3]:

- ✓ Membrane damage tears, pinholes, blisters, and brine impurity precipitation.
- ✓ Electrode deactivation mechanisms related to the decrease of the anode performance or its failure in critical situations.

The coating deactivation intensifies the activation overpotential, η, and it can be a consequence of four important chemical and physical phenomena [34]:

I. A loss of active surface sites by blockage owing to insoluble surface layers (e.g., MnO_2, $BaSO_4$, Fe oxides, etc.) or impurities in the solution.

II. A selective electrochemical dissolution on the surface related to the depletion of RuO_2 (via the loss of Ru-based adsorbed intermediates, which are crucial to the chlorine and oxygen evolution reactions).

III. Erosion of the electroactive species on the coating, instigated by the gas bubble accumulation in the electrode surface, the movement of fluids in the compartments and the abrasion between elements or auxiliary parts of the electrolyser, such as the gaskets.

IV. The formation of an insulating TiO_2 layer between the Ti-substrate and the coating interface.

The corrosion of the coating in the electrode surface increases during the service time of the electrode. Figure 2.7 represents the different mechanisms of the deactivation of the anode, with a DSA® based configuration.

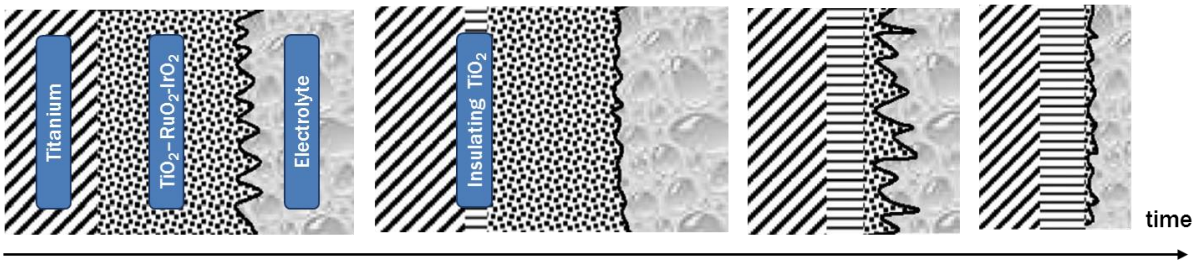

Figure 2.7 Corrosion of the compact part of the oxide layer in a typical DSA® anode used for the chlorine production (adapted from [63, 64]).

The industrial electrochemical dissolution of RuO_2 during the NaCl electrolysis is a recognized mechanism. The erosion and loss of Ru-based intermediates can be involved in the chlorine and oxygen evolution reaction, depending on the operating conditions. The RuO_2 dissolution rate increases due to:

- ✓ An increase in the current density [65];
- ✓ An increase of the OER [66];
- ✓ A decrease of the brine concentration [67];
- ✓ An increase in the number of shutdown operations of the electrolysis cells.

The Pourbaix diagram represents the dependence of the electrochemical reaction as a function of the pH of a solution and potential applied. Figure 2.8 shows this diagram for the Ru-H_2O-Cl^- system at 298 K for a solution with of 264 g·dm^{-3} NaCl [68].

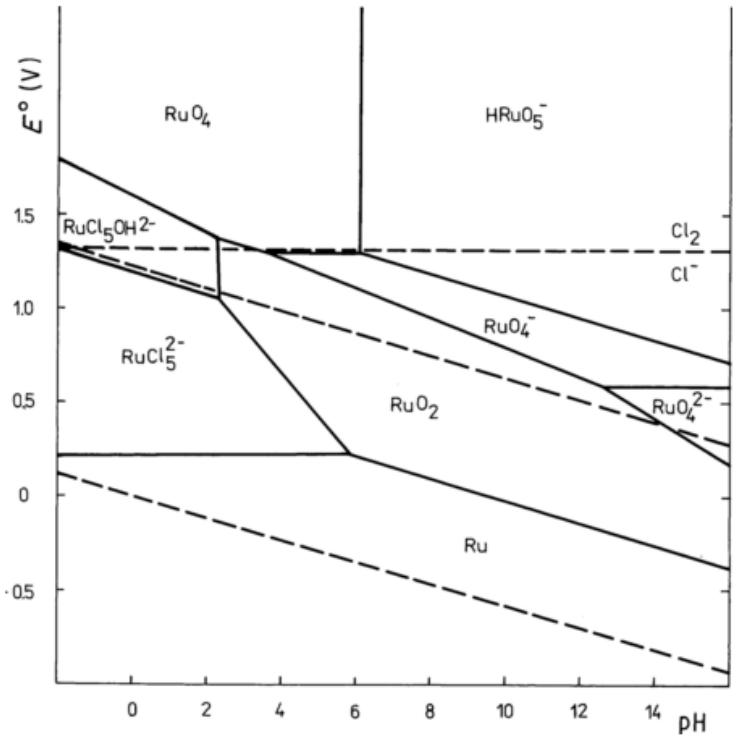

Figure 2.8 Pourbaix diagram for the Ru-H_2O-Cl^- system at 298 K in a solution of 264 g·dm^{-3} NaCl (source: [68]).

The associated reactions of Figure 2.8 are represented by Equations (2.41) to (2.42). RuO_2 corrosion rate is minimal at a pH 2, wherein, $RuOHCl_5^{2-}$ is formed in lower pH (Equation 2.42) and, at pH above 4, RuO_2 losses can occurs by direct oxidation, where RuO_4^- is formed (Equation 2.43) [34].

$$RuO_2 + 2Cl^- + 2H^+ \rightarrow RuOHCl_5^{2-} + H_2O \quad (2.41)$$

$$RuO_2 + 2H_2O \rightarrow RuO_4 + 4H^+ + 4e^- \quad (2.42)$$

$$RuO_2 + H_2O \rightarrow RuO_2.OH + H^+ + e^- \quad (2.43)$$

$$RuO_2.OH \rightarrow RuO_3 + H^+ + e^- \quad (2.44)$$

$$RuO_3 \rightarrow RuO_2 + \frac{1}{2}O_2 \quad (2.45)$$

The depletion of the Ru from the coating can also arise during the oxygen generation due to the oxidation of the absorbed intermediates (RuO_2·OH and RuO_3) [34]. Although, the chlor-alkali manufacturers take some preventive actions to minimize the loss of the ruthenium species in the coating surface, if the mass fraction of ruthenium in the surface is less than a mass fraction of 20 %, it is recommended to stop the use of the anode. An *ex-situ* analysis procedure was then developed for the anode characterization, which can allow quantifying the metal oxides in the coating periodically, indicating what is its composition for a specific service time of the anode.

Accelerated ageing tests

The service time of the DSA® type electrode is, approximately, eight years for regular electrolysis of NaCl operation. In this way, the mechanistic studies of the anode degradation are not developed in industrial conditions because the test time will be not reasonable for reproducing. Instead, it is usual to perform accelerated ageing tests of the electrodes to represent a shorter period and the loss of catalytic activity on the electrode surface. These studies are only applied to small fragments of an electrode because it involves the destruction of the material.

The first electrochemical characterization studies of the industrial electrodes were performed *in-situ* using radiochemical techniques and it was executed almost exclusively by Soviet Union scientists between 1960-1990 [6]. In 2004, Gajic-Krstajic *et.al.* [69] employed another technique, the spectrophotometric method, which allowed similarly sensitive detection of ruthenium. The spectrophotometric method allowed avoiding handling of

radioactive materials and gives an understanding of the degradation process for different service times, being a quick test that can be also executed online. Nowadays, others sophisticated, and precise methods are developed to follow the degradation of DSA® electrodes, such as the inductively coupled plasma mass spectrometry (ICP-MS) and the electrochemical quartz crystal microbalance (EQCM) techniques.

To study the ageing mechanism of the anode in an acceptable period, the electrodes are exposed to operating conditions that force the loss of activity of the active site in the electrode surface. The most used technique implicates that the anodes are in contact with a sulphuric acid solution, which promotes the oxygen evolution reaction and the respective degradation of the coating surface and, in this case, it is the only kinetics happening [70]. In this way, it is possible to determine a relationship between the increase in the reaction of the evolution of oxygen and the deactivation of the coating as a function of the service time passed. in these studies, it can only be assessed the relationship between OER and the electrode degradation. However, what occurs in the industrial process can be different. The CER kinetics and other mechanisms that involves Cl^- intermediates can also affect to the degradation of the element [71].

The ageing test of the ruthenium-based electrode started with a sulphuric acid electrolyte and soft operating conditions, such as a diluted solution and room temperature, to study its effects on the deactivation of the ruthenium active sites in the electrode surface. The processes occurring at the electrode will not be the same as those which occur during regular operation of the electrodes in sodium chloride solutions, as shown the work of by Hoseinieh *et al* [28]. In the ageing test of a ruthenium-based electrode with a solution of 1 M H_2SO_4, it was observed quick passivation of the electrode that resulted in the dissolution of the metal oxides deposited on the electrode surface. However, in an ageing test of a ruthenium-based electrode, with a solution of 0.50 M NaCl, it was also observed another deactivation mechanism, namely the formation of an insulating layer of TiO_2 on the coating-substrate interface that minimized the electric conductivity of the material. Nevertheless, in both cases, the abrasion of the surface electrode was minimized independent of the operating conditions applied but, in the industrial process, these physical degradations are relevant.

As the purpose of the accelerated ageing tests is observing the comportment of an isolated component of the electrolysis membrane cells, it is common to use a three electrodes configuration, excluding the effect of the membrane and the industrial cathodes.

Figure 2.9, shows an example of the ageing test of DSA® using a brine solution performed by Silva *et al.* (adapted from [72]), where a three electrodes configuration was adopted. The testing electrode is the DSA®, the counter electrode is a mesh of platinum, Pt, and the reference electrode is composed by Ag | AgCl, KCl (3 M) [72].

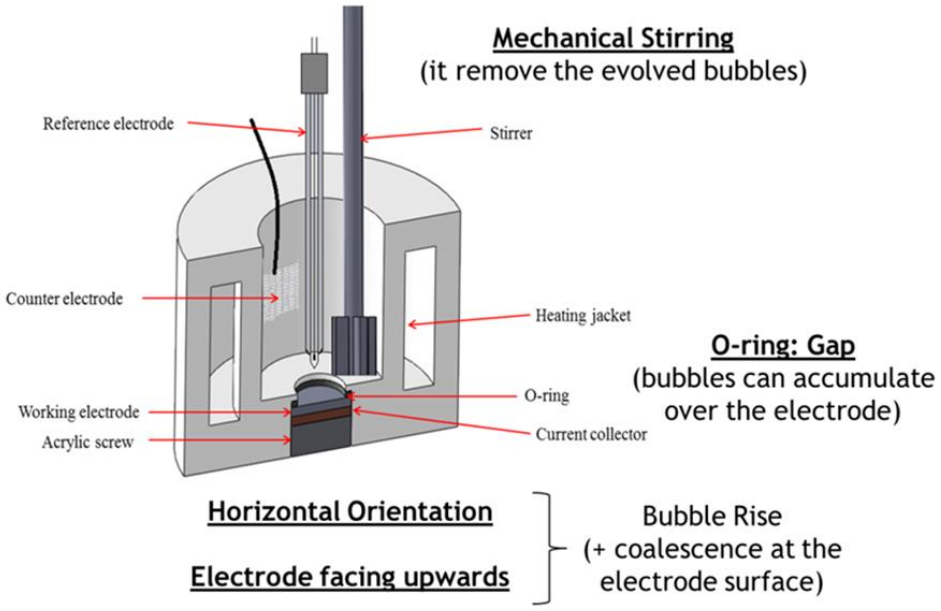

Figure 2.9 Schematic cross-section of the test cell (adapted from [72]).

This cell allowed to minimize some of the side effects of the electrolysis process, such as the gas bubbles accumulation along the electrode surface and it is rising out of the cell. The mechanical stirring was included to quickly remove the gas bubbles of active site where it was formed, minimizing the mass concentration limitations. It was referred that the horizontal electrode configuration was selected to increase the coalescence of gas bubbles on the electrode surface. The O-ring was used to create a gap between electrode and electrolyte compartment, which also reduce the bubbles gas accumulation. As for the working electrode placement at the bottom of the cell, the aim was to facility the removed the electrode for a continuous *ex-situ* characterization, which complement the electrochemical characterization performed during the accelerated deactivation test.

For an electrochemical characterization of the cell, its potential was collected as a function of time when the cell was operating in a potentiostatic mode, or the current density was collected as a function of time when a test cell is operated in a galvanostatic mode [35]. At different times, the experiment cycle was stopped to apply some electrochemical

techniques (e.g., using electrochemical impedance spectroscopy, cyclic voltammetry and polarization curves techniques) and, for an *ex-situ* characterization of the electrode surface (e.g., using the X-ray photoelectron spectroscopy) [72].

Gas bubbles accumulation

The formation of gas bubbles on the surface of the electrode and its rise out of the cell can be beneficial to the electrochemical process since it increases the mass transfer of the diffusion-controlled species to the electrode surface, due to the rising gas bubbles form on the electrolyte layer close to the electrode. This is helpful up to a point as it also promotes the mixture of the electrolyte. However, when the gas bubbles coalescence or the respective get free from the electrode or membrane surface is not correct, the gas bubble accumulation can contribute to the degradation of the electrodes [60, 73]. During the gas bubble coalescence, the electrode surface forces the current to circulate through smaller areas of the electrode, increasing the current density increases and the overpotential of the reaction, which can damage the electrode surface; and, the circuit of the electrolyte between the compartment are blocked by bubbles, damaging the membrane surface.

Figure 2.10 demonstrates the gas bubbles accumulation on the electrolyser for a commercial electrolyser by Uhde [15].

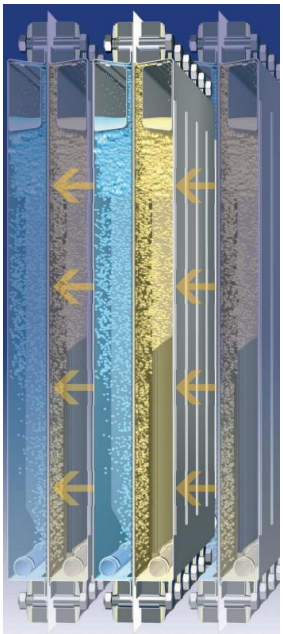

Figure 2.10 Structure of a membrane electrolyser with zero-gap over the full membrane area with gas bubbles accumulation (source: [15]).

The evolution of the gas bubbles increases the ohmic resistance in the electrolytic cell, which motivated several the studies about the bubble effects on the energy consumption of the chlor-alkali process. From them it was concluded that, if the kinetic of the reaction is convection-limited due to concentration gradients or temperature gradients, the gas dissolved will be transported for the bulk solution by mass diffusion and convection. If the kinetics of the reaction is diffusion-limited and the solubility of the gas dissolved in the electrolyte is low, the nucleation of gas bubbles occurs at the electrode surface. After a long period, there is a saturation of the electrolyte and the concentration of the products become constant, making the kinetics being more susceptible to the efficiency of the diffusion of the electrolyte species to the electrode surface and the products between the electrode surface and the electrolyte [73].

The increase of separation rate and coalescence of rising bubbles formed can be achieved, by maximizing the homogenization of the solution [73]. The gas bubble accumulation increases with the increase of the current density applied and with the increase of the gas pressure. On the other hand, the gas bubbles accumulation decreases with the increase of the flow rate of the feed and the temperature of the electrolyte. There are more factors that influence the density of gas bubbles in the solution, such as the nature of the gas formed; the electrolyte composition; the electrode surface texture and geometry; and the position of the electrode on the cell, although the latter is more relevant for experimental studies [73].

In conclusion, the presence of gas bubbles dispersed in the electrolyte can have a strong effect on the ionic conductivity of the electrolyte solutions and it can cause coating damage. Moreover, gas bubbles can plug the electrode surface, reducing the active area of the electrodes and affect the current and concentration distribution in the bulk solution. The conjugation of these effects can affect the ohmic resistance of the electrolyte and, consequently, affects the energy required.

2.2.6 Recoating of the deactivated electrodes

In the membrane cell technology, the anode reactivation occurs every 8 to 10 years of service, preventing the rapid growth of the activation overpotential that affects the rate of the chlorine production and it can even force a stop of the chlorine production. This is a standard schedule for preventive maintenance for this type of electrodes.

Over the time of anode operation, there are Ru losses at the coating layer. It is known that when the concentration RuO_2 in the DSA® is less than 20 mol % or the ruthenium loading is less than 2 $g \cdot m^{-2}$, the overpotential of the anode increases considerably, which is represented in Figure 2.11 [34].

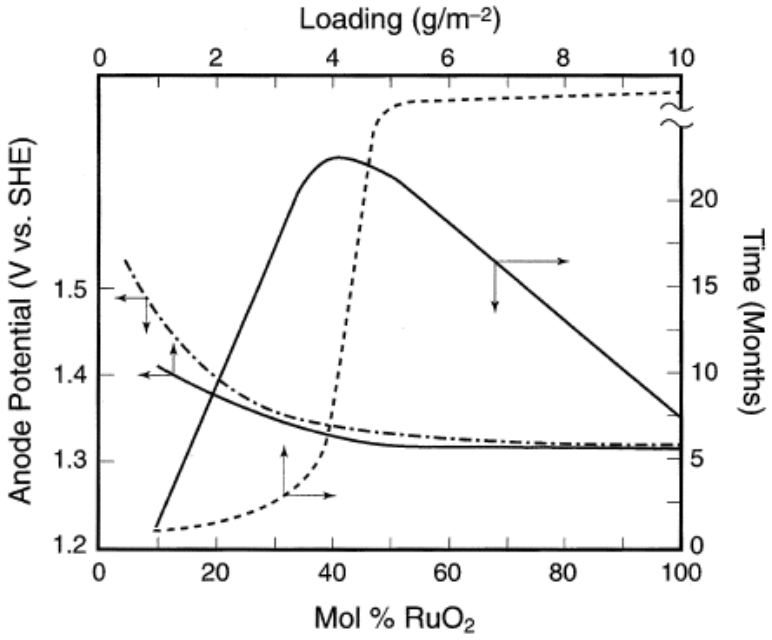

Figure 2.11 Anode potential at 3.0 $kA \cdot m^{-2}$ and the operating life with mol % RuO_2 and percentage loading for a 40 mol %, determined in 300 $g \cdot dm^{-3}$ at pH 2.0 - 2.5 and 353 K (source: [34]).

An example of the metal coating profile, after 1000 days in operation, is shown in Figure 2.12. The concentrations are expressed as a function of the depth of the coating, where the surface corresponds to the interception with y-axis and the interface coating-substrate is the opposite depth value.

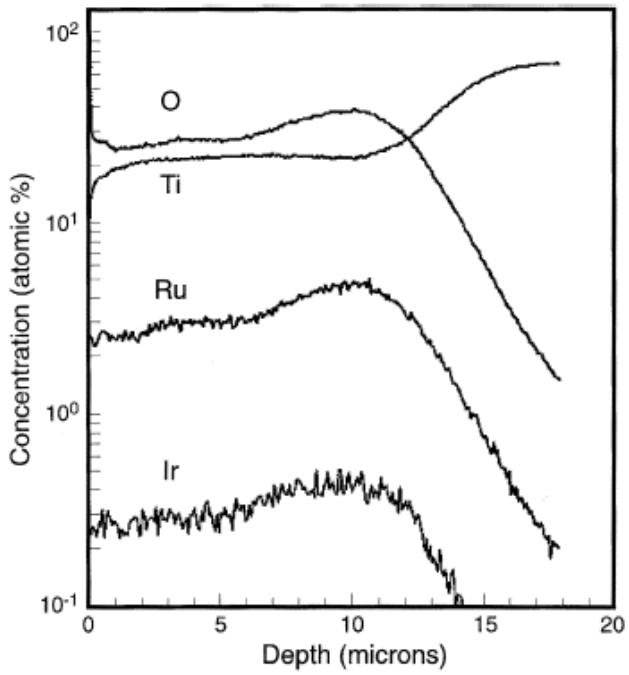

Figure 2.12 DSA® composition after 1000 days of operation (source: [34])

The anode then should be replaced or recoated, with the objective of restoring its electrocatalytic activity. This maintenance step is called recoating of the anode. The reactivation process consists of the removal of deactivated coating of the electrode and a recoating step of the DSA®, which allows resetting the metal oxide active sites on the surface. In accelerated ageing tests in sulphuric acid solutions, it was proved that the deposition of platinum had a service time that was equivalent of a new DSA® anode coating, as shown in Figure 2.13 [34].

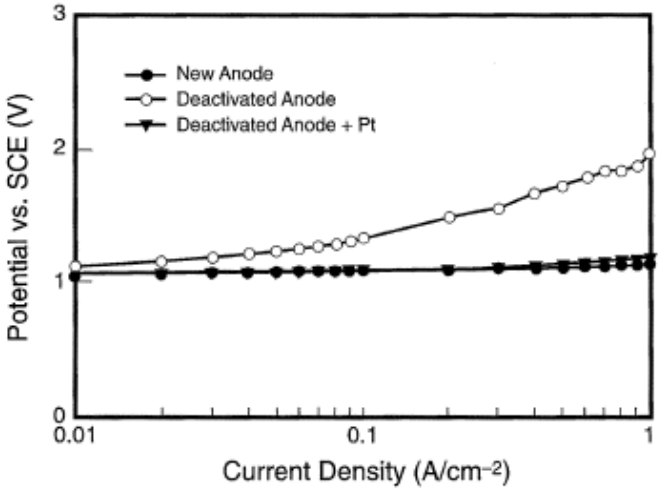

Figure 2.13 Effect of Pt-doping on the anode potential (source: [34]).

Platinum has good catalytic activity and ionic conductivity that favour the chlorine production but, its higher cost makes it inviable for the initial coating of the anode. At the instant, the anode reaches deactivation, the Ru residual load is still significant because the loss of active sites by dissolution and erosion occurs mainly in the outer part of the surface of the coating layer. So, in the recoating step, the metal quantity required per meter of an electrode is considerably less. Combining the previous factors it is considered, although platinum is expensive it should be considered as a good alternative for the recoating [34].

A good practice to following in the electrodes maintaining is, then, to replacement the anode, after two recoating of the electrode mesh [34]. If the main cause of deactivation of the electrode is an increase of the TiO_2 insulating layer thickness or the Ti-support degradation, the recoating step are not efficient. In the case, the mesh replacement is the only options because the depositing of noble metals on the surface allows the compensation of the number of active sites lost due to coating dissolution or erosion but, it does not solve the problem.

Related to the cathode reactivation, for a bipolar electrode the schedule it is the same as the anode, in this case, 8 to 10 years of service. For the cathode, it is also common to use an online recoating technique, especially when there is a significant loss of nickel on the surface in a short period of time. A platinum solution, or more recently a voltage reduction solution (VRS), is fed to the cathode compartment of the electrolysis. The metal species introduced have an affinity for the cathode surface where they end up depositing, increasing the number of active sites available for the hydrogen evolution reaction. This technique is not yet a recurring practice for the reactivation process of the anode.

2.3 NOTATION

	Description	Units
A	Cross-sectional area of the current flow	m^2
b	Tafel slope	V
CER	Chlorine evolution reaction	-
DSA	Dimensionally stable anode	-
E	Cell potential	V
E^0	Equilibrium cell potential	V
$E_{0,c}$	Redox potential of the cathodic reaction for the operating conditions	V
$E_{0,a}$	Redox potential of the anodic reaction for the operating conditions	V
F	Faraday constant	$C \cdot mol^{-1}$
ΔG	Gibbs free energy	J
HER	Hydrogen evolution reaction	-
j	Current density	$A \cdot m^{-2}$
j_0	Exchange current density	$A \cdot m^{-2}$
l	Length of the conductor	m
MDI	Diphenyl methylene diisocyanate	-
N	Number of electrons involved in the electrode reaction	-
OER	Oxygen evolution reaction	-
PVC	Polyvinyl chloride	-
R	Universal gas constant	$J \cdot K^{-1} \cdot mol^{-1}$
R_c	Conductor resistance	Ω
[S]	Active site	-
T	Absolute temperature	K
α	Charge transfer coefficient	-
σ	Conductor conductivity	$S \cdot m^{-1}$
ε	Gas void fraction	-
η	Activation overpotential	V
ρ	Resistivity of the electrolyte	$\Omega \cdot m^{-1}$
ρ_0	Resistivity of the pure eletrolyte	$\Omega\ m^{-1}$
z	Charge number	-

2.4 REFERENCES

1. EuroChlor, *The membrane cell process*. (Available from: http://www.eurochlor.org/media/7812/membrane_300dpi2.pdf, accessed 18/4/2016).

2. O'Brien, T., Bommaraju, T., Hine, F., *Handbook oh chlor-alkali technology*, ed. Springer. 2005, New York.

3. Dias, A. C., *Chlor-alkali membrane cell process: study and characterization*, in *Chemical Engineering Department*. 2010, University of Porto.

4. Schmittinger, P., Florkiewicz, T., Curlin, L., Luke, B., Scannell, R., Navir, T., Zelfer, E., Bartsch, R., *Ullmann's encyclopedia of industrial chemistry*. 2012, Weinheim.

5. EuroChlor, *Questions and Answers on the Chlor-Alkali Sector and the EU Emission Trading System (ETS).* 2010.

6. Karlsson, R., Cornell, A., *Selectivity between oxygen and chlorine evolution in the chlor-alkali and chlorate processes.* Chem Reviews, 2016. 116(5): p. 2982-3028.

7. Shimoaka, T., Wakai, C., Sakabe, T., Yamazaki, S., Hasegawa, T., *Hydration structure of strongly bound water on the sulfonic acid group in a Nafion membrane studied by infrared spectroscopy and quantum chemical calculation.* Physical Chemistry Chemical Physics, 2015. 17: p. 8843--8849.

8. Jalalia, A. A., Mohammadib, F., Ashrafizadehc, S. N., *Effects of process conditions on cell voltage, current efficiency and voltage balance of a chlor-alkali membrane cell.* Desalination, 2009. 237: p. 126–139.

9. Mauritz, K. A., Moore, R. B., *State of understanding of Nafion.* Chemical Reviews, 2004.

10. Kiros, Y., Bursell, M., *Low energy consumption in chlor-alkali cells using oxygen reduction electrodes* International Journal of Electrochemical Science, 2008. 3: p.444- 451.

11. Rausch, S., Wend, H., *Morphology and utilization of smooth hydrogen-evolving Raney-Nickel cathode coatings and porous sintered-nickel cathodes.* Journal of Electrochemical Society, 1996. 143: p. 2852-2862.

12. Kuhn, A. T., Mortimer, C. J., *The kinetics of chlorine evolution and reduction on titanium-supported metal oxides especially RuO2 and IrO2.* Journal of The Electrochemical Society, 1973. 120(2): p. 231.

13. Trasatti, S., *Electrocatalysis: understanding the success of DSA®.* Electrochimica Acta, 2000. 45: p. 2377-2385.

14. Trasatti, S., *Electrolysis in the evolution of oxygen and chlorine.* Electrochimica Acta, 1984. 29: p. 1503-1512.

15. ThyssenKrupp *Uhde chlorine engineers*. (Available from: www.uhdenora.com/chlor_alkali.asp, accessed 08/01/2018)

16. Duby, P., *The-history of progress in dimensionally stable anodes.* 1993.

17. Beer, H. B., *The invention and industrial development of metal anodes.* Journal of The Electrochemical Society, 1980. 127: p. 303-307.

18. DeNora, *DSA® anodes for chlorine evolution*. (Available from: http://www.denora.com/markets-products/electrodes/anodes/chlorine-evolution.html, accessed 08/11/2019).

19. Over, H., *Surface chemistry of ruthenium dioxide in heterogeneous catalysis and electrocatalysis: from fundamental to applied research.* Chemical Review, 2012. 112(6): p. 3356-426.

20. Ayres, G. H., Booth, M. H., *Catalytic decomposition of hypochlorite solution by iridium compounds: II kinetic studies.* 1955.

21. Hayfield, P. C., *Development of the noble metal/oxide coated titanium electrode, PART III: coated titanium anodes in widely ranging oxygen evolving situations.* Platinium Metals Rev., 1998. 42: p. 116-122.

22. Beer, H. B., *Improvements in or relating to electrodes for electrolysis.* 1969. GB 1,147,442.

23. Trasatti, S., *Ruthenium dioxide: a new interesting electrode material. solid state structure and electrochemical behaviour.* . Electroanalytical Chemistry and Interfacial Electrochemistry, 1971. 29.

24. Beer, H. B., *Improvements in or relating to the manufacture of electrodes.* 1970. GB 1,195,871.

25. Beer, H. B., *Electrode and coating therefor.* 1972. US 3,632,498.

26. Beer, H. B., *Method of chemically plating base layers with precious metals of the platinum group.* 1966. US 3,265,526.

27. Takasu, Y., Nishiki, Y., Sugimoto, W., Nakamatsu, S. , *Structural analyses of RuO2–TiO2/Ti and IrO2–RuO2–TiO2/Ti anodes used in industrial chlor-alkali membrane processes.* Journal of Applied Electrochemistry, 2010. 40: p. 1789-1795.

28. Hoseinieh, S., Ashrafizadeh, F., Maddahia, M., *A comparative investigation of the corrosion behavior of RuO2–IrO2–TiO2 coated titanium anodes in chloride solutions.* Journal of The Electrochemical Society, 2010. 157.

29. Kuznetsova, E., Petrykin, V., Sunde, S., Krtil, P., *Selectivity of nanocrystalline IrO2-based catalysts in parallel chlorine and oxygen evolution.* Electrocatalysis, 2014. 6(2): p. 198-210.

30. Wang, S., Xu, H., Yao, P., Chen, X. , *Ti/RuO2-IrO2-SnO2-Sb2O5 anodes for Cl2 evolution from seawater.* Electrochemistry, 2012. 80(7): p. 507-511.

31. Chen, S., Zheng, Y., Wang, S., Chen, X., *Ti/RuO2–Sb2O5–SnO2 electrodes for chlorine evolution from seawater.* Chemical Engineering Journal, 2011. 172(1): p. 47-51.

32. Comninellis, C., Vercesi, G. P., *Problems in DSA | coating deposition by thermal decomposition.* Journal of Applied Electrochemistry, 1992. 21: p. 136-142.

33. Yousefpour, M., Shokuhy, A., *Electrodeposition of TiO2–RuO2–IrO2 coating on titanium substrate.* Superlattices and Microstructures, 2012.

34. Bommaraju, T., Chen, C., Birss, V., *Deactivation of thermally formed RuO2 + TiO2 coatings during chlorine evolution: mechanisms and reactivation measures*, in *Modern chlor-alkali technology*. 2000, International Chlorine Symposium - Blackwell Science: UK.

35. Brett, C., Brett, A., *Electrochemistry: principles, methods and applications*. 2005: Oxford University Press.

36. Noren, D. A., Hoffman, M. A., *Clarifying the Butler–Volmer equation and related approximations for calculating activation losses in solid oxide fuel cell models.* Journal of Power Sources, 2005.

37. O'Hayre, R., Cha, S., Colella, W., Prinz, F., *Fuel cell fundamentals*. 2006, New York: Wiley.

38. Faita, G., Fiori, G., *Anodic discharge of chloride ions on oxide electrodes.* Journal of Applied Electrochemistry, 1972. 2: p. 31-35.

39. Trasatti, S., *Progress in the understanding of the mechanism of chlorine evolution at oxide electrodes.* Electrochimica Acta, 1987. 32: p. 369-382.

40. Erenburg, R. G., Krishtalik, L. I., Bystrov, V. I. , *Mechanism evolution and ionization of chlorine on a ruthenium oxide electrode.* Russian Journal of Electrochemistry, 1972. 8.

41. Erenburg, R. G., Krishtalik, L. I., Yaroshevskaya, I. P. , *Mechanism of evolution and ionization of chlorine on a ruthenium oxide electrode.* Russian Journal of Electrochemistry, 1975. 11: p. 1068-1972.

42. Erenburg, R.G., Krishtalik, L. I., Yaroshevskaya, I. P. , *Kinetics of chlorine evolution and ionization at ruthenium oxide and ruthenium-titanium oxide electrodes.* Russian Journal of Electrochemistry, 1975. 11: p. 1072-1074.

43. Erenburg, R., Krishtalik, L., Yaroshevskaya, I., *Liberation and ionization of chlorine on ruthenium-titanium oxide electrodes at increased current densities.* Russian Journal of Electrochemistry, 1975. 11: p. 1236-1239.

44. Janssen, L., Starmans, L., Visser, J., Barendrecht, E., *Mechanism of the chlorine evolution on a ruthenium oxide/titanium oxid electrode and on a ruthenium electrode.* Electrochemical Acta, 1977. 22: p. 1093-1100.

45. Augustynski, J., Frankenthal, R., Kruger, J. , *Passivity of metals.* Electrochemical Society, 1978.

46. Erenburg, R. G., *Mechanism of the chlorine reaction of ruthenium-titanium oxide electrodes.* Russian Journal of Electrochemistry, 1984. 20: p. 1602-1607.

47. Fernandez, J., Gennero de Chialvo, M. Chialvo, A., *Kinetic study of the chlorine electrode reaction on Ti/RuO2 through the polarisation resistance Part I: experimental results and analysis of the pH effects.* Electrochimica Acta 4, 2002. 47: p. 1129–1136.

48. Fernandez, J., Gennero de Chialvo, M. Chialvo, A., *Kinetic study of the chlorine electrode reaction on Ti/RuO2 through the polarisation resistance Part II: mechanistic analysis.* Electrochimica Acta, 2002. 47: p. 1137–1144.

49. Fernandez, J., Gennero de Chialvo, M. Chialvo, A., *Kinetic study of the chlorine electrode reaction on Ti/RuO2 through the polarisation resistance Part III: proposal of a reaction mechanism.* Electrochimica Acta, 2002. 47: p. 1145–1152.

50. Kim, J., Kim, C., Kim, S., Yoon, J., *A review of chlorine evolution mechanism on dimensionally stable anode (DSA).* Korean Chemical Engineering Research, 2015. 53: p. 531-539.

51. Bergner, D., *Reduction of by-product formation in alkali chloride membrane electrolysis.* 1989.

52. Gorodetskii, V., Pecherskii, M., Yanke, M., Yanke, V., Buné, N., Busse-Machukas, V., Kubasov, V., Losev, V., *Effect of acidity on the electrochemical and corrosion behavior of titanium-ruthenium oxide anodes in chloride solutions.* Russian Journal of Electrochemistry, 1981. 17: p. 513-517.

53. Jaksic, M. M., *Mutual effect of current density, pH, temperature, and hydrodynamic factors on current efficiency in the chlorate cell erocess.* J. Electrochem. Soc., 1974. 121: p. 70-80.

54. Kosevic, M., Stopic, S., Bulan, A., Kintrup, J., Weber, R., Stevanović, J., Panic, V., Friedrich, B., *A continuous process for the ultrasonic spray pyrolysis synthesis of RuO2/TiO2 particles and their application as a coating of activated titanium anode.* Advanced Powder Technology, 2017. 28(1): p. 43-49.

55. Eberil, V., Fedotova, N., Novikov, E., Mazanko, A., *Studying the link between the potential of a metal-oxide anode, the current efficiency for chlorate, and the current losses for the oxygen and chlorine evolution in a wide range of the chlorate electrolysis conditions.* Russian Journal of Electrochemistry, 2000. 36: p. 1463-1470.

56. Buné, N., Portnova, M., Filatov, V., Losev, V., *Effects of foreign anions on the kinetics of chlorine and oxygen evolution on the ruthenium-titanium oxide anodes under the conditions of chlorine evolution.* Russian Journal of Electrochemistry, 1984. 20: p. 1291-1295.

57. Wanngard, J., *Cost saving in chlorine plants by benefiting from the unique properties of titanium: Chapter 23*, in *Modern chlor-alkali technology* E.A. Science, Editor. 1992.

58. Trasatti, S., Buzzanca, G., *Ruthenium dioxide: a new interesting electrode material, solid state structure and electrochemical behaviour.* . Electroanalytical Chemistry and Interfacial Electrochemistry, 1971. 29.

59. Arikawa, T., Murakami, Y., Takasu, Y., *Simultaneous determination of chlorine and oxygen evolving at RuO2/Ti and RuO2-TiO2/Ti anodes by differential electrochemical mass spectroscopy.* Journal of Applied Electrochemistry, 1998. 28: p. 511-518.

60. Vogt, H., Stephan, K., *Local microprocesses at gas-evolving electrodes and their influence on mass transfer.* Electrochimica Acta, 2015. 155: p. 348-356.

61. Burrows, I., Denton, D., Harrison, J., *Chlorine and oxygen evolution on various compositions of RuO2/TiO2 electrodes.* Russian Journal of Electrochemistry, 1978. 23: p. 493–500.

62. Karlsson, R., *Theoretical and experimental studies of electrode and electrolyte processes in industrial electrosynthesis*, in *KTH Royal Institute of Technology*. 2015, KTH Royal Institute of Technology: Stockholm.

63. Hoseinieh, S., Ashrafizadeh, F., Maddahia, M., *A comparative investigation of the corrosion behavior of RuO2–IrO2–TiO2 coated titanium anodes in chloride solutions.* Journal of The Electrochemical Society, 2010. 157: p. E50-E56.

64. Jovanovic, V. M., Dekanski, A., Despotov, P., Nikoli, B. Z., Atanasoski, R. T., *The roles of the ruthenium concentration profile stabilizing component and the substrate on the stability of the oxide coatings.* Journal of Electroanalytical Chemistry, 1992. 339: p. 147-165.

65. Iwakura, C., Hirao, K., Tamur, H., *Anodic evolution of oxygen on ruthenium in acid solutions.* Electrochimica Acta, 1977.

66. Loucka, T., *The reason for the loss of activity of titanium anodes coated with a layer of RuO2 and TiO2.* Journal of Applied Electrochemistry, 1977. 7: p. 211-214.

67. Novikov, E. A., Eberil, V. I., Mazanko, A. F., *Corrosion and electrochemical behavior of metal-oxide anodes during electrolysis with an ion-exchange membrane.* Russian Journal of Electrochemistry, 2000. 36: p. 861-865.

68. Loucka, T., *The potential-pH diagram for the Ru-H2O-Cl- system at 25 ºC.* Journal of Applied Electrochemistry, 1990. 20: p. 522-523.

69. Gajic-Krstajic, L., Trisovic, T., Krstajic, N., *Spectrophotometric study of the anodic corrosion of Ti/RuO2 electrodes in acid sulfate solution.* Corrosion Science, 2004. 46: p. 65-74.

70. Karlsson, R., Cornell, A., *Selectivity between oxygen and chlorine evolution in the chlor-alkali and chlorate processes.* Chemical Reviews, 2016. 116(5): p. 2982-3028.

71. Cherevko, S., Reier,T., Zeradjanin, A., Pawolek, Z., Strasser, P., Mayrhofer, K., *Stability of nanostructured iridium oxide electrocatalysts during oxygen evolution reaction in acidic environment.* Electrochemistry Communications, 2014. 48: p. 81-85.

72. Silva, J. F., *Study of dimensionally stable anodes for chlor-alkali electrolysis*, in *Chemical Engineering Department*. 2016, University of Porto.

73. Joe, J. M., *Aspects of power reduction in the chlor-alkali membrane electrolysis*. 1989, Technical University of Eindhoven: Eindhoven.

3 PERFORMANCE HISTORY ANALYSIS OF AN INDUSTRIAL ELECTROLYSER

Abstract: The history of the potential and electrical current evolution of an industrial chlor-alkali membrane electrolyser is a powerful tool to track its operational efficiency progress over time and for deciding the required maintenance instants. For this reason, the performance of a dedicated industrial NaCl electrolyser was systematically analysed as a function of its service time for about eight years, recording the cell potential versus current density. The documented potential values were normalized considering the initial current density, which allowed to reduce data scattering due to small fluctuations of the current density values. The ohmic overpotential contribution, associated to the ion-exchange membranes, showed an average relative error smaller than 3 % and the activation overpotential, related to the performance of the electrodes, displayed an average relative error of 6 %. Thus, the proposed approach enables rigorous assessing of the performance of industrial chlor-alkali membrane electrolysers for adequate scheduling of its maintenance, which leads to significant operational and economic improvements of the chlor-alkali process.

Keywords: chlor-alkali membrane electrolyser; energy consumption; overpotential; service time

* This chapter was published on Filipa Franco, Jorge Prior, Svetlozar Velizarov and Adélio Mendes, A Systematic Performance History Analysis of a Chlor-Alkali Membrane Electrolyser under Industrial Operating Conditions, *Applied Science*, 2019, 9 (DOI: http://dx.doi.org/10.3390/app9020284).

3.1 INTRODUCTION

Chlorine gas is an important chemical commodity in the modern industry, mainly produced via electrolysis of a concentrated aqueous solution of sodium chloride, which demands high-energy consumption. In 2019, the European chlorine production represented nearly 11 million tonnes, and the membrane electrolyser technology corresponded to *ca.* 64 % of the chlorine production capacity [1]. It should be stressed that the electrolysis units installed during the last decades are almost exclusively based on membrane technology, which is considered the best available technique in the chlor-alkali industry. Membrane technology presents numerous advantages over older technologies, such as, higher energy efficiency, lower environmental impact, and higher purity of the produced caustic soda that the mercury method. Developments in the membrane and electrodes fields are further driving this process to improved energy efficiency levels [2].

A membrane electrolyser module consists of a set of single cells. In the case study, considered in the present work, the investigated membrane electrolyser was connected in parallel, and its membrane cell elements were disposed in series on a stack arrangement, where the electrodes had two different coating surfaces corresponding to the anode and to the cathode, respectively. This configuration is the most common in the modern chlor-alkali industry; therefore it is considered in this study [3].

Its three major components are a cation-exchange membrane, a dimensionally stable anode (DSA®) and a nickel-based cathode. At the anode, chloride oxidation to chlorine occurs releasing electrons to the cathode half-reaction, where hydrogen and hydroxyl ions are produced from the water reduction; the sodium ions migrate across the membrane to the cathode compartment and combine with the hydroxyl ions produced at the cathode, thus originating sodium hydroxide [4]. The thermodynamic redox potential for the operating conditions applied (temperature and electrolyte composition) is 2.23 V *vs.* SHE [5], corresponding to a value of 2.19 V *vs.* SHE at 298 K.

$$2\mathrm{NaCl\,(aq)} + 2\mathrm{H_2O\,(l)} \rightarrow \mathrm{Cl_2(g)} + \mathrm{H_2(g)} + 2\mathrm{NaOH\,(aq)} \qquad (3.1)$$

The growth of the electromembrane processes and the availability of the selective and stable ionically conductive materials has opened a very promising field for the chlor-alkali

industry [2]. Nowadays, the bilayer cation-exchange membrane is usually made of perfluorinated sulfonated materials with low ohmic resistance and high selectivity. The membrane configuration allows the movement of Na^+ cations and water molecules while preventing the back migration of Cl^- and OH^- anions, even under high current densities and ion concentration gradients [6]. The membrane is made by a thick layer of tetrafluoroethylene functionalized with sulfonic acid groups at the anode side and a thinner layer of tetrafluoroethylene functionalized with carboxylic groups at the cathode side. The sulfonic functionalized layer assures proton conductivity, while the carboxylic functionalized layer plays a major role for electrostatic repulsion of OH^- anions. The electrodes should be in close contact with the cation-exchange membrane, to minimize the ohmic overpotentials on the electrolyte phase. Reduced spacing between the electrode and the membrane allows also for reducing the mass transport overpotential related to the removal of the gaseous products from the inter-electrode phase [2].

As for the electrodes, the development of dimensionally stable anodes contributed to energy savings in the chlorine industry due to their low activation overpotentials and stability [7-9]. DSA® anodes were developed and commercialized back to the 1970s; it is made of a mixture of ruthenium and titanium oxides applied on a titanium substrate. Ruthenium oxides have excellent electrocatalytic properties, but other transition metal oxides are also used to increase the coating stability during chlorine evolution reaction, of which iridium oxides present the best mechanical properties [7, 8]. Therefore, nowadays, the composition of the electrodes used in industrial chlor-alkali processes is based on TiO_2-RuO_2-IrO_2 applied to Ti-support. Traditionally, the ruthenium-titanium based oxides exhibit chlorine overpotentials between 40 and 60 mV, for current densities of 0.20 - 0.25 $kA.m^{-2}$ with 5.0 M NaCl solutions and temperatures of around 358 K. However, after prolonged operation, the electrocatalytic activity decreases and the anode overpotential can reach 300 - 400 mV at the final stage with an exponential evolution, a point, at which the anode is considered ‘deactivated’ [10].

Previous research works showed that anode deactivation contributes significantly to increase electricity consumption. The deactivation mechanisms of the electrodes are dependent on the operating conditions, where the pH of the brine and the electrolysis temperature are the most important parameters [11-13]. One of the best practices in the chlor-alkali industry is anolyte acidification that helps to reduce the oxygen content in the cell gas

products. The pH of the brine is most commonly lowered by adding HCl for neutralizing the back-migration of OH^- into the anolyte, which leads to the formation of oxygen at the anode [11, 12].

The main anodic reaction is the chlorine evolution reaction, CER, which requires a thermodynamic potential of 1.36 V at 298 K *vs.* SHE (Standard Hydrogen Electrode) [6].

$$2Cl^-\,(aq) \rightarrow Cl_2(g) + 2e^- \qquad (3.2)$$

In addition to the chlorine evolution, the undesired oxygen, mainly by water oxidation:

$$2H_2O\,(l) \rightarrow 4H^+(aq) + O_2(g) + 2e^- \qquad (3.3)$$

In which electrode potential is 1.23 V *vs.* SHE at 298 K [6], also occurs, especially outside the optimum pH "window" of 2 to 4 [11]. This reaction is thermodynamically advantageous but the DSA electrode strongly favours the CER. Industrially, the ratio of the chloride ions in the anolyte inlet to the total amount of electric current used by the anode, so-called anodic current efficiency, is monitored to assess the relevance of the parasitic reactions as water oxidation. Typically, DSA® anodes have an anodic current efficiency between 95 % and 97 % [14].

Carbon steel electrodes were first used in diaphragm cell for the hydrogen evolution reaction, HER, at the cathode compartment. In the 1990s, after the successful commercialization of ion-exchange membrane-based cells, cathodes with new compositions (such as nickel or nickel with ruthenium oxide-coated, so-called Raney nickel cathodes, Ni-Al) and greater surface areas became available and displaying higher corrosion stability and catalytic activity for the HER. In the chlor-alkali typical operating conditions, nickel is a competitive material, because it combines a good electrocatalytic activity with stability under alkaline conditions and supports higher temperatures (up to *ca*. 353 K) [15]. Raney nickel cathodes exhibit an overpotential up to *ca*.120 mV in the high current density region [6].

The cathode promotes the half-reaction of water decomposition to produce hydroxide ions and hydrogen and the associated thermodynamic potential is -0.83 V *vs.* SHE at 298 K [6].

$$2H_2O\,(l) + 2e^- \rightarrow H_2(g) + 2OH^-(aq) \qquad (3.4)$$

Consequently, sodium hydroxide is formed from the hydroxide and sodium ions. If hydroxide ions migrate into the anode side, in addition to losing the cathodic product, it would combine with dissolved chlorine gas to produce hypochlorite ions, which is an unwanted side reaction:

$$Cl_2(g) + 4OH^-(aq) \rightarrow 2ClO^-(aq) + 2H_2O(l) + 2e^- \quad (3.5)$$

The energy efficiency of the chlor-alkali process depends on the overpotentials associated with each component, namely the membrane, the electrodes, and the concentration polarization. The overall cell potential is the sum of cathode, anode, membrane, electrolyte and hardware [6]:

$$E = E_{\text{therm}} + \eta_a + (-\eta_c) + (R_{\text{mem}} + R_{\text{hw}} + R_{\text{sol}}) \cdot j \quad (3.6)$$

where E_{therm} represents the redox thermodynamic potential for the operating conditions (temperature and composition), the $\eta_{\text{act}} = \eta_a + (-\eta_c)$ represents the anodic and cathodic activation overpotentials. The membrane, hardware and electrolyte-related overpotentials can be calculated using the Ohm's law, $\eta_\Omega = R_\Omega \cdot j = (R_{\text{mem}} + R_{\text{hw}} + R_{\text{sol}}) \cdot j$ [5]. However, Equation (3.6) does not consider the concentration overpotential term because the concentration of NaCl and NaOH in the anode and the cathode are high, therefore, the electrolyte resistance can be considered negligible.

Most of the maintenance of an electrolyser is related to the membrane, which affects the ohmic resistance proportionally to the extent of the affecting area. A preventive maintenance strategy is usually followed based on the potential of the cell, replacing the membrane before electrolyte exchange between the cathode and anode compartments destroys the electrodes.

The DSA® activation overpotential grows exponentially at the final stage of its service time due to the deactivation of the electrode [10]. This overpotential increase is a result of the coating erosion, selective electrochemical dissolution of ruthenium, blockage of the active surface site due to insoluble species and the formation of an insulating TiO_2 layer at the coating-substrate interface [10, 16]. The overpotential associated with the cathode surface corrosion grows smoothly making possible, until a certain extent, to keep the current density by increasing the cell's potential [13].

For the reasons given above the deactivation of the electrode, an excessive electrode service time contributes to an increase in the energy operating costs of NaCl electrolysis. However, the recoating or replacing of the electrodes is very expensive due to the use of noble metal oxides on the electrode surface. Therefore, scheduling the maintenance instants of an electrolyser should be carefully made, balancing the increase of energy costs over time, based on the evolution of the potential as a function of time for a specific current density, and the obtained productivity with the replacement costs and the substantial catalyst losses increase that happens during the shutdowns and start-ups of the electrolyser [10]. Therefore, it is essential to have a rigorous criterion to decide when to perform the preventive maintenance of the electrodes and membranes. It should be emphasized, for instance, that the undercurrent performance of a cell compromises the whole stack for cells associated in series.

3.2 EXPERIMENTAL

Bondalti uses electrolyser modules with bipolar cell configuration. Each bipolar electrode has an effective area of around 3 m^2 equipped with DSA® anodes and Raney nickel cathodes [6]. The performance history of one of the industrial bipolar electrolysers was recorded and analysed for eight years. A bipolar electrolyser is a stack of cells connected in series; the cathode of one cell is connected directly to the anode of the adjacent cell, receiving then the same electrical current – Figure 3.1. The potential was measured for each cell and used to assess the performance of the electrolyser.

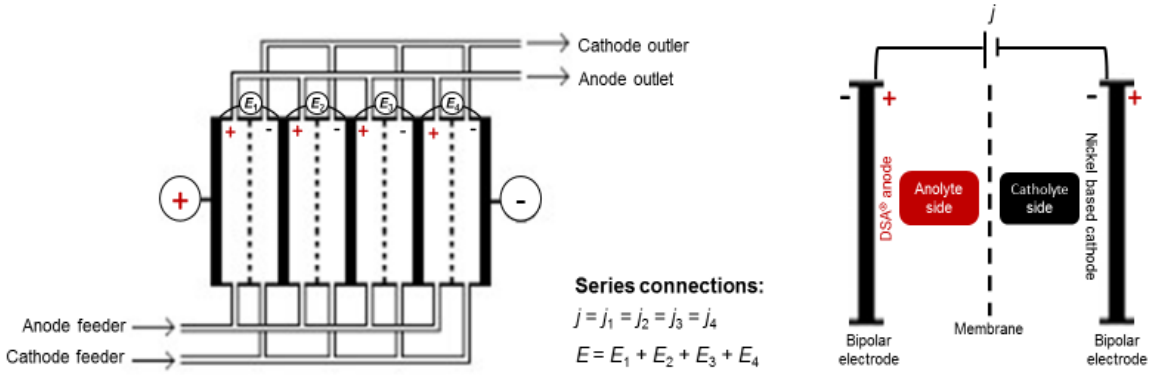

Figure 3.1 Scheme of a bipolar electrolyser where the stack consists of four cells connected in series: the potential between the terminals, E, is the sum of the individual potential of the cells and the same current density, j, flows through the cells.

During the period of analysis, the membranes of the electrolyser were replaced every four to five years of service time, whereas the electrodes were usually replaced or recoated after the eight years of operation. It was, therefore, decided to record the current density for the electrolyser and the potential of each cell every 15 minutes for eight years.

The electrolyser was operated under mostly constant operating conditions; specifically, the feed was a 5.0 M NaCl aqueous solution, the temperature was *ca.* 358 K and pH close to the membrane between 4 and 4.5 [17].

3.2.1 Model assumptions

The loss of energy efficiency in a chlor-alkali process is mostly related to the activation overpotentials and ohmic overpotentials associated with the membrane, hardware, and electrolyte. At each electrode, the activation overpotential, η_{act}, is related to the electrochemical kinetics and affects the total current density, j, which according to the Butler-Volmer equation, relates to the activation overpotential as follows [18]:

$$j = j_0 \cdot \left[e^{\left(\frac{\alpha \cdot n \cdot F \cdot \eta}{R \cdot T}\right)} - e^{\left(\frac{-(1-\alpha) \cdot n \cdot F \cdot \eta}{R \cdot T}\right)} \right] \tag{3.7}$$

where η represents a potential loss due to activation, j_0 is the exchange current density of the reaction, α is the transfer coefficient, n is the number of the electrons exchanged in the reaction, F is the Faraday constant, T is the absolute temperature and R is the universal gas constant. At high current densities, the second term in Equation (3.7) can be neglected and the overpotential is given by the Tafel equation [18]:

$$\eta = -\frac{R \cdot T}{\alpha \cdot n \cdot F} \cdot \ln j_0 + \frac{R \cdot T}{\alpha \cdot n \cdot F} \cdot \ln j \tag{3.8}$$

Parameters α and j_0 depend on the composition and pH of the electrolyte and on nature and surface characteristics of the coatings of the electrodes. The overpotential can now be obtained by linear regression:

$$\eta = b \cdot (-\ln j_0 + \ln j) \tag{3.9}$$

where parameter b is called Tafel slope. Under Tafel conditions, normally for $\eta > 50$ mV [6], Equation (3.9) can be introduced into Equation (3.6):

$$E = [E_{\text{therm}} - (b_{\text{a}} \cdot \ln j_{0,\text{a}}) + (b_{\text{c}} \cdot \ln j_{0,\text{c}})] + [(b_{\text{a}} - b_{\text{c}}) \cdot \frac{\ln j}{j} + (R_{\text{mem}} + R_{\text{hw}} + R_{\text{sol}})] \cdot j \qquad (3.10)$$

E as a function of j, as described by Equation (3.10), is not linear but experimentally it follows a mostly linear relationship over the current density range of 2 kA·m^{-2} to 5 kA·m^{-2}, corresponding to the Tafel region. In this way, E *vs.* j values can be fitted using Equation (3.11), where k-factor corresponds to the slope of the E *vs.* j curve and E_0 is the interception or the open circuit potential [6]:

$$E = E_0 + k \cdot j \qquad (3.11)$$

where:

$$E_0 = E_{\text{therm}} - (b_{\text{a}} \cdot \ln j_{0,\text{a}}) + (b_{\text{c}} \cdot \ln j_{0,\text{c}}) \qquad (3.12)$$

$$k = (b_{\text{a}} - b_{\text{c}}) \cdot \frac{\ln j}{j} + (R_{\text{mem}} + R_{\text{hw}} + R_{\text{sol}}) \qquad (3.13)$$

This linear approach is usually called the k-factor analysis. Since the overall ohmic resistance is dominant, it is usually considered that the k-factor depends mostly on the ohmic overpotential, where the membrane has a major contribution [18].

Blair *et al.* [19] proposed to record the potential of small groups of cells connected in series and to compare it with a reference potential. An alarm would be activated, and the supply of energy to the cell disconnected, whenever the measured potential varies from the reference potential by more than an actual potential [18]. In a day-to-day operation, the imposed current density fluctuations result in a potential change. Consequently, it is important to remove these fluctuations from the overpotential analysis. Themblay *et al.* [20] proposed an improvement to the previous approach by Blair *et al.* correcting the real potential for a reference constant current density, according to the Equation (3.14).

$$E_{j,\mathrm{ref}} = E_0 + (E - E_0) \cdot \frac{j_{\mathrm{ref}}}{j} \tag{3.14}$$

where $E_{j,\mathrm{ref}}$ is the corrected potential for a reference current density (j_{ref}). Here, it is assumed again that the ohmic overpotentials dominate within the Tafel region.

This work aims at estimating the overpotentials related to the membrane and to the activation of the anode and the cathode. Therefore, the experimental values of *E vs. j* were analysed, removing the values outside of the Tafel region and calculating a monthly average for producing a pair of values per month. These values outside of the Tafel region are mostly related to shut down and start-up occurrences; consequently, it was only considered the pair of values with a potential higher than 2.3 V and current densities of higher than 2 kA·m^{-2}. Industrially, a set of cells or even the whole membrane electrolyser is normally considered for the potential *versus* current analysis. For this reason, *E* values considered are the average of all cells corrected for a reference current density value using Equation (3.14). In this equation, the reference current density was set to the average current density of the first operating month and E_0 was obtained based on Equation (3.11), upon fitting to the experimental results for each month. Consequently, Equation (3.14) can thus be written for each operating month as:

$$E_{ji,0} = E_0 + (E - E_0) \cdot \frac{j_{i,0}}{j} \tag{3.15}$$

where E_0 was estimated based on Equation (3.11) for each month of membranes and electrodes set i, $j_{i,0}$ is the average current density of the first operating month, and *j* is the average current density of the actual month. For each month, the corrected potential outlier values, $E_{ji,0}$, were removed based on the "box-and-whisker" statistical analysis [21]. From Equation (3.15) fitting it becomes possible to associate the increase of the corrected potential to the activation and ohmic overpotentials:

$$\eta'_{\mathrm{act}} = E_0 - E_{\mathrm{therm}} \tag{3.16}$$

$$\eta'_{\Omega,\mathrm{i}} = (E - E_0) \cdot \frac{j_{\mathrm{i},0}}{j} \tag{3.17}$$

where η'_{act} is the activation overpotential for each set of electrodes and $\eta'_{\Omega,i}$ the ohmic overpotential associated with each set of membranes and electrodes i.

3.3 RESULTS AND DISCUSSION

The monthly potential, E, and current density, j, histories of an industrial electrolyser between 2008 and 2016 are shown in Figure 3.2.

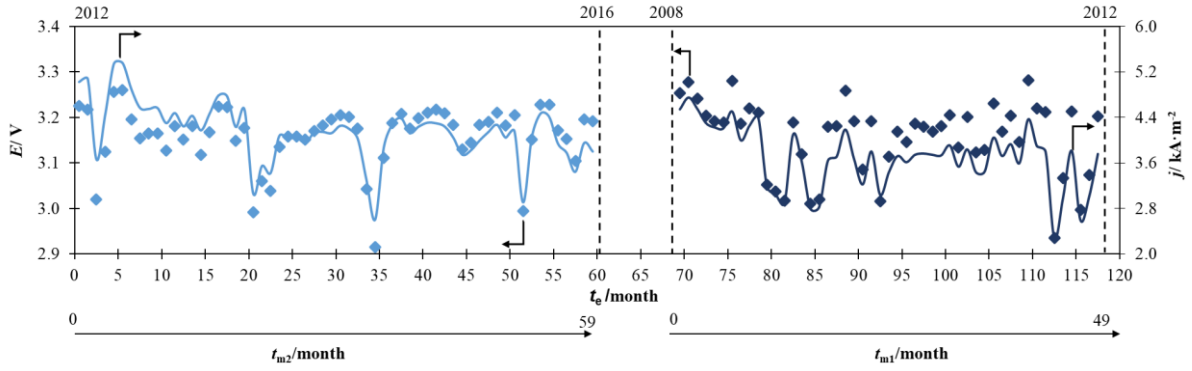

Figure 3.2 Potential (♦), E, and current density (−), j , as a function of the electrode and membrane service times, respectively t_e and t_{mi}.

During the studied period, two sets of membranes and two sets of electrodes were inserted in the electrolyser. Chronologically, the data collection began in 2008, at the middle age of the electrodes (69 months) and with fresh membranes. At instant corresponding to an age equal to 117 months of the electrodes and equal to 48 months of the membranes, both electrodes and membranes were replaced and the time counting of the electrodes and membranes, respectively t_e and t_{mi}, was reset to 0 – see Figure 3.2. The first set of membranes was named #m1 and the second #m2; likewise, the first and second set of electrodes were named #e1 and #e2, respectively – see Figure 2. For each month in Figure 3.2, parameters E_0 and k was calculated by Equation (3.11), which are plotted in Figure 3.3.

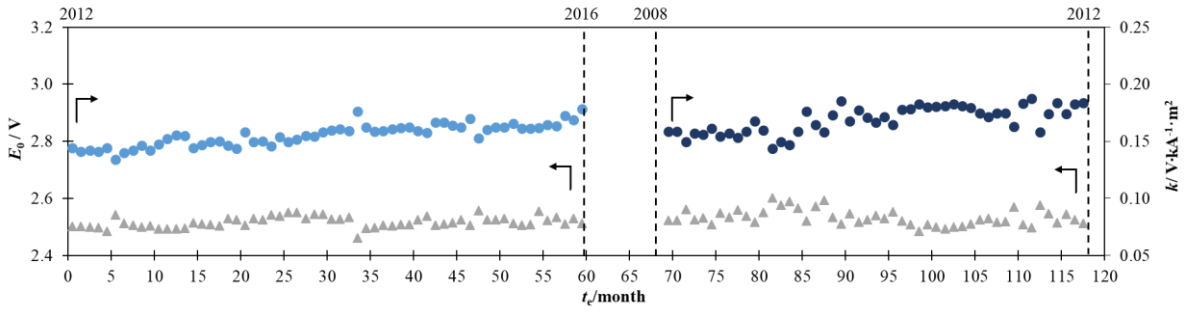

Figure 3.3 The monthly E_0 (●) and k (▲) values obtained from the polarization curves analysis.

Typically, E_0 takes a value between 2.20 and 2.60 V and k-factor between 0.05 and 0.15 $V \cdot kA^{-1} \cdot m^{-2}$, when the membrane surface area is equal to 1.5 m^2, according to the book of good operating principals for the chlor-alkali industry [22]. For a membrane area of 5.4 m^2, E_0 should be between 2.40 and 2.80 V and the k-factor between 0.15 and 0.25 $V \cdot kA^{-1} \cdot m^{-2}$. For the actual electrolyser, electrodes display a surface area around 3 m^2. The first sets of electrodes and membranes (#e1 and #m1) display E_0 values between 2.40 and 2.60 V and k between 0.14 and 0.19 $V \cdot kA^{-1} \cdot m^{-2}$ – see Figure 3.3. After their replacement (corresponded to #e2 and #m2 period), E_0 values are between 2.46 and 2.56 V and k-factor between 0.13 and 0.18 $V \cdot kA^{-1} \cdot m^{-2}$ – see Figure 3.3. These results are within the reported normal range of k-factor. In this period, the k-factor values are smaller, which also indicates a smaller ohmic resistance related to the use of the different type of membranes.

Figure 3.4 shows the normalized potential, $E_{ji,0}$ and the correspondent ohmic resistance, equal to $(E - E_0) \cdot j^{-1}$, as a function of the respective electrode service time, t_e, and membrane service time, t_{mi}.

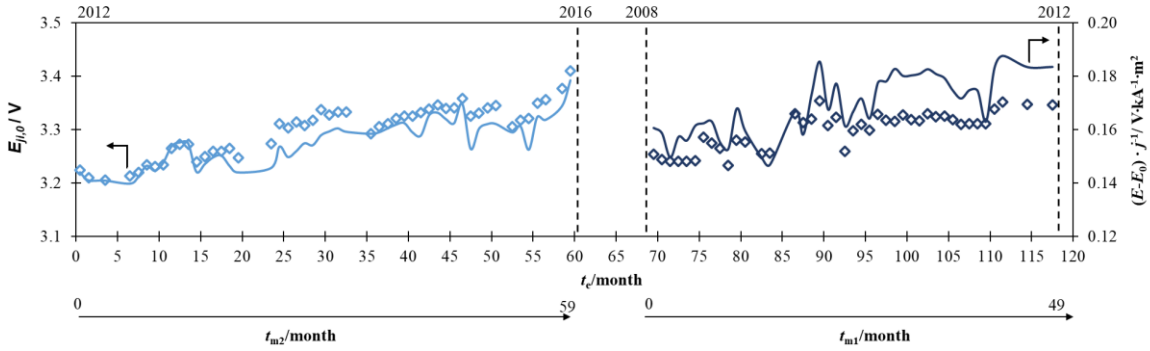

Figure 3.4 Normalized potential (◊), $E_{ji,0}$, and the correspondent ohmic resistance (−), $(E - E_0) \cdot j^{-1}$, as a function of the electrode and membrane service times, respectively t_e and t_{mi}.

Figure 3.4 shows that $E_{j2,0}$ starts at 3.22 V and increases *ca.* 200 mV over the 2012-2016 period, for the set #e2 and #m2 and for the set #e1 and #m1, over the 2008-2012 period, the initial value of the normalized potential is about the same ($E_{j1,0} = 3.25$ V) but, the potential increase is smaller, approximately 100 mV. Comparing the Figures 3.2 and 3.4, it can be observed that the potential normalization methodology allows for smoothing the production peaks and determining the effective progression of the potential over time due degradation of the elements of the electrolyser. Between the 79 and 95 months of the electrode service time, the ohmic resistance displays various peaks. These peaks are related to an experimental period

to the maintenance of the membrane procedure that was discontinued, and no other peaks are observed afterwards. After the 95 months of the electrode service time, the normalized potential remains to increase slowly but, the ohmic resistances sharp growth. In this case, the electrodes contribution for the ohmic resistance was not negligible due to a significant deactivation, as assigned in Equation (3.13); the timely replacement or recoating of the electrodes prevented an expectable exponential growth of the potential [6, 8].

Figure 3.5 plots the activation and ohmic overpotentials (η'_{act} and $\eta'_{\Omega,i}$) obtained from Equations (3.16) and (3.17). It shows that the ohmic overpotential increases around 170 mV between 2012 and 2016 and 100 mV during the period from 2008 to 2012, which are within the same order of the normalized potential increase, $E_{ji,0}$. However, it is difficult to identify a trend for the activation overpotential since it remains mostly constant.

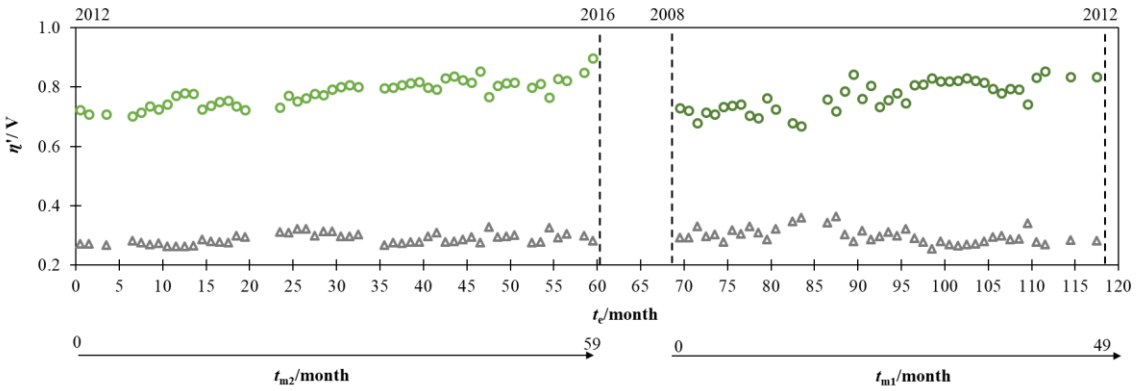

Figure 3.5 Activation overpotential (Δ) and ohmic overpotential (○) as a function of the electrode and membrane service times, respectively t_e and t_{mi}.

Figure 3.6 shows $E_{j2,0}$ and $E_{j1,0}$ (Figure 3.6a), $\eta'_{\Omega,2}$ and $\eta'_{\Omega,1}$ (Figure 3.6b) and η'_{act} (Figure 3.6c) as a function of the respective service time and regression analyses in Table 3.1.

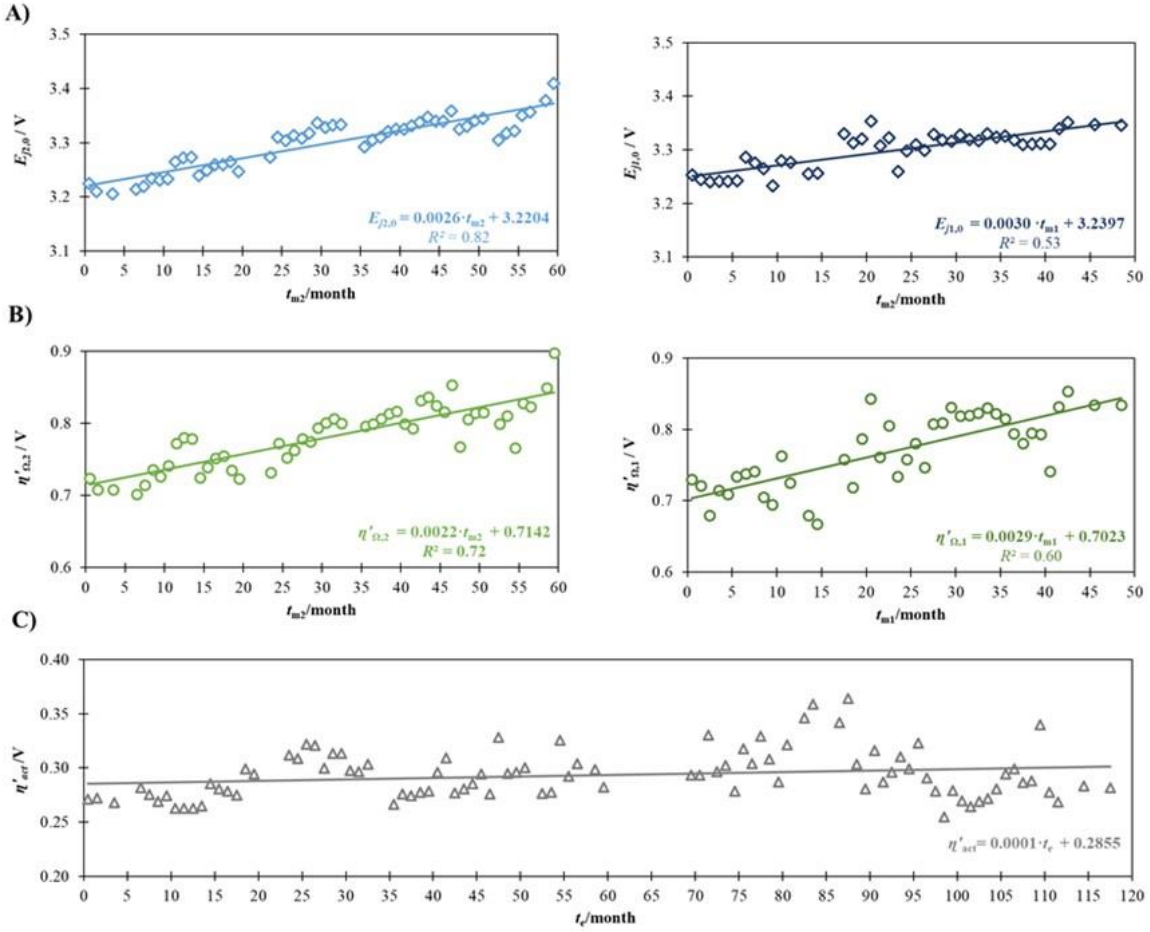

Figure 3.6 A) Normalized potential, $E_{ji,0}$, as a function of the electrode and membrane service time, t_{mi}; B) Associated ohmic overpotential, $\eta'_{\Omega,i}$,as a function of the electrode and membrane service time, $t_{mi;}$ C) associated activation overpotential, η'_{act}, as a function of the respective electrode service time, $t_{e.}$

Table 3.1 Regression analysis of the $E_{ji,0}$, $\eta'_{\Omega,i}$ and η'_{act} as a function of the respective service time.

Linear regression	R^2		**Coefficient**	***p*-value**
$E_{j2,0}$ *vs.* t_{m2}	0.82	intercept	3.2204	<0.05
		slope	0.0026	<0.05
$E_{j1,0}$ *vs.* t_{m1}	0.67	intercept	3.2495	<0.05
		slope	0.0021	<0.05
$\eta'_{\Omega,2}$*vs.* t_{m2}	0.72	intercept	0.7142	<0.05
		slope	0.0022	<0.05
$\eta'_{\Omega,1}$*vs.* t_{m1}	0.60	intercept	0.7023	<0.05
		slope	0.0029	<0.05
η'_{act} *vs.* t_e	0.04	intercept	0.2855	<0.05
		slope	0.0001	<0.05

From Figure 3.6 and Table 3.1, a linear trend with the time of the normalized potential and ohmic overpotential, when the analysis is applied to each stage of the electrolyser history, is clearly observable. The observed trends show a small increase of the activation overpotential over time, which is related to the electrode catalytic activity, and of the ohmic overpotential, mostly related to the performance of the membranes.

The average of the relative error, ε, between the actual values of $E_{ji,0}$, $\eta'_{\Omega,\mathrm{i}}$ and η'_{act} and the corresponding linear regression is given in Table 3.2, together with the actual values for each instance.

Table 3.2 Relative error between the actual values of $E_{ji,0}$, $\eta'_{\Omega,i}$ and η'_{act} and the corresponding linear regression, for the first and second stages of the data analysis.

	t_{e} (month)	t_{m} (month)	$E_{ji,0}$ (V)	$\bar{\varepsilon}_{E_{ji,0}}$ (%)	η'_{act} (V)	$\bar{\varepsilon}_{\eta'_{\mathrm{act}}}$ (%)	$\eta'_{\Omega,i}$ (V)	$\bar{\varepsilon}_{\eta'_{\Omega,i}}$ (%)
#e2, #m2	0.5	0.5	3.23	0.5	0.271	6	0.723	2
	29.5	29.5	3.34		0.314		0.793	
	59.5	59.5	3.41		0.282		0.897	
#e1, #m1	69.5	0.5	3.25	0.4	0.293		0.730	3
	89.5	20.5	3.30		0.281		0.843	
	99.5	30.5	3.33		0.279		0.819	
	117.5	48.5	3.35		0.282		0.834	

The average relative error of the activation overpotential is 6 % and of the ohmic overpotential is 3 %. Concerning the average of the relative error of the normalized potential, it is quite small, < 0.5 %. It can, therefore, be concluded that the methodology presented allows for discriminating the performance over operation time of the most critical elements in an electrolyser: electrodes and membranes, which can be therefore used for scheduling their preventive maintenances. The developed methodology allows estimating the energy cost of a given set of membranes/electrodes over its period of operation based on the overpotential increase. Moreover, if the costs of acquisition and replacement of all elements and its respective amortization period are known, the average value of the maintenance costs can be calculated. Thus, the intersection between the maintenance cost and operating cost can be considered as the ideal replacement time for each set of membranes/electrodes.

3.4 CONCLUSIONS

A methodology was proposed to follow the ageing of electrodes and membranes of a chlor-alkali membrane electrolyser. The developed methodology is based on the potential difference and current density histories of an industrial bipolar electrolyser data collected every 15-minute for about approximately eight years.

The NaCl electrolysis data was organized monthly and the values outside of the Tafel region were removed, which permitted to calculate the average of all cells' potential and the current density. The monthly open-circuit cell potential was obtained from potential and current density curves of the electrolyser. The cell potential was then normalized taking into account the initial current density (when occurs the membranes or membranes and electrodes replacements) and depending on the type of elements used; this procedure allows removing from the experimental data the potential variations associated to small current fluctuations. This normalisation made possible to associate the ohmic and activation overpotentials increase with the electrode and membrane service time. In the considered case study, the calculated average relative error of the activation overpotential was 6 % and of the ohmic overpotential was 3 %. The overpotential histories associated with the membrane (ohmic overpotential) and to the electrodes (activation overpotentials) allow deciding the best instant for servicing actions. This decision, therefore, balances the maintenance costs with the over-energy consumption and the risks of a complete failure of the membranes/electrodes.

3.5 NOTATION

	Description	Units
b	Tafel slope	V
b_a	Anodic Tafel slope	V
b_c	Cathodic Tafel slope	V
CER	Chlorine evolution reaction	-
DSA	Dimensionally stable anode	-
E	Cell potential	V
$E_{j,\mathrm{ref}}$	Corrected potential for a reference current density	V
E_{therm}	Redox thermodynamic potential for the operating conditions	V
F	Faraday constant	$C \cdot mol^{-1}$
HER	Hydrogen evolution reaction	-
i	Number of a set of membranes	-
j	Current density	$A \cdot m^{-2}$
j_0	Exchange current density	$A \cdot m^{-2}$
$j_{0,a}$	Exchange current density for the anodic reactions	$A \cdot m^{-2}$
$j_{0,c}$	Exchange current density for the cathodic reactions	$A \cdot m^{-2}$
j_{ref}	reference current density	$A \cdot m^{-2}$
k	*k*-factor value	Ω
N	Number of electrons involved in the electrode reaction	-
OER	Oxygen evolution reaction	-
R	Universal gas constant	$J \cdot K^{-1} \cdot mol^{-1}$
R_{mem}	Ohmic resistance related to the membrane	Ω
R_{hw}	Ohmic resistance related to the hardware	Ω
R_{sol}	Ohmic resistance related to the electrolyte	Ω
R_Ω	Ohmic resistance of the cell	Ω
SHE	Standard hydrogen electrode	-
T	Absolute temperature	K
α	Charge transfer coefficient	-
η	Activation overpotential	V
η_a	Anodic activation overpotentials	V
η_c	Cathodic activation overpotentials	V
η_Ω	Ohmic overpotential	V
η'_{act}	Activation overpotential for each set of electrodes	V
$\eta'_{\Omega,i}$	Ohmic overpotential associated with each set of elements	V
z	Charge number	-

3.6 REFERENCES

1. EuroChlor, *The chlor-alkali industry in Europe*. (Available from: http://www.eurochlor.org/the-chlorine-universe/the-chlor-alkali-industry-in-europe.aspx, accessed 10.06.2018).

2. Paidar, M., Fateev, V. Bouzek, K., *Membrane electrolysis—History, current status and perspective.* Electrochimica Acta, 2016. 209: p. 737-756.

3. O'Brien, T., Bommaraju, T., Hine, F.,*Chlor-alkali technologies*, in *Handbook of Chlor-Alkali Technology*, Springer, Editor. 2005: New York. p. 387-442.

4. O'Brien, T., T. Bommaraju, T., Hine, F., *Introduction*, in *Handbook of Chlor-Alkali Technology*, Springer, Editor. 2005: New York. p. 1-16.

5. Dias, A., *Chlor-alkali membrane cell process: study and characterization, PhD thesis*. 2010, University of Porto.

6. O'Brien, T., T. Bommaraju, and F. Hine, *Chemistry and Electrochemistry of the Chlor-Alkali Process*, in *Handbook of Chlor-Alkali Technology*. 2005, Springer: New York. p. 75-386.

7. Beer, H., *The invention and industrial development of metal anodes.* Journal of The Electrochemical Society, 1980. 127: p. 303-307.

8. DeNora, *DSA® anodes for chlorine evolution*. (Available from: http://www.denora.com/markets-products/electrodes/anodes/chlorine-evolution.html, accessed 08/11/2019).

9. Trasatti, S., *Electrocatalysis: understanding the success of DSA®.* Electrochimica Acta, 2000. 45: p. 2377-2385.

10. Bommaraju, T., Chen, C., Birss, V., *Deactivation of thermally formed RuO2+TiO2 coatings during chlorine evolution: mechanisms and reactivation measures*, in *Modern chlor-alkali technology*. 2000, International Chlorine Symposium - Blackwell Science: UK.

11. Karlsson, R. Cornell, A., *Selectivity between oxygen and chlorine evolution in the chlor-alkali and chlorate processes.* Chemical Reviews, 2016. 116(5): p. 2982-3028.

12. Sandin, S., Karlsson, R., Cornell, A., *Catalyzed and Uncatalyzed Decomposition of Hypochlorite in Dilute Solutions.* Industrial & Engineering Chemistry Research, 2015. 54(15): p. 3767-3774.

13. Sohrabnejad-Eskan, I., Goryachev, A., Exner, K. S., Kibler, L. A., Hensen, E., Hofmann, J. P., Over, H. *Temperature-dependent kinetic studies of the chlorine evolution reaction over RuO2(110) model electrodes.* ACS Catalysis, 2017. 7(4): p. 2403-2411.

14. *Chlor-alkali simulation using ESP* (Available from: http://support.olisystems.com/ApplicationBriefs/Briefs%20-%20Chlor%20Alkali.pdf).

15. Rausch, S., Wend, H., *Morphology and utilization of smooth hydrogen-evolving Raney-nickel cathode coatings and porous sintered-nickel cathodes.* Journal of The Electrochemical Society, 1996. 143: p. 2852-2862.

16. Hoseinieh, S., Ashrafizadeh, F. Maddahia, M. *A comparative investigation of the corrosion behavior of RuO2–IrO2–TiO2 coated titanium anodes in chloride solutions.* Journal of The Electrochemical Society, 2010. 157: p. E50-E56.

17. Bondalti, *Manual Operatório: Eletrólise AGC - Processo*. 2019: Estarreja.

18. O'Hayre, R., Cha, S., Colella, W., Prinz, F., *Fuel cell fundamentals*, in *Fuel cell fundamentals*. 2006, Wiley: New York.

19. Blair, J., Dircks, K., *Method and apparatus for monitoring fuel cell performance*. 1992.

20. Tremblay, G., Berriah, S., Brillon, D., Guena, T., *Method and system for acquisition, monitoring, display and diagnosis of operational parameters of electrolyzers*. 2003.

21. McClave, J. T., Benson, P .G., Sincich, T., *Methods for describing sets of data*, in *Statistics for Business and Economics*. 2010.

22. Tremblay, G., Lademann, H., Berriah, S., Veillette, M. *Method for ensuring and monitoring eletrolyzer safety and performances, US Patent 20110240483 A1*. 2012, Recherche 2000 Inc., Quebec (CA).

4 STUDY OF THE CHLORINE EVOLUTION REACTION KINETICS OVER DSA® ELECTRODES

Abstract: The chlorine evolution reaction, CER, is the main anodic reaction on the chlor-alkali production. However, the electrolyte is an aqueous solution, and it is necessary to consider the unwanted oxygen evolution reaction, OER, from the water electrolysis. Understanding the CER mechanism is essential to maximize the selectivity of the chlorine production at the DSA® anode. A parametric study was performed to analyse the effect of the electrolyte composition and temperature for the CER over a DSA® industrial electrode, where sodium chloride concentration was varied from 2.50 M to 5.20 M, the sodium chlorate (principal impurity) concentration was varied from 0.0 M to 1.0 M and the pH was varied from 0 to 9 (by acidification with HCl). Electrochemical characterization techniques were applied to analyse the chlorine evolution reaction, namely cyclic voltammetry, and polarization curves in the CER region. The kinetic parameters were calculated from the iR-corrected polarization curves and the results obtained are consistent with the literature values for ruthenium-based electrodes. In acid solutions, the reversible electrode potential increases with chloride activity -70 mV/decade and a bend were observed around 1.25 V *vs.* SHE for the general of the experiments. This value is related to the oxidation of ruthenium on the electrode surface, which is involved in the chlorine evolution reaction as intermediate species.

Keywords: chlor-alkali, anode, DSA, kinetics, chlorine

*This chapter was presented by Filipa Franco on the First International Young Researchers Symposium on Applications of Electrochemical Technology (IYRS-AET) of the 3rd International Congress of Chemical Engineering (ANQUE-ICCE).

4.1 INTRODUCTION

Chlorine has been produced industrially for nearly 120 years; presently, 95 % of it is obtained by an electrochemical process. The membrane cell technology is the most used in Europe, corresponding to 66 % of the installed capacity, being Bondalti Chemicals S.A. one of the most important players in the Iberian Peninsula [1].

The catalytic electrolysis of a concentrated sodium chloride solution (brine) yields chlorine, hydrogen, and sodium hydroxide. The chlorine evolution reaction (CER) is the main anodic reaction, where two chloride anions need to be successively discharged and recombined thereby forming gaseous chlorine over dimensionally stable anodes, DSA®, as illustrated by the Equation (4.1), where RuO_2 is the main catalytically active component.

$$2Cl^- (aq) \rightarrow Cl_2(g) + 2e^- \quad (4.1)$$

Understanding the CER mechanism is essential to allow maximizing the selectivity of the chlorine production at the anode because brine is an aqueous solution and there is necessary to consider the unwanted oxygen evolution reaction (OER) from the water electrolysis. The OER from water electrolysis can be written as:

$$2H_2O (l) \rightarrow 4H^+(aq) + O_2(g) + 2e^- \quad (4.2)$$

The OER is thermodynamically preferred to CER, E^0_{OER} = 1.23 V *vs.* SHE, which is lower than the corresponded value for the CER, E^0_{CER} = 1.36 V *vs.* SHE. However, the CER mechanism comprehends two-electron process and the OER is a four-electron process. In the DSA®, the limiting step of CER is much faster than the limiting step of OER in the anode and the CER prevails whenever the applied potential is > 1.36 V *vs.* SHE [2, 3].

4.1.1 Mechanisms for chlorine evolution reaction

Chlorine evolution on a metal oxide active site generally occurs according to Equation (4.3) and (4.4) or (4.3) and (4.5), which are respectively, the Volmer-Heyrovsky and the Volmer-Tafel mechanisms. In 1972, Erenburg *et al.* (cited by [4]) proposed that the chlorine evolution mechanism comprehends the chloride adsorption on the metal oxide

(Volmer or discharge step), which may react with a chloride ion in solution leading to the formation and desorption of chlorine (Heyrovsky or electrochemical desorption step) or, with a second adsorbed chloride ion to form a desorbed chlorine molecule (Tafel or recombination step**)**. In both cases, the ruthenium dioxide active sites at the DSA® is represented by [S]:

$$[S] + Cl^- \rightleftharpoons [S]Cl_{ads} + e^- \text{ (Volmer or discharge step)} \quad (4.3)$$

$$[S]Cl_{ads} + Cl^- \rightarrow Cl_2 + [S] + e^- \text{ (Heyrovsky or electrochemical desorption step)} \quad (4.4)$$

$$2[S]Cl_{ads} \rightarrow Cl_2 + 2[S] \text{ (Tafel or recombination step)} \quad (4.5)$$

If the second step of the mechanism, or Heyrovsky step, is rate-limiting (corresponding the sum of Equations 4.3 and 4.4), the characteristic Tafel slope is ca. 40 mV/decade of current density but, assuming that the Volmer-Tafel mechanism prevails (Equations 4.5 and 4.6), the characteristic Tafel slope is ca. 30 mV/decade of current density. The Volmer-Tafel mechanism prevails at higher potentials (> 1.20 V *vs.* SHE) and both mechanisms are not pH dependent.

On a ruthenium dioxide-coated electrode and in acid medium, the mechanism is consistent with a low Tafel slope of *ca*. 40 mV/decade of current and then with the Volmer-Heyrovsky mechanism. In 1975, it was proposed a new CER mechanism, which is pH dependent and where the first step is the adsorption of a chloride ion on an active site, SCl^+_{ads}; in the following year it was demonstrated that this reaction is actually pH dependent (cited by [5]). Fernández *et al.* [6-8], in 2002, published three articles addressing the CER using a new electrochemical method based on the polarization resistance analysis close to the reversible potential of the chlorine evolution, at a ruthenium oxide coating. The first article confirms the inhibition of the CER at high H^+ concentrations [6]. The second article assesses the Volmer-Krishtalik mechanism, where it considers that the adsorbed chloride ion is reduced in an intermediate step, $SCl_{ads}{}^+$, but the authors concluded that this mechanism can only partially describe the CER [7]. The last article proposes a reaction mechanism for the chlorine evolution which include the deactivation of ruthenium oxide sites by protonation besides the adsorption of chloride ion followed by chlorine evolution, as described by Equations (4.6) to (4.10), *z* is the charge number [8]:

$$[S]^{z} + H^{+} \rightleftharpoons [S]^{z+1}H \quad (4.6)$$

$$[S]^{z} \rightleftharpoons [S]^{z+1} + e^{-} \quad (4.7)$$

$$[S]^{z+1} + Cl^{-} \rightleftharpoons [S]^{z+1}Cl_{ads} + e^{-} \quad (4.8)$$

$$[S]^{z+1}Cl_{ads} + Cl^{-} \rightleftharpoons Cl_2 + [S]^{z} \quad (4.9)$$

or, $$2[S]^{z+1}Cl_{ads} \rightleftharpoons Cl_2 + 2[S]^{z} \quad (4.10)$$

where, S^z and S^{z+1} are active sites with *z* and *z*+1 oxidation state. Although the protonation is not directly involved in the mechanism, the availability of active sites for the CER is pH dependent. The chlorine evolution needs the active sites oxidation and occurs afterwards either by the consecutive adsorption of chloride species by the reaction between two adsorbed chloride species.

4.1.2 Reversible potential of the chlorine evolution reaction, E_{rev}

The anodic polarization curves on a DSA® anode display a bend to high Tafel slope, at *ca*. 1.20 V *vs.* Ag/AgCl (~1.40 V *vs.* SHE). Cornell *et al.* [9, 10] studied this system using a rotating disc apparatus and did not observe any change for different speeds. As so they proposed that the bend is neither related to an ohmic drop nor to mass-transport limitations of the reactants and/or products on the electrode surface, since increasing the velocity of the rotating electrode disc this overpotential did not disappear. These authors proposed that this overpotential is related to a change in the electrode catalytic activity, which affects the reaction kinetics [9, 10].

The onset of the polarization curve is associated with the reversible potential, E_{rev}, and the respective current density, j_{rev}. The exchange current density is a critical parameter to the industrial process because it determines the maximum of current efficiency for the chlorine evolution. When the potential deviates substantially from $E_{rev,}$ the effective current density decreases as a result of the parasitic oxygen evolution reaction increase, which can be accelerated by the electrolyte composition [10, 11].

Eberil *et al.* associate the bend of the polarization curves to the oxidation of ruthenium species to Ru^{VIII} in the coating of the DSA® [12]. The reversible potential identified, 1.40 V *vs.* SHE, coincides with the onset of the formation of gaseous ruthenium oxide, RuO_4. For potentials above of 1.40 *vs*. SHE, the anode coating material is unstable and liable to corrode in acid media during the chlorine evolution [10]. The oxidation of Ru^{IV} to Ru^{VIII} can be included in the reaction mechanism for chlorine evolution on the ruthenium dioxide based catalysts, and it has already been considered in a study which combined the kinetics analysis with *ex-situ* characterization by XPS [12]. Consequently, the proposed mechanism for the chlorine evolution reaction on ruthenium dioxide sites integrates the Volmer-Heyrovsky-Tafel mechanism (associated to the evolution on Ru metal) with previous steps where Ru intermediates are formed as a result of the interaction with the side atoms [10]:

$$RuO_x(OH)_y + \delta H^+ + \delta e^- \rightarrow RuO_{x-\delta}(OH)_{y+\delta}, \qquad 0 \leq \delta \leq 2 \qquad (4.11)$$

4.1.3 Electrolyte parameters influence

The selectivity between the desired chlorine evolution and the parasitic oxygen evolution is influenced by different factors: effects of the process parameters (temperature and the concentrations of the main intermediates and reactants), presence of impurities in the electrolyte (such as those possibly released from the electrodes and construction materials or due to brine recirculation and accumulation of by-products, especially, sodium chlorate) and the electrode morphology and composition [13]. In this study, it was decided to study only the effects that are possible to be industrially set using electrochemical techniques to characterize the systems.

Sodium chloride and sodium chlorate concentration

The main anodic side reaction of the chlor-alkali process is the chloride oxidation to chlorine, as represented by Equation (4.1). However, the oxygen evolution is the most important side reaction and it is a consequence of the water oxidation, Equation (4.2), or the hypochlorite oxidation under chlorate conditions at pH > 4.

To avoid the mass transport limitations and maximize the current efficiencies for chlorine evolution, a chloride brine near saturation should be used, *ca*. 5.40 M, but industrially

a slightly lower concentration is used to prevent crystallization. In this way, it is possible to minimize the competitive adsorption of the other species on the electrode surface and, to prevent the anodic oxygen evolution [11, 14]. As example, the sodium chlorate concentration increases in the anolyte, the number of chlorate molecules absorbed in the active sites also increases. Using ultrapure brine has yet another advantage; an increase in chloride concentration corresponds to a decrease in the reversible potential of the chlorine evolution, which contributes to increase the current efficiency of the chlorine production [10, 11, 14].

Several studies report the effects of the chloride and chlorate concentration on DSA® type electrodes. Cornell *et al.* [10] analysed the chloride concentration dependency on the critical anode potential, varying the chloride concentration between 0.0 and 5.0 M and compensating the ionic strength with chlorate at a pH around 6.5. In this range, it was found a linear relationship between the reversible potential and the logarithm of the chloride concentration (Nernst relation), which corresponds to a decrease of -90 mV/decade of current density, proportional to the oxidation of the ruthenium species in the coating.

It should be highlighted that, for 5.0 M $NaClO_3$ and 0.0 M NaCl at pH = 6.5, the onset of the slope polarization curve is *ca.* 1.20 V *vs.* Ag/AgCl, which is associated to the oxygen evolution under Ru^{VIII} sites, as referred in the previous section. These results are reinforced by Nylén [11], who reproduced the study but, for an anolyte with pH = 2. The slope for the polarization curves obtained was the same and is the same for the interval $2 < pH < 6.5$; this implies that the polarization slope is just related to the chloride concentration.

Electrolyte pH

In the chlor-alkali process, it is essential to have a low pH in the bulk electrolyte to reach a faster reaction kinetics to the chlorine evolution and suppressing the oxygen evolution [11]. The oxygen rate evolution in chlor-alkali processes is 1.5 - 2 % in membrane cells without anolyte acidification, and the oxygen levels in the chlorine gas are < 0.5 % with careful acidification [13]. The literature indicates that chlorine selectivity is maximized for a pH of *ca.* 1 - 2 [13]; however, the best practice in membrane technology is to keep the anolyte at $2 < pH < 3$, since the cation-exchange membranes are unstable in solutions with higher proton activities [15]. However, the pH of the inlet electrolyte on the industrial cell is basic, but it is necessary to keep in mind that the bulk conditions can differ from those at the electrode

surface, where the electrochemical reactions occur. The pH in the vicinity of the electrode surface is around 4 to 5 due the parasitic reactions.

While the reversible electrode potential of CER depends on the pH only indirectly, the reversible electrode potential of the OER increases with the pH – see the Equation (4.2). The parasitic formation of oxygen gas changes the pH at the electrode surface since it produces H^+ ions. On the other hand, the dissolved chlorine can be hydrolysed to form hypochlorous acid, HClO, and hypochlorite species, ClO^-, which also contribute to decreasing the pH [11, 13].

$$Cl_2\,(aq) + H_2O\,(l) \rightarrow H^+(aq) + HClO\,(aq) + Cl^-(aq) \qquad (4.12)$$

$$2HClO\,(aq) + ClO^-(aq) \rightarrow ClO_3{}^- + 2H^+(aq) + 2Cl^-(aq) \qquad (4.13)$$

The pH of the anolyte also plays a role in the stability of the anode due to changes in the ruthenium-water-chlor balance, denoted by RuO_2-H_2O + Cl^- <=> RuO_2-Cl^--H_2O [3, 8, 16]. When the ruthenium species display the highest oxidation state – Ru^{VIII}, the active site deactivates contributing to the reduction the chlorine evolution on the DSA® surface. The Pourbaix diagram indicates the stable forms of ruthenium as a function of the potential *E* and electrolyte pH; it also shows the areas where CER or OER are favoured. Figure 4.1 (adapted from [17]) shows that the most suitable operating conditions for the CER are for $E < 1.49$ V *vs.* SHE and pH < 4. For these conditions, the adsorption of chloride on the terminal on-top oxygen atoms of the ruthenium dioxide is energetically favoured, so, this structure can be considered as a precursor for the chlorine evolution reaction [3].

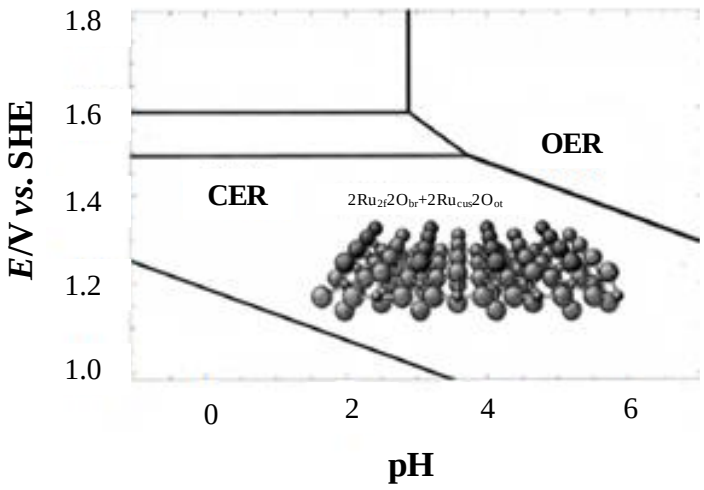

Figure 4.1 Pourbaix diagram of ruthenium-based DSA® electrodes (source: [17]).

The polarization curves are recurrently used to discuss the indirect dependence between the chlorine evolution and the electrolyte pH, in chlorate or chlor-alkali conditions. For chlorate production (high sodium chloride concentration, *ca*. 343 K and pH = 6.5), Cornell *et al.* [10] suggested that the oxygen evolution prevails over the chlorine evolution for low potentials, $E < 1.15$ V *vs.* Ag/AgCl, which corresponds to the water oxidation conditions. In this case, the mechanism is clearly pH dependent. However, the polarization curves display no discontinuity for higher potentials, $E > 1.15$ V *vs.* Ag/AgCl, when the chloride evolution on-sets; it should be emphasised that for these potentials the polarization curves are pH independent. Later, Nylén and Fernandez *et al.* [6-8, 11] studied different chloride concentration but for pH values between 1 and 2 and, the results obtained support the mechanism proposed by Fernandez *et al.* [6-8, 11], which includes ruthenium oxidation in the chlorine evolution mechanism for pH < 2.

Electrolyte temperature

The effect of temperature in the electrolysis is complex and the least mentioned in the literature, probably because the kinetic studies are often conducted at room temperature. At higher temperatures, the viscosity of the electrolyte decreases, improving the mass-transport (mass transport effect), the reversible half-cell potential of the chlorine evolution decreases, E^0_{CER} (thermodynamic effect), but also the exchange of current density j_0 increase (kinetic effect) [2].

The reversible potential of the CER as a function of the temperature, $E_{T,\mathrm{CER}}$, can be calculated from Equation (4.14):

$$E_{T,\mathrm{CER}} = E^0_{\mathrm{CER}} + \frac{\Delta\hat{s}}{n \cdot F} \cdot (T - T_0) \tag{4.14}$$

where $\Delta\hat{s}$ is the entropy of the chemical reaction, assumed independent of the reference temperature, T_0, n is the number of electrons involved in the reaction and F is the Faraday constant [18]. The temperature of the membrane cells is typically near to 358 K.

Nylén [11] also assessed the effect of temperature but under chlorate conditions based on the polarization curve and on the indirect calculation of apparent activation enthalpy. The results showed two linear zones; at low potentials, *ca.* 1.10 V *vs.* Ag/AgCl, where the OER is

higher than CER and at for > 1.20 V *vs.* Ag/AgCl, where the CER is higher than OER. For the CER range, the Tafel slope was 45 mV/decade of current density for a temperature equal to 343 K. It is intended to adjust the temperature so that the chlorine evolution reaction occurs preferably, requiring the lowest possible overpotential value.

4.1.4 Aim of the study

In the chlor-alkali process, energy consumption represents the highest fraction of the operating costs. To minimize the overpotentials and preserving the good condition of the electrode surface, it is important to study the effect of the process parameters on the chlorine evolution reaction over DSA® electrodes, such as sodium chloride and sodium chlorate concentration, electrolyte pH and temperature. A parametric study was therefore developed taking as the reference condition the ones recommended as the best practice for the chlor-alkali process, namely: $2 < pH < 4$, $353\ K < T < 363\ K$ and sodium chloride concentration around 5.0 M. For each operating condition, it was performed an electrochemical characterization of the cell, namely cyclic voltammetry, and polarization curves in the CER region, which allow the calculation of the kinetic parameters of the chlorine evolution.

4.2 EXPERIMENTAL

4.2.1 Electrochemical cell setup

The scheme of electrochemical cell assembly (working electrode, reference, and counter electrode) used for the kinetic analysis of the CER is represented in Figure 4.2. The reactor consists of a 400 mL jacketed cylindrical cell with easy access to the working electrode through the cell bottom with a horizontal orientation. Using a water circulation bath is pumped through the jacket to control the electrolyte temperature in the cell at a constant temperature.

To minimize the mass transfer limitation problems due to gas bubbles accumulation on the electrode surface, a mechanic stirrer (set at 500 rpm) with the propeller located near to the DSA® electrode plate, was used. This electrochemical cell setup allows performing similarly to the rotating disk setup because it allows keeping the electrolyte-electrode interface mostly without gas bubbles and the concentration polarization very low.

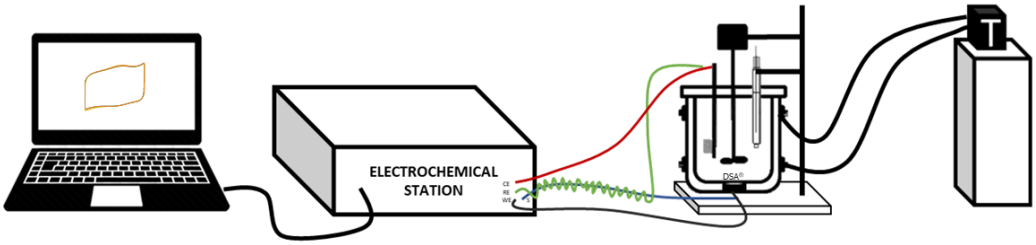

Figure 4.2 Representation of the electrochemical cell setup used.

Electrodes

The working electrodes were cut round shape from a DeNora DSA® plate, 3 mm thick and with 2 cm^2 of effective area, made of RuO_2-IrO_2-TiO_2 coated titanium. A platinum wire was used as a counter electrode, and the electrode potentials were measured against a Red-Rod type electrode supplied by HACH, which contains Ag/AgCl saturated in 3 M KCl and is significantly stable at temperatures around 343 K, which is difficult for a normal Ag/AgCl reference electrodes.

Electrolyte

The electrolyte was prepared from industrial brine with 5.20 M NaCl, 0.11 M $NaClO_3$ and 0.015 M Na_2SO_4 (pH = 2). The initial pH was set using an industrial HCl solution with a mass fraction of 32 %, previously diluted to 0.01 M HCl. When necessary, demineralized water was added to the brine to obtain the desired NaCl concentration. The industrial solutions were supplied by Bondalti. For studying the $NaClO_3$ concentration effect, it was used a different electrolyte. Initially, industrial salt was diluted in ultrapure water and filtered, and the pH adjusted to 2 with HCl. Additional $NaClO_3$ salt was then added to obtain the desired $NaClO_3$ concentrations, using sodium chlorate 99^+ wt. % supplied by ACROS.

4.2.2 Experimental conditions

The experiments performed to investigate the effects of electrolyte composition and temperature are presented in Table 1. Any additional conditions are indicated in the text.

Table 4.1 Initial conditions of the experiments performed on the CER tests.

Effect studied	**[NaCl] (M)**	**[$NaClO_3$] (M)**	**pH**	***T*** **(K)**
Standard condition	5.0	0.11	2	353
Sodium chloride concentration	0.0	0.0	2	353
	2.50	0.05	2	353
	4.50	0.09	2	353
	4.25	0.09	2	353
	4.50	0.09	2	353
	4.75	0.10	2	353
	5.20	0.11	2	353
Sodium chlorate concentration	5.0	0.0	2	353
	5.0	0.05	2	353
	5.0	0.25	2	353
	5.0	0.50	2	353
	5.0	1.0	2	353
Electrolyte pH	5.0	0.11	0	353
	5.0	0.11	1	353
	5.0	0.11	4	353
	5.0	0.11	7	353
	5.0	0.11	9	353
Electrolyte pH corresponding to the CER	5.0	0.11	2.5	353
	5.0	0.11	3	353
	5.0	0.11	3.5	353
	5.0	0.11	4	353
	5.0	0.11	4.5	353
Temperature	5.0	0.11	2	298
	5.0	0.11	2	348
	5.0	0.11	2	353
	5.0	0.11	2	358
	5.0	0.11	2	363

4.2.3 *In-situ* electrochemical characterization techniques

Cyclic voltammetry (CV) and potential polarization curves (PC) were performed using an IM6ex Zahner electrochemical station to characterize the cell system. The working electrode was polarized until no further changes in the electrochemical performance. For the preconditioning the working electrode, the following steps were performed:

(i) 10 potential cycles from 0 V and 1.25 V *vs.* SHE (corresponding to 1.45 V *vs.* Ag/AgCl in 3 M KCl at room temperature) at a scan rate of 50 mV s^{-1}.

(ii) 300 s polarization at 0.50 V *vs*. SHE.

Cyclic voltammetry

Cyclic voltammetry is an electrochemical characterization technique that allows obtaining information about one or more chemical species in the system by registering electric current-potential density (voltammogram) curves at different scan rates. One of the main characteristics of the voltammogram is peaks occurrences corresponding to redox pairs, by formed due to reactions that involve transitions of the active species on the surface of the electrode. The oxidation-reduction reactions can be more kinetically controlled or affected by mass transfer species diffusion to the electrode surface. By scan rate modification, it is possible to verify which mechanisms prevail.

In the first part, a DSA® commercial working electrode was used, and the electrolyte was a solution with 5.0 M NaCl and pH 2 (acidified with HCl), which was referred to as a standard condition. At 298 K, ten potential cycles were performed between 0 V *vs*. SHE and 1.25 V *vs.* SHE at a scan rate between 10 and 200 mV·s^{-1}. These potential limits were chosen to avoid possible Faradaic interference due to the occurrence of chlorine and oxygen evolution reactions [19].

Voltammetric measurements were performed between 0.0 V and 1.25 V *vs*. SHE, which allows covering the capacitive/pseudocapacitive region of the DSA® type electrode, as well as the beginning of the chlorine evolution around 1.20 V *vs.* SHE. Ten potential cycles were performed at a scan rate of 20 mV·s^{-1} at 298 K. The voltammograms were independent of the electrolyte homogenization on the electrode surface, before the chlorine evolution reaction, and therefore were carried out in electrolyte without stirring.

Polarization curves

Polarization curves analyses were performed to a dataset of the voltammograms obtained exclusively in the chlorine evolution reaction around 1.20 V *vs.* SHE, and 1.60 V *vs.* SHE, at a scan rate of 10 $mV \cdot s^{-1}$. In this technique, the working electrode was not exposed to reverse electric current, which could contribute to the deactivation of the electrode surface.

Data evaluation from polarization curves

The electric potential-current density measurements (*E vs. j*) were made to quantitatively describe the electrochemical performance of a membrane electrolysis cell or an individual compartment of the cell. For the anodic part, the *E vs. j* curve is described by Equation (4.15).

$$E = E_{\mathrm{rev}} + \eta_a + R_\Omega \cdot j \tag{4.15}$$

where E_{rev} is the reversible potential on the operating conditions, R_Ω is the ohmic resistance of the system and η_{a} correspond to the activation overpotential of the anodic electrode. The Tafel slope analysis leads to two crucial parameters: the Tafel slope and the exchange current density. The Tafel slope provides insights concerning the reaction mechanism for different operating conditions, and the exchange current density is associated to the catalytic activity [20], which were obtained by the η *vs.* log *j* relationship to high overpotentials:

$$\eta_a = b \cdot \log\left(\frac{j}{j_{\mathrm{rev}}}\right) \tag{4.16}$$

where j is the current density and j_{rev} the exchange current density. The Tafel slope, b, can be also decomposed on Equation (4.17).

$$b = \ln 10 \cdot \frac{R \cdot T}{\alpha \cdot F \cdot n} \tag{4.17}$$

Equation (4.17) includes the universal gas constant, $R = 8.314$ $J \cdot mol^{-1} \cdot K^{-1}$, the temperature, T, the number of electrons involved in the reaction, n, the electron transfer coefficient for the chlorine evolution, α, and Faraday's constant, $F = 96485$ $C \cdot mol^{-1}$.

To obtain the overpotential values, it is first necessary to subtract the ohmic resistance of the *E vs. j* curves analysis and calculate the reversible potential. The ohmic resistance, R_Ω, is related to the mass transport limitations of reactants to the anode surface, and consecutive gas bubbles accumulation. Both effects become significant at high current densities because a higher demand of reactants and removal of products are needed to have a similar composition on the electrode to the bulk. This becomes more difficult with the increase of current density and it is needed to remove these limitations from the value analysis. Combining the Equations (4.15) and (4.16), the R_Ω is estimated from the first derivate of the potential with the respect to the current density, in the chlorine evolution range:

$$\frac{dE}{dj} = \frac{b}{j} + R_\Omega \tag{4.18}$$

The reversible half-cell potential of the chlorine evolution, E^0_{CER}, is only useful under standard-state conditions, namely room temperature, atmospheric pressure, and unit activities of all species. For non-standard-state conditions, the reversible potential is affected by operating temperature, as expressed by Equation (4.14), and the influence of the contributions from reactant activity (indirectly, concentration) and the product pressures, which is expressed by Nernst equation [18]. In summary, the reversible potential is estimated for the specific operating conditions and the electrolyte compositions using Equation (4.19).

$$E_{\mathrm{rev}} = E^0_{\mathrm{CER}} + \frac{\Delta\hat{s}}{n \cdot F} \cdot (T - T_0) + \frac{R \cdot T}{n \cdot F} \cdot ln\left(\frac{{a_{\mathrm{Cl_2}}}^{n/2}}{{a_{\mathrm{Cl^-}}}^{n}}\right) \tag{4.19}$$

where, $a_{\mathrm{Cl_2}}$ correspond to the partial pressure of chlorine gas and $a_{\mathrm{Cl^-}}$ is the activity of the chloride anion, which is obtained to ASPEN simulation for each specific test electrolyte composition and temperature.

4.3 RESULTS AND DISCUSSION

4.3.1 Cyclic voltammetry

a) Scan rate

The voltammograms allow to identify the peaks of current density which are related to the solid-state surface redox transition of active species, If the oxidized/reduced species are at the electrode surface (reaction not limited by the diffusion), the peak of the current density should increase linearly with the scan rate [18]. In this case, the current density of the peak is proportional to the square root of the scan rate.

The cyclic voltammograms of the DSA®, obtained with an electrolyte solution of 5.0 M NaCl and pH 2 (acidified with HCl) for a scan rate between 10 and 200 $mV \cdot s^{-1}$, in the potential region from 0 to 1.25 V *vs.* SHE, are shown in Figure 4.3.

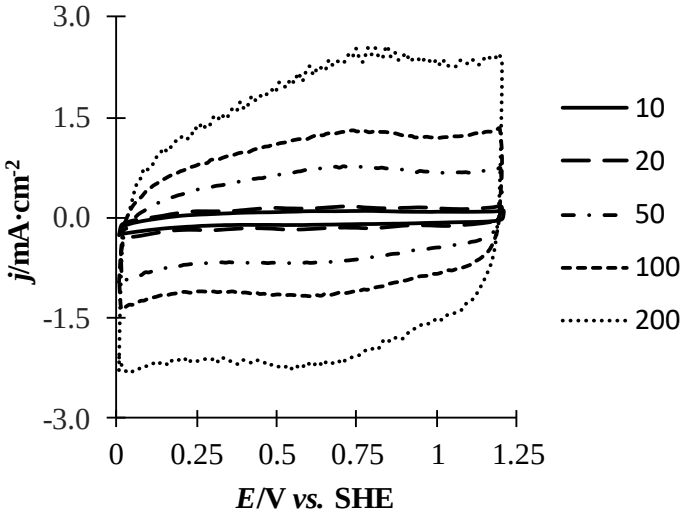

Figure 4.3 Voltammograms obtained for a DSA® inserted in an electrolyte solution of 5.0 M NaCl and pH 2 (acidified with HCl), at room temperature and for a scan rate from 10 to 200 $mV \cdot s^{-1}$.

Figure 4.3 shows two peaks of current density, the first near to 0.75 V *vs.* SHE and the second for E > 1.15 V *vs.* SHE. The first peak should be related to the Ru^{3+}/Ru and Ir^{3+}/Ir^{4+} surface redox reactions, while the second peak should be related to the Ru^{3+}/Ru^{4+} redox reaction [21, 22]. For the first peak at *ca*. 0.75 V *vs.* SHE, the current density for the anode, $j_{pa,}$ and the cathode part, j_{pc}, are plotted as a function of the scan rate in Figure 4.4A and as a

function of the square root of the scan rate in Figure 4.4B. From this experiment it is not possible to state clearly that chemical reaction, and not the mass transport, is the limiting mechanism. Still, the literature indicates that reaction 4.19 is a surface reaction and then the chemical reaction should be the limiting mechanism [21, 22].

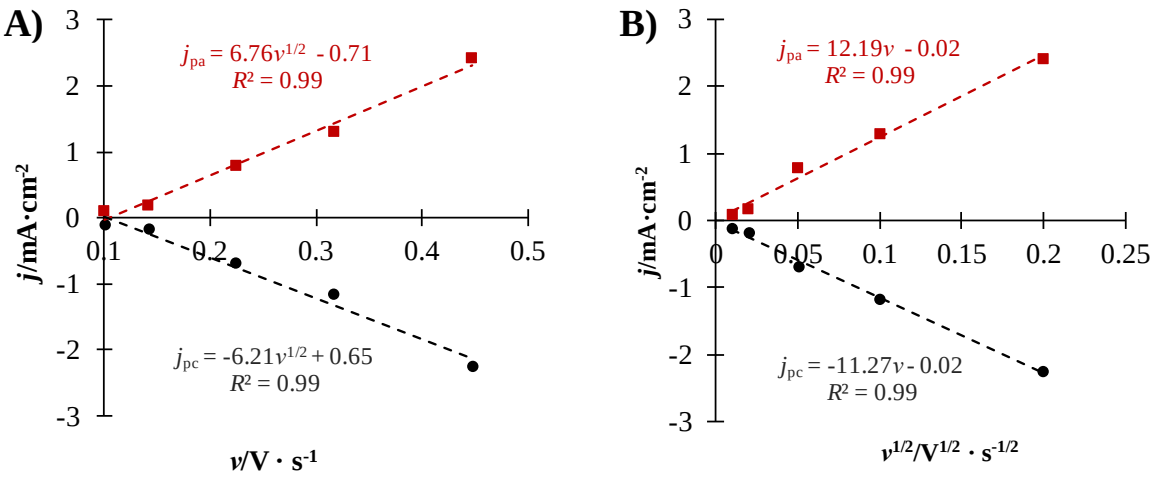

Figure 4.4 First peak of current density relative to oxidation (red) and reduction (black) as a function of: A) scan rate; B) square root of the scan rate .

Figure 4.5 plots four voltammograms at a scan rate of 20 mV·s^{-1}, where the high reproducibility of the reads can be observed.

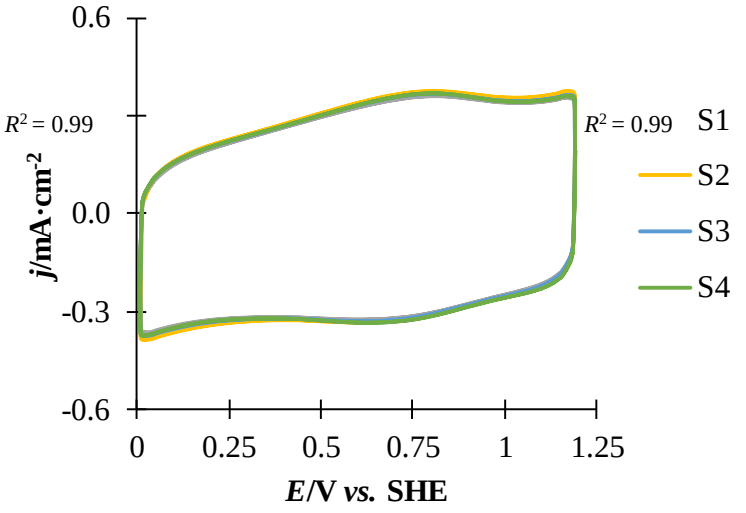

Figure 4.5 Repeatability of the voltammograms obtained for DSA® and electrolyte with 5.0 M NaCl, and pH 2 (acidified with HCl), room temperature, and a scan rate of 20 mV·s^{-1}.

b) Effect of the sodium chloride concentration

As was already mentioned, the interactions between the electrolyte and the metal oxides on the surface of the electrodes are relevant for the initial stage of the chlorine evolution reaction. Figure 4.6 presents six voltammograms as a function of the NaCl concentration, from 2.50 M to 5.0 M. As chloride ions concentration increases the exchange current density associated to the metal oxide transitions, potentials of ca. 0.75 V *vs.* SHE (on the first peak) and 1.20 V *vs.* SHE (on the second peak), get smaller, which is desirable to accelerate the chlorine evolution kinetics rates.

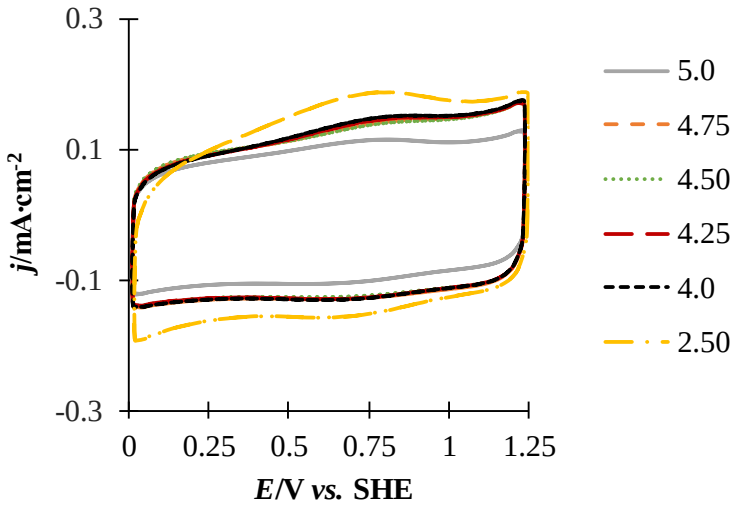

Figure 4.6 Voltammograms obtained for DSA® and electrolyte with NaCl concentrations increasing between 2.50 and 5.0 M, pH 2 (acidified with HCl), room temperature, and a scan rate of 20 $mV \cdot s^{-1}$.

c) Effect of the sodium chlorate concentration

Figure 4.7 plots five voltammograms for sodium chlorate concentrations, from 0 to 1.0 M. It can be observed that for higher concentrations of this contaminant, the peaks are smaller meaning that the redox ruthenium reaction develops to a smaller extent, so the active sites are unavailable to catalyse the chlorine evolution.

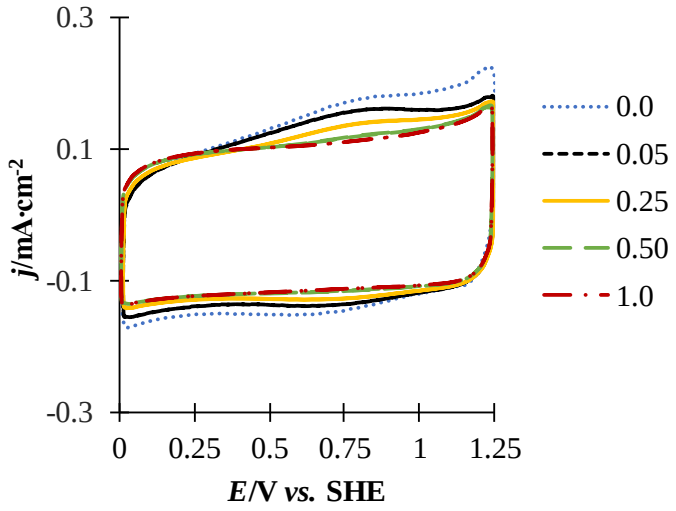

Figure 4.7 Voltammograms obtained for DSA® and electrolyte with 5.0 M NaCl and pH 2 (acidified with HCl), $NaClO_3$ concentration from 0.0 to 1.0 M, room temperature, and a scan rate of 20 $mV \cdot s^{-1}$.

d) Effect of the electrolyte pH

Equation 4.11 shows that the ruthenium oxidation depends linearly on the concentration of H^+. For lower pH values, and consequently higher H^+ concentrations, the electric potential associated of this oxidation transition increases. Figure 4.8 shows the cyclic voltammograms obtained to a DSA® contacting a concentrated sodium chloride solution, 5.0 M NaCl, at different pH values between 1 and 7. In this case, additional experiments were performed, between pH 2 and 4.5, which corresponded to the optimal pH range condition for the chlorine evolution.

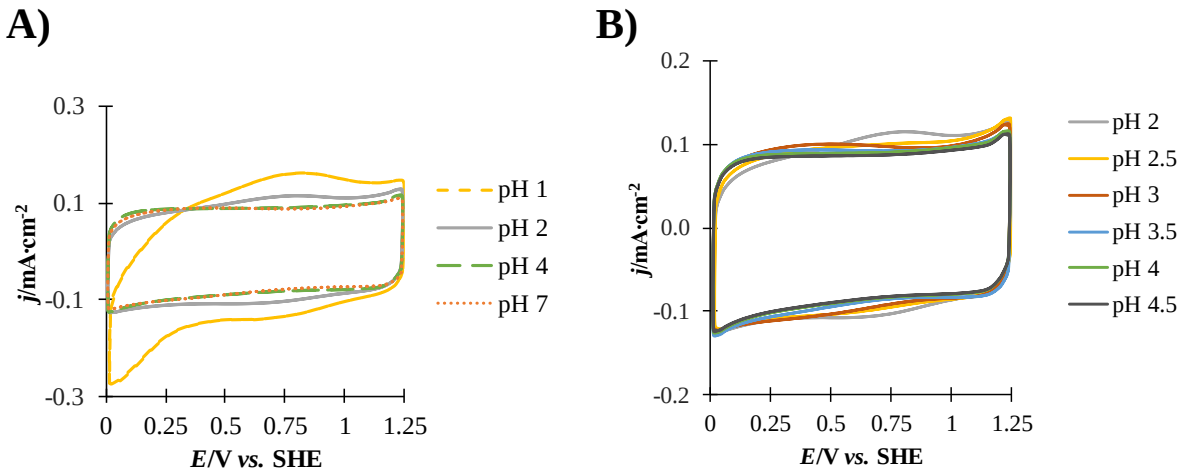

Figure 4.8 Voltammograms obtained for DSA® and electrolyte with 5.0 M NaCl and pH 2 (acidified with HCl), room temperature, and a scan rate of 20 $mV \cdot s^{-1}$: A) pH between 1 and 7; B) pH between 2 and 4.5, corresponding to the chlorine evolution reaction range.

From Figure 4.8A, it can be observed that Ru^{3+}/Ru transition peak is more pronounced for more acidic solutions. At pH = 1, the H^+ concentration is so high that the reduction of H^+ to H_2 is highly preferred, corresponding to 0.0 V *vs.* SHE, and the voltammogram shows a peak at this potential for the H^+ reduction. Figure 4.8B, obtained for the pH range, within which the chlorine evolution is more pronounced, shows a Ru^{3+}/Ru peak deviation to lower electric potentials as the pH increases. Regarding the current density peak related to the Ru^{3+}/Ru^{4+} pair, there are no noticeable changes.

4.3.2 Predicting reversible electrode potential

The reversible electrode potential predicted, for each group of operating conditions, was calculated using Equation (4.19), and it is shown in Table 4.2.

The reversible electrode potential was computed using the activities of the chloride and chlorine species obtained for each operating condition using ASPEN; It was considered that the approximation of the pressure felt on the electrode surface could be like that of the electrolyte, that accounted for the water vapour pressure of the solution at each temperature. If he reactor were completely isolated or under a slow vacuum, without agitation and high current density forming significant amounts of gases that immediately dissolve in the electrolyte, as usual in the industrial process, the water vapour pressure could already have significant impact in the reversible potential [23].

As it can be seen in Table 4.2, almost all conditions indicate a reversible potential of *ca*. 1.20 V *vs.* SHE, which agrees with the values presented in the literature, based on the conversion of the reference electrode value to the respective temperatures [6-8, 10, 11, 14]. However, the two parameters with the largest influence of the reversible potential electrode are sodium chloride concentration and temperature. Temperature is the parameter that presents the largest influence, e.g. 1.32 V *vs.* SHE at 298 K and 1.21 V *vs.* SHE at 358 K and followed by the NaCl concentrations where the reversible potential is 1.26 V *vs.* SHE for sodium chloride concentrations equal to 2.50 M and 1.23 V *vs.* SHE for 5.20 M, directly related to the variation of chloride activity. From the values obtained, it is apparent that for higher pH ranges, the reversible potentials obtained based on concentrations and activity coefficients are closer compared with more acidic solutions.

Table 4.2 Reversible electrode potential of the chlorine evolution, E_{rev}, and the respective auxiliary parameters for each group of tests (standard operating condition, S, sodium chloride concentration, [NaCl], sodium chlorate concentration, [$NaClO_3$], electrolyte pH and temperature, *T*.

Effect studied		$\boldsymbol{\rho}$ **(kg · dm^{-3})**	$\boldsymbol{a_{Cl^-}}$	$\boldsymbol{a_{Cl_2}}$	$\boldsymbol{E_{rev}}$ **(V *vs.* SHE)**
Standard Condition	S	1162	4.99	0.55	1.23
[NaCl] (M)	2.50	1075	1.88	0.55	1.26
	4.0	1128	3.57	0.55	1.25
	4.25	1137	3.91	0.55	1.24
	4.50	1145	4.25	0.55	1.24
	4.75	1154	4.61	0.55	1.24
	5.20	1169	5.30	0.55	1.23
[$NaClO_3$] (M)	0.0	1154	4.90	0.55	1.24
	0.05	1157	4.93	0.55	1.24
	0.25	1170	5.10	0.55	1.23
	0.50	1186	5.32	0.55	1.23
	1.0	1217	5.79	0.55	1.23
Electrolyte pH	0	1176	6.85	0.55	1.23
	4	1162	4.96	0.55	1.24
	7	1162	4.96	0.55	1.24
	9	1162	4.96	0.55	1.24
T (K)	298	1154	4.86	0.98	1.32
	343	1158	4.93	0.72	1.26
	348	1162	6.03	0.64	1.25
	358	1170	5.09	0.47	1.24
	363	1193	5.18	0.35	1.23

*S: 5.0 M NaCl, 0.11 M NaClO3, pH 2 (acidified with HCl) and 353 K.

4.3.3 Polarization curves

This section reports the polarization curves obtained with the DSA® electrode in different solutions where the effect of a) NaCl concentration; b) $NaClO_3$ concentration; c) electrolyte pH and d) temperature were studied.

a) Effect of the sodium chloride concentration

Figure 4.9 shows the polarization curves for different concentrations of sodium chloride, between 2.50 M and 5.20 M.

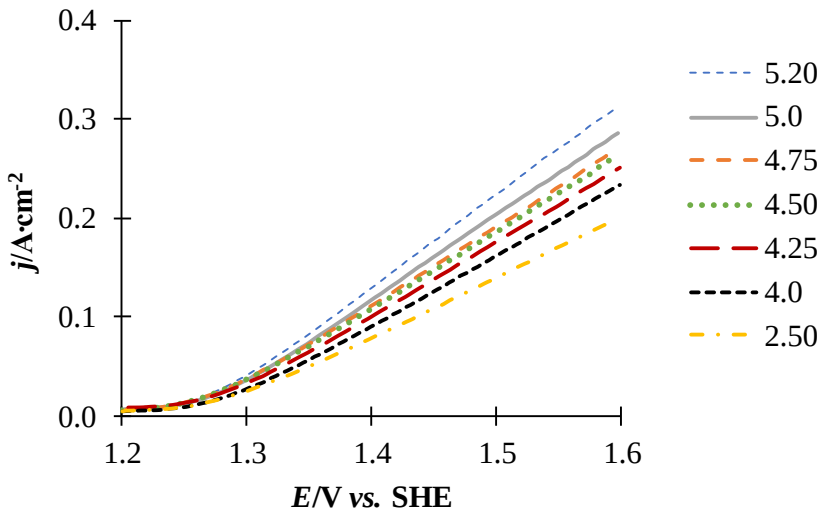

Figure 4.9 Polarization curves obtained for an electrolyte with different NaCl concentration (between 2.50 M and 5.20 M); the other conditions were 0.11 M $NaClO_3$ and pH 2 (acidified with HCl) at 353 K.

The pH of the electrolyte was set to 2 for minimizing the effect of oxygen evolution. The following discussion assumes that, within the analyzed potential range, the CER prevails and then the observed current density variations depend exclusively on the chlorine evolution kinetics. By increasing the NaCl concentration the corresponding current density increases, which is related to the decrease of the reversible potential balanced by the increase of the ohmic overpotential related to the increase of the gas hold-up. Above a given threshold, the evolution of the bubbles imposes a substantial increase in the electrolyte ohmic overpotential, which imposes a practical limit to the maximum current density. Table 4.3 shows the parameters determined from the polarization curves of Figure 4.9.

Table 4.3 Parameters of the polarization curves analysis for electrolytes with different NaCl concentrations (between 2.50 M and 5.20 M); the other conditions were: 0.11 M $NaClO_3$ and pH 2 (acidified with HCl) at 353 K.

[NaCl] (M)	a_{Cl^-}	E_{rev} **(V *vs.* SHE)**	R_Ω **(Ω)**	b **(mV)**	j_{rev} **(mA·cm^{-2})**	α
5.20	5.3	1.23	1.0	46	4.6	0.76
5.0	5.0	1.23	0.9	47	4.9	0.75
4.75	4.6	1.23	1.1	48	6.1	0.74
4.50	4.3	1.23	1.1	49	7.3	0.72
4.25	3.9	1.23	1.1	49	6.0	0.72
4.0	3.6	1.25	1.2	50	6.9	0.71
2.50	1.9	1.26	1.4	53	14.9	0.67

The Tafel slope obtained ranged from 53 mV for 2.50 M to 46 mV for 5.20 M NaCl. For the reference operating conditions, 5.0 M NaCl, the estimated Tafel slope was 47 mV, which is just above the 45 mV mentioned by Nylén [11].

A linear relationship between the E_{rev} and ln[NaCl] with a slope of approximately -99 mV/decade Cl^- concentration and an intercept around 1.28 V *vs*. SHE was obtained [10, 11]. These values are similar to the ones obtained by Nylén and Cornell *et al*. [10, 11], for the concentration range and for two different electrolyte pHs; these researchers obtained -90 mV/decade Cl^- concentration and an intercept around 1.30 V *vs*. SHE. Since the present work was done with an industrial brine, this observation indicates that the possible contaminants of the solution are not relevant for the CER kinetics; this is an important result allowing for comparing the results obtained with those reported in the literature. However, the Tafel slope was obtained based on Cl^- concentration but more accurate values can be obtained if chemical activities are used. Figure 4.10 shows the individual trends between the kinetic parameters (A - E_{rev}; B - j_{rev}, C - b, D - α) and activity of Cl^-, following relationship established by Equation (4.18) and the data presented in Table 4.3.

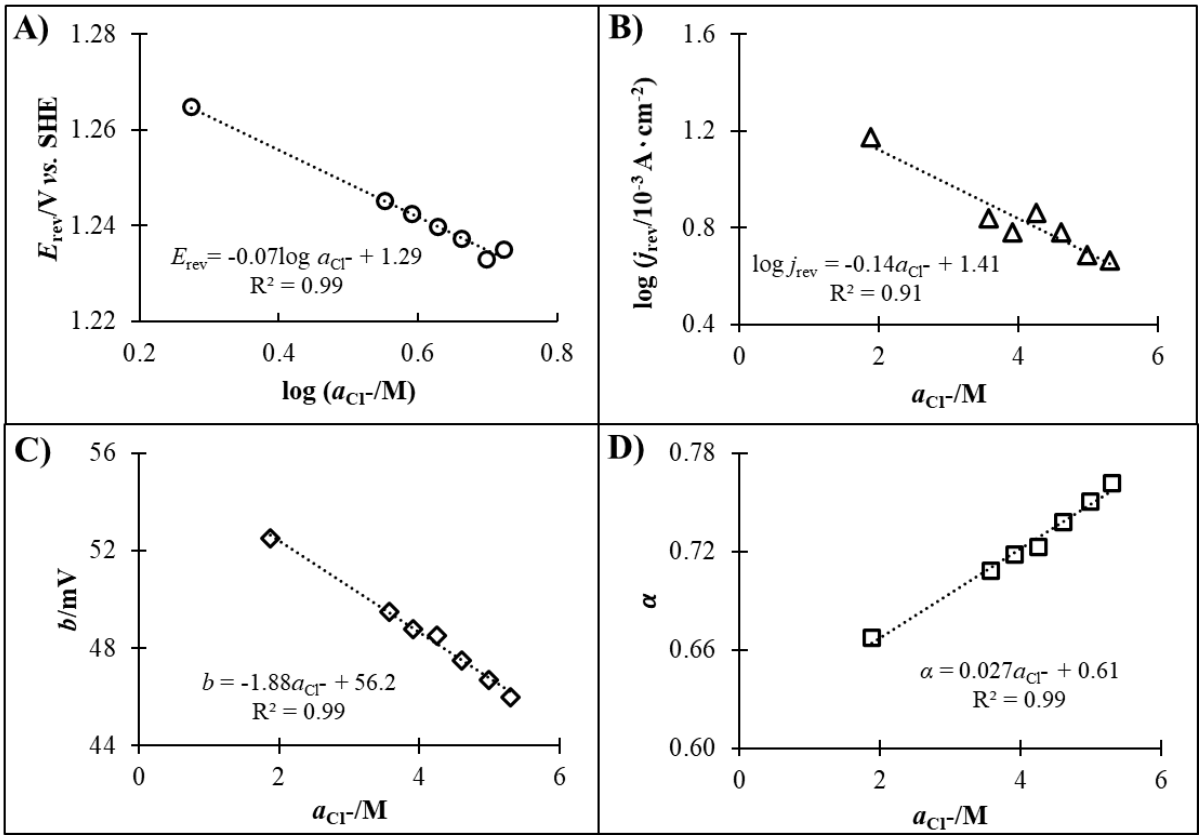

Figure 4.10 A) Reversible potential, E_{rev}, as a function of the logarithm of the chloride activity, a_{Cl^-}; B) The logarithm of exchange current density, j_{rev}, as a function of a_{Cl^-}; C) Tafel slope, b, as a function of a_{Cl^-}; D) Charge transfer coefficient, α, as a function of a_{Cl^-}. Data from Table 4.3 correspondent to the effect of the sodium chloride concentration.

The E_{rev} dependence for the analysed NaCl concentrations as a function of the Cl^- activities shows a slope *ca*. -70 mV/decade of chloride activity, is now rather different from the previous result (a slope equal to -99 mV/decade Cl^- concentration), which indicates that activities and not concentrations should be used for this system; the interception value, 1.28 V *vs*. SHE, is, however, like the previous one. Figure 4.10B shows that the exchange current density does not change much, except for the most diluted solution. Figure 4.10C and Figure 4.10D give the Tafel slope and charge transfer coefficient where the determination coefficient is quite high, indicating a very good correlation. The value estimated for the standard condition was 0.76 which agrees with the results obtained by Silva [24].

b) Effect of sodium chlorate concentration

In the chlor-alkali process, the main parasitic reaction is the production of $NaClO_3$. The effect of its presence at the anode side was therefore studied. To a 5.0 M NaCl solution, prepared with pure salt, different concentrations of $NaClO_3$ were added, its range between 0.0 M to 1.0 M; normally, the maximum concentration of $NaClO_3$ which can be found at the process feed is *ca.* 0.1 M. The obtained polarization curves are presented in Figure 4.11.

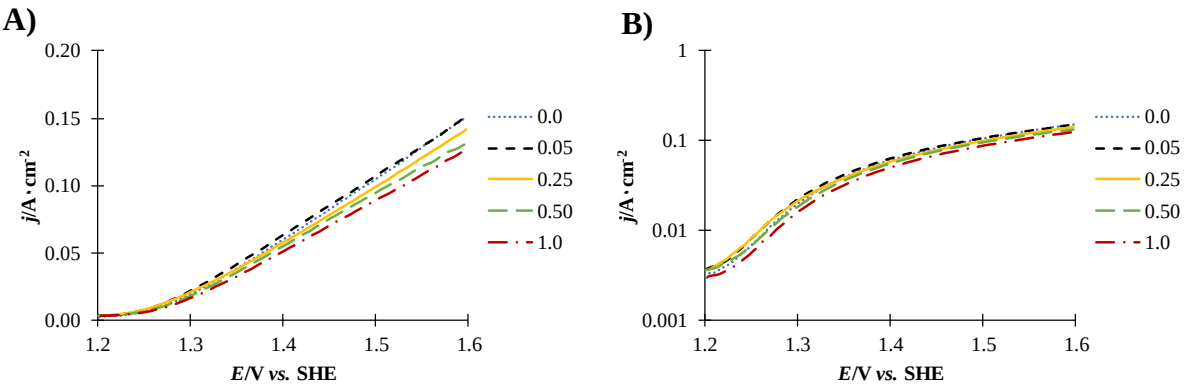

Figure 4.11 Polarization curves obtained for an electrolyte with different $NaClO_3$ concentration (between 0.0 M and 1.0 M); the other conditions were: 5.0 M NaCl and pH 2 (acidified with HCl) at 353 K. The exchange current density, j_{rev}, is shown in two scales: A) normal; B) semi-logarithmic.

The chlorine evolution over the oxygen is favoured for low $NaClO_3$ concentration and pH from 2 to 3 – acidified solutions. In the present case, the pH of the solution was 2 so the OER was suppressed and any deviations should be associated with the CER kinetics. As it can be seen in Figure 4.11B, no significant changes are observed in the current density, *j*, obtained for low potentials, which is different from what was observed by Cornell *et al.* but these authors kept the pH at 6.5, where the oxygen evolution is promoted [10].

Table 2 shows that the kinetic parameters display minor variations for the $NaClO_3$ concentration range studied.

Table 4.4 Parameters of the polarization curves analysis for electrolytes with different $NaClO_3$ concentrations (0.0 to 1.0 M), 5.0 M NaCl and pH 2 at 353 K.

[$NaClO_3$] (M)	a_{Cl^-}	E_{rev} (V *vs.* SHE)	R_Ω (Ω)	b (mV)	j_{rev} (mA·cm^{-2})	α
0.0	4.9	1.24	1.0	46	9.2	0.76
0.05	4.9	1.24	1.0	46	7.6	0.76
0.25	5.1	1.23	1.1	47	7.2	0.74
0.50	5.3	1.23	1.1	48	5.0	0.73
1.0	5.8	1.23	1.1	49	3.2	0.72

Table 4.4 shows that the kinetic parameters display minor variations for the $NaClO_3$ concentration range studied. For the exchange current density, j_{rev}, the values obtained were between 7.6 and 3.2 mA · cm^{-2}. Excluding the value for the pure NaCl solution, which deviates greatly from the others (correspondent to 4.9 mA · cm^{-2}), the current density decreased with the chlorate concentration in the system. Figure 4.12 shows the trends of the kinetic parameters as a function of the chloride activity.

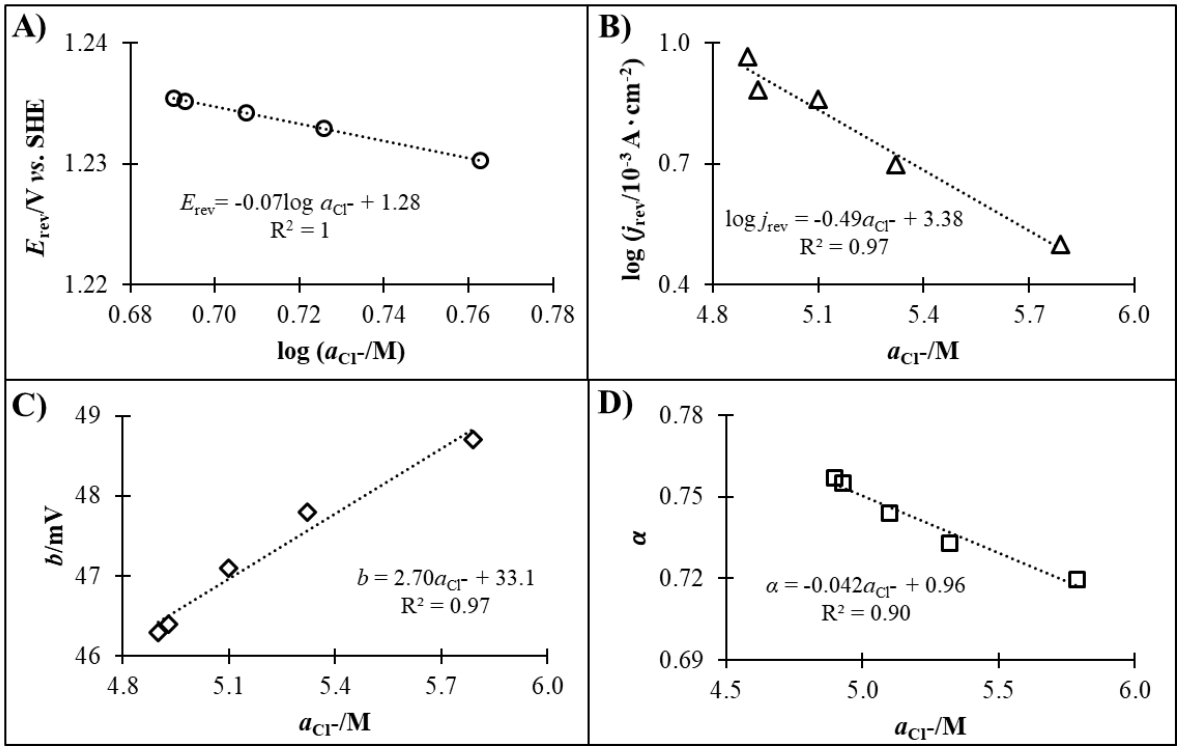

Figure 4.12 A) Reversible potential, E_{rev}, as a function of the logarithm of the chloride activity, a_{Cl^-}; B) The logarithm of exchange current density, j_{rev}, as a function of a_{Cl^-}; C)Tafel slope, b, as a function of a_{Cl^-}; D) Charge transfer coefficient, α, as a function of a_{Cl^-}; Data from Table 4.4 correspondent to the effect of the sodium chlorate concentration.

As discussed previously, E_{rev} *vs.* a_{Cl^-} is very similar to that observed in the study of the effect of NaCl concentration (Figure 4.12A), approximately -70 mV/dec a_{Cl^-}. Since the solutions were acidified, with a pH *ca*. 2, CER is favoured over the OER, and the production of more $NaClO_3$ is prevented. On the other hand, the feed concentration of $NaClO_3$ is too low to hinder the CER by occupying active sites at the catalyst surface. Additionally, it was observed that for a highest concentrated solution (*ca.* 1.0 M $NaClO_3$) than the one normally observed in the feed, the Tafel slope increases from 46 mV to 49 mV and j_{rev} decreases from *ca*. 9.2 mA·cm^{-2} to 3.2 mA·cm^{-2} indicating that $NaClO_3$ is already occupying active sites and producing oxygen by decomposition of chlorates.

c) Effect of the electrolyte pH

Figure 4.13 plots the polarization curves for a 5.0 M NaCl, 0.11 M $NaClO_3$ electrolyte at 353 K with pH varying between 0 and 9; Figure 4.13A displays the polarization curves in linear coordinates while Figure 4.13B displays in semi-logarithmic coordinates.

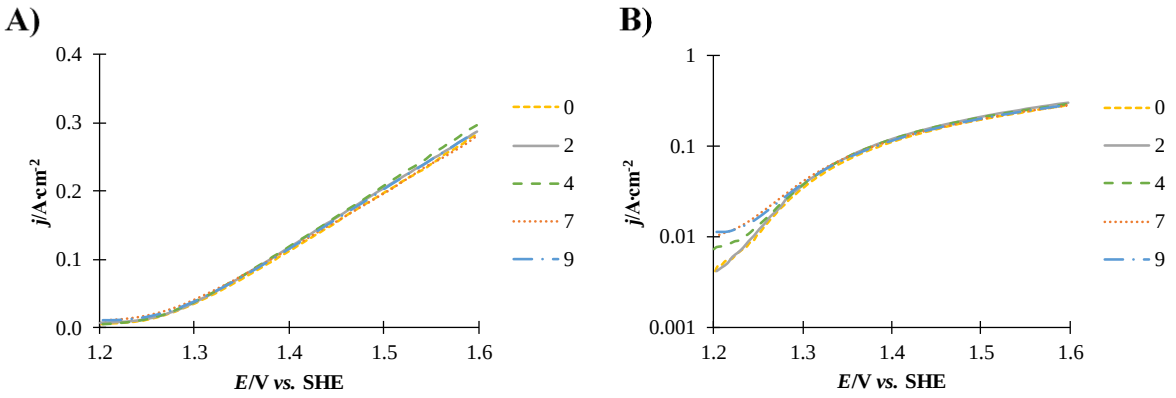

Figure 4.13 Polarization curves obtained for an electrolyte with different electrolyte pH (between 0 and 9 adjusted with HCl); the other conditions were 5.0 M NaCl, 0.11 M $NaClO_3$ and at 353 K. The exchange current density, j_{rev}, is represented in two scales: A) normal; B) semi-logarithmic.

The polarization curves show noticeable differences at low potentials, E < 1.25 V *vs.*SHE, for different concentrations of H^+ / pH values, as evidenced in Figure 4.13B. This region corresponds to a transition between the OER and CER dominant mechanisms, and the water oxidation can be significantly retarding the chlorine evolution, as previously discussed. However, for high potentials, CER is the main reaction, depending only indirectly on the pH value as it affects the oxidation state of ruthenium catalyst, as suggested by Fernandéz *et al*. [6-8, 11]; the pH has only a noticeable effect when it is low enough (pH < 2) – see Figure 4.13A.

Table 4.5 shows the parameters determined by the data analysis of Figure 4.13 for the effect of electrolyte pH.

Table 4.5 Parameters of the polarization curves analysis for electrolytes with different electrolyte pH (between 0 and 9); other conditions are: 5.0 M NaCl, 0.11 M $NaClO_3$ and at 353 K.

pH	a_{Cl^-}	E_{rev} **(V *vs.* SHE)**	R_Ω **(Ω)**	***b*** **(mV)**	j_{rev} **(mA·cm^{-2})**	***α***
0	6.85	1.23	1.0	40	1.9	0.88
2	4.99	1.24	1.0	47	4.6	0.75
4	4.96	1.24	0.9	49	4.7	0.72
7	4.96	1.24	1.0	66	8.1	0.53
9	4.96	1.24	1.0	69	7.3	0.50

From Table 4.5 it can be highlighted that the main differences were obtained for the most acidified solution, pH = 0 when the activity of Cl^- is seriously affected by high H^+ concentration. It should be emphasized that j_{rev} and b values increase with the pH for pH > 4 and for the same Cl^- activity. In the case of 2 < pH < 4, the polarization curve is mostly independent of the pH; for pH > 4, the polarization curves are independent of the pH. Figure 4.14 shows the kinetic parameters for different pH values or H^+ activities and Table 4.6 presents the results of the analysis of the previous polarization curves.

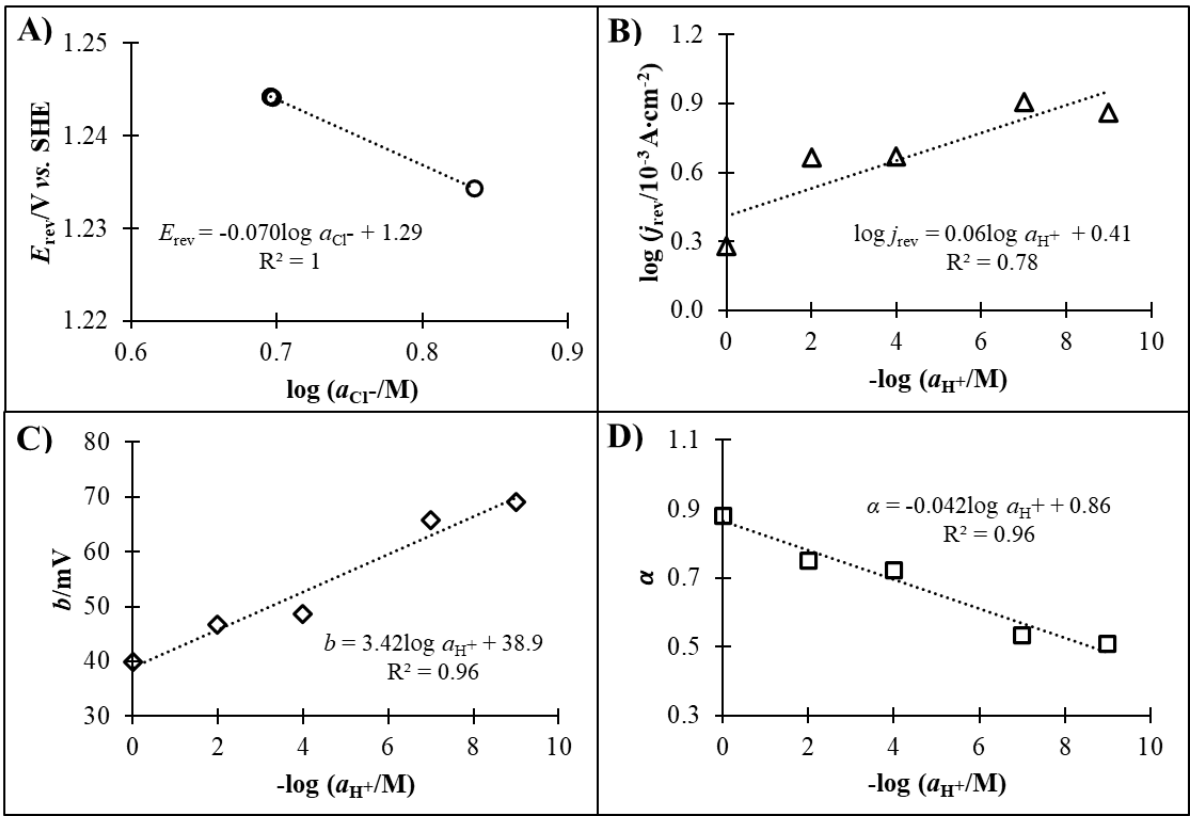

Figure 4.14 A) Reversible potential, E_{rev}, as a function of the logarithm of chloride activity, a_{Cl^-}; B) The logarithm of exchange current density, j_{rev}, as a function of the logarithm of chloride activity, a_{Cl^-}; C) Tafel slope, b, as a function of - log a_{H^+} or pH; D) Charge transfer coefficient α, as a function of -log a_{H^+}. Data from Table 4.5 correspondent to the effect of the electrolyte pH.

For pH > 2 it is observed that E_{rev} is constant with the activity of Cl^-; for pH = 0, E_{rev} decreases substantially. On the other hand, the current density, j_{rev}, is pH dependent for pH > 4 and for the same activity of Cl^-; j_{rev} changes also for different activities of Cl^-.

Figure 4.14C shows the Tafel slope coefficient as a function of the pH while Figure 4.14D presents the charge transfer coefficient, also as a function of the pH. At pH = 9, a Tafel slope of *ca*. 60 mV was reported [25]. It is known that the Tafel slope value characteristic of the OER is 60 mV for acidic solutions or 120 mV for the basic solutions (pH > 7); the Tafel slope value characteristic of the CER is 40 mV [25]. At pH = 9, b = 69 mV, the CER should compete already with the OER [25]. This observation is further reinforced by the decrease in the correspondent charge transfer coefficient value.

d) Effect of temperature

The effect of temperature on the NaCl electrolysis was investigated using the reference electrolyte solution (5.0 M NaCl, 0.11 M $NaClO_3$ at pH = 2), at different temperatures between 298 K and 363 K; Figure 4.15 plots the obtained polarization curves.

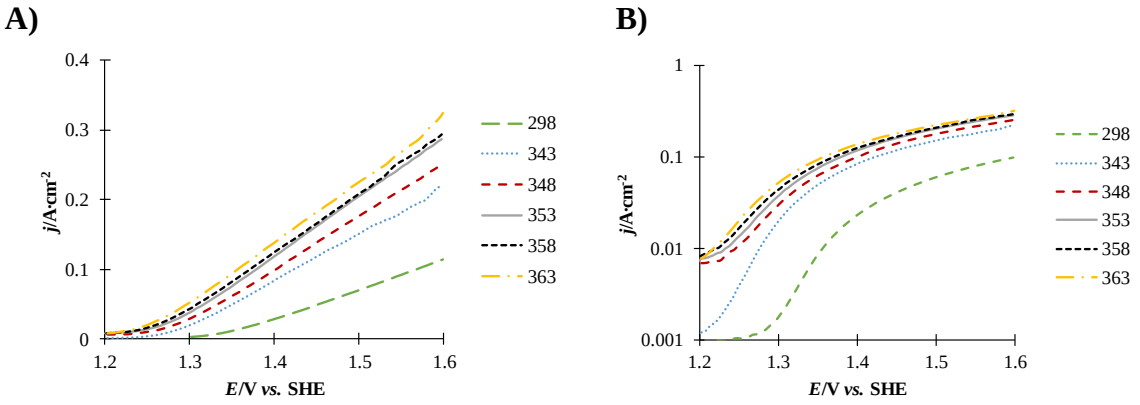

Figure 4.15 Polarization curves obtained for an electrolyte at different temperatures (between 298 and 363 K); the other conditions were 5.0 M NaCl, 0.11 M $NaClO_3$ and pH 2 (acidified with HCl), at two different scales: A) normal; B) semi-logarithmic.

Figure 4.15A shows that for 298 K E_{rev} is 1.3 V, a value higher than previously observed at 353 K – 1.25 V *vs.* SHE – as expected. On the other hand, the current density decreases substantially for 298 K, following a reaction exponential decrease with the temperature; these results are in agreement with those reported by Nylén. [11].

Table 4.6 Parameters of the polarization curves analysis for electrolytes with different temperatures (between 298 and 363 K); the other conditions were: 5.0 M NaCl, 0.11 M $NaClO_3$ and pH 2.

T (K)	a_{Cl^-}	E_{rev} (V *vs.* SHE)	R_Ω (Ω)	b (mV)	j_{rev} (mA·cm^{-2})	α
298	4.9	1.32	2.0	39	3.3	0.76
343	4.9	1.26	1.2	45	4.3	0.75
348	5.0	1.25	1.1	46	6.7	0.75
353	5.0	1.24	1.0	47	7.1	0.75
358	5.1	1.24	1.0	47	7.7	0.75
363	5.2	1.23	0.9	48	8.3	0.75

From Table 4.6 it can be concluded that at room temperature the ohmic resistance, which is required to be exceeded and, consequently, the oxidation of chloride to chlorine rate is lower. It is also evident that, the E_{rev} decreases with the increasing temperature and j_{rev} increases directly, which are the parameters most affected by this parameter. The filled symbol has been excluded from the linear relationship – an outlier.

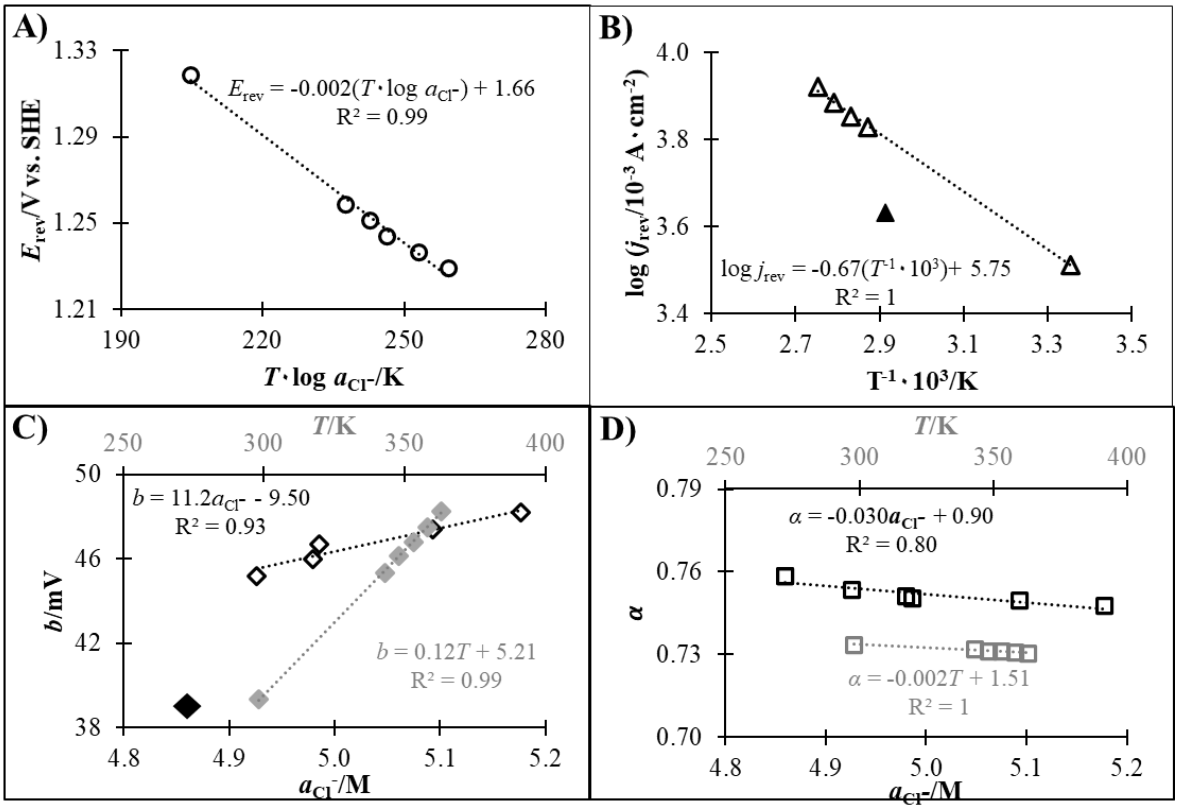

Figure 4.16 A) Reversible potential, E_{rev}, as a function of the product between the temperature, T, and the logarithm of the chloride activity, a_{Cl^-}; B) The logarithm of exchange current density, j_{rev}, as a function of T; C) Tafel slope, b, as a function of a_{Cl^-} and T; D) Charge transfer coefficient α, as a function of $a_{Cl^-}$and T. Data from Table 4.6 correspondent to the effect of the temperature.

Figure 4.16 shows the trends between the data of Table 4.6 at different temperatures. E_{rev} depends on the temperature directly and through the Cl^- activity, as indicated by Equation (4.13). A similar effect is observed for the Tafel slope, b, and for the charge transfer coefficient, α, which depends directly on the temperature and through Cl^- activity, as indicated by Equation (4.16).

4.4 CONCLUSIONS

Polarization curves on commercial DSA® anodes in different electrolytes were obtained between 1.20 and 1.60 V *vs.* SHE. A parametric study was performed to analyse the effect of the electrolyte composition (sodium chloride concentration, sodium chlorate concentration, and electrolyte pH) and the temperature. The mass transport limitations were minimized using a mechanical stirred on the electrode surface and an adequate reactor design, permitting the analysis of the electrochemical kinetics. For a potential of *ca*. 1.25 V *vs.* SHE, so-called reversible electrode potential, it was identified a bend in the polarization curve assigned to the oxidation of the active sites, namely ruthenium intermediate species. This observation was also supported by the cyclic voltammetry analysis and reported by several authors; it is related to the first step mechanism of the chlorine evolution reaction which depends on the pH of the electrolyte (H^+ activity).

The variation of the chloride oxidation kinetic parameters (exchange current density and the charge transfer coefficient) obtained was analysed taking into account the activity of ions Cl^- and H^+, and temperature, using the polarization curves results. The interception value obtained is equal to 1.28 V *vs.* SHE and the charge transfer coefficient is around 0.75, for the standard operating conditions. The reversible electrode potential decreases as the chloride activity increases, with a factor of -70 mV/decade of the chloride activity in acid solutions; the chloride activity increases with sodium and chlorate concentration. The pH of the electrolyte has an important effect on the reaction rate. If the solution has a pH below 2, the oxidation of the active sites of the DSA® electrode is inhibited and, consequently, the chlorine evolution is affected. In this study, for pH = 1 it the active sites did not change its oxidation state when performing the cyclic voltammetry analysis. However, when the pH was above 4, the Tafel slope obtained was higher than the 45 - 50 mV recorded for the remaining points, which was assigned to the oxygen evolution by parasite reactions that depend directly on the pH, namely by the water oxidation. Finally, it is observed that for 298 K, E_{rev} is 1.32 V *vs*. SHE, a higher value than previously observed at 353 K, namely 1.24 V *vs*. SHE and the current density also decreases with the temperature - according to the literature. However, a second analysis is performed because, in concentrated NaCl solutions, the chloride activity has a *J*-shape increase with the temperature, which corresponds to an opposite effect on the reversible potential. Temperature is also considered an important parameter for the process because it has a double effect on the chlorine evolution reaction.

4.5 NOTATION

	Description	Units
a_{Cl^-}	Activity of the chloride anion	M
a_{Cl_2}	Activity of the chlorine gas	M
b	Tafel slope	V
CER	Chlorine evolution reaction	-
DSA	Dimensionally stable anode	-
E	Cell potential	V
E^0_{CER}	Thermodynamic potential for chlorine evolution reaction	V
E^0_{OER}	Thermodynamic potential for oxygen evolution reaction	V
E_{rev}	Reversible cell potential	V
E_T	Reversible cell potential as a function of the operating temperature	V
F	Faraday constant	$C \cdot mol^{-1}$
j	Current density	$A \cdot m^{-2}$
j_{rev}	Reversible current density	$A \cdot m^{-2}$
k	*k*-factor value	Ω
N	Number of electrons involved in the electrode reaction	-
OER	Oxygen evolution reaction	-
R	Universal gas constant	$J \cdot K^{-1} \cdot mol^{-1}$
R_Ω	Ohmic resistance of the cell	Ω
$\Delta\hat{s}$	Entropy of the chemical reaction	$J \cdot K^{-1}$
SHE	Standard hydrogen electrode	-
[S]	Active site	-
T	Absolute temperature	K
T_0	Reference temperature	K
α	Charge transfer coefficient	-
η	Activation overpotential	V
η_a	Anodic activation overpotentials	V
z	Charge number	-

4.6 REFERENCES

1. EuroChlor, *How is chlorine produced*. (Available from: http://www.eurochlor.org/the-chlorine-universe/how-is-chlorine-produced.aspx, accessed 01/11/2019).

2. Sohrabnejad-Eskan, I., Goryachev, A., Exner, K. S., Kibler, L. A., Hensen, E. Hofmann, J. P., Over, H., *Temperature-dependent kinetic studies of the chlorine evolution reaction over RuO2(110) model electrodes.* ACS Catalysis, 2017. 7(4): p. 2403-2411.

3. Exner, K. S., Anton, J., Jacob, T., Over, H., *Full kinetics from first principles of the chlorine evolution reaction over a RuO2 (110) model electrode.* Angew Chem Int Ed Engl, 2016. 55(26): p. 7501-4.

4. Erenburg, R. G., Krishtalik, L. I., Bystrov, V. I., *Mechanism of chlorine evolution and ionization on a ruthenium oxide electrode.* Elektrokhimiya 1972. 8: p. 1740.

5. Trasatti, S., *Progress in the understanding of the mechanism of chlorine evolution at oxide electrodes.* Electrochimica Acta, 1987. 32: p. 369-382.

6. Fernandez, J., Gennero de Chialvo, M., Chialvo, A., *Kinetic study of the chlorine electrode reaction on Ti/RuO2 through the polarisation resistance Part I: experimental results and analysis of the pH effects.* Electrochimica Acta 4, 2002. 47: p. 1129–1136.

7. Fernandez, J., Gennero de Chialvo, M., Chialvo, A., *Kinetic study of the chlorine electrode reaction on Ti/RuO2 through the polarisation resistance Part II: mechanistic analysis.* Electrochimica Acta, 2002. 47: p. 1137–1144.

8. Fernandez, J., Gennero de Chialvo, M., Chialvo, A., *Kinetic study of the chlorine electrode reaction on Ti/RuO2 through the polarisation resistance Part III: proposal of a reaction mechanism.* Electrochimica Acta, 2002. 47: p. 1145–1152.

9. Kelly, E. J., Heatherly, D. E., Vallet, C. E., White, C. W., *Application of ion implantation to the study of electrocatalysis: I. chlorine evolution at Ru-implanted titanium electrodes.* Journal of Electrochemistry Society, 1987. 134: p. 1667-1675.

10. Cornell, A., Hakansson, B., Lindbergh, G., *Ruthenium based DSA in chlorate electrolysis critical anode potential and reaction kinetics.* Electrochimica Acta, 2003. 48: p. 473-481.

11. Nylén, L., *Critical potential and oxygen evolution of the chlorate anode*, in *Department of Chemical Engineering and Technology*. 2006, KTH – Chemical Science and Engineering: Stockholm.

12. Eberil, V. I., Fedotova, N. S., Novikov, E. A., Mazanko, A. F., *Studying the link between the potential of a metal-oxide anode, the current efficiency for chlorate, and the current losses for the oxygen and chlorine evolution in a wide range of the chlorate electrolysis conditions.* Russian Journal of Electrochemistry, 2000. 36: p. 1463-1470.

13. Karlsson, R., Cornell, A., *Selectivity between oxygen and chlorine evolution in the chlor-alkali and chlorate processes.* Chemical Reviews, 2016. 116(5): p. 2982-3028.

14. Karlsson, R., *Theoretical and experimental studies of electrode and electrolyte processes in industrial electrosynthesis*, in *KTH Royal Institute of Technology*. 2015, KTH Royal Institute of Technology: Stockholm.

15. O'Brien, T., Bommaraju, T., Hine, F., *Plant Commissioning and Operation*, in *Handbook of Chlor-Alkali Technology*, Springer, Editor. 2005: New York. p. 1217-1294.

16. Povar, I., Spinu, O., *Ruthenium redox equilibria: 3. Pourbaix diagrams for the systems Ru-H2O and Ru-Cl--H2O.* Journal of Electrochemical Science and Engineering, 2016. 6(1): p. 145.

17. Exner, K. S., Anton, J., Jacob, T., Over, H., *Controlling selectivity in the chlorine evolution reaction over RuO(2)-based catalysts.* Angewandte Communications 2014. 53(41): p. 11032-5.

18. O'Hayre, R., Cha, S. W., Colella, W., Prinz, F. B., *Fuel cell fundamentals*, in *Fuel cell fundamentals*. 2006, Wiley: New York.

19. Bommaraju, T., Chen, C., Birss, V. *Deactivation of thermally formed RuO2+TiO2 coatings during chlorine evolution: mechanisms and reactivation measures*, in *Modern chlor-alkali technology*. 2000, International Chlorine Symposium - Blackwell Science: UK.

20. Exner, K. S., Anton, J., Jacob, T., Over, H., *Microscopic insights into the chlorine evolution reaction on RuO2(110): a mechanistic initio atomistic thermodynamics study.* Electrocatalysis, 2014. 6(2): p. 163-172.

21. Jovanovic, V. M., Dekanski, A., Despotov, P., Nikoli, B. Z., Atanasoski, R. T., *The roles of the ruthenium concentration profile stabilizing component and the substrate on the stability of the oxide coatings.* Journal of Electroanalytical Chemistry, 1992. 339: p. 147-165.

22. Panic, V., Dekanski, A., Milonjic, S., Atanasoski, R., Nikolic, B., *RuO2-TiO2 coated titanium anodes obtained by the sol-gel procedure and their electrochemical behaviour in the chlorine evolution reaction.* Colloids and Surfaces, 1999. 157: p. 269-274.

23. Wendt, W., Kreysa, G., *Electrochemical thermodynamics*, in *Electrochemical engineering: science and technology in chemical and other industries*, Sringer, Editor. 2014.

24. Silva, J. F., *Study of dimensionally stable anodes for chlor-alkali electrolysis*, in *Chemical Engineering Department*. 2016, University of Porto.

25. Fang, Y., Liu, Z., *Mechanism and Tafel Lines of Electro-Oxidation of Water to Oxygen on RuO2 (110).* JACS, 2010. 132: p. 18214–18222.

5 GENERAL CONCLUSIONS

The most energy efficient technology for the electrolysis of NaCl is the membrane technology, which is used by Bondalti Chemicals S.A. In the past, the elements of the electrochemical membrane cells were improved, and new performance evaluation tools were developed to improve the process. However, scientific knowledge is still dominated by the suppliers of electrodes and membranes.

For the dimensionally stable anodes (DSA®), the final stage of service time can be critical, as energy consumption increases quickly from linearly to exponentially with time. On one hand, the risk of abrupt failure of the anodes in this final step is a critical point for the maintenance decision, with the anodes being replaced mainly according to the recommendations of the suppliers. On the other hand, the anode coating is made of a mixture of expensive metal oxides, such as ruthenium oxide, and the extension of its service life is, therefore, of great relevance for chlorine and alkali producers.

This work is divided in two parts: a data analysis focusing the potential and current density histories of an industrial chlor-alkali membrane electrolyser; and, an experimental parametric study of the chlorine evolution kinetics over DSA® anodes, which is related to the chlorine current efficiency of the process.

A methodology was proposed to follow the ageing of electrodes and membranes of the NaCl electrolysis. The method used was based on the potential and current density data histories of an industrial bipolar electrolyser, collected for about eight years. At approximately half of the period studied there was a simultaneous replacement of electrodes and membranes event. Currently, the electrodes had around 10 years of operation and the membranes 5 years, due to the service time of the electrodes is approximately twice the service time of the membranes. Nevertheless, it should be mentioned that the type of membrane and electrodes used was not modified, as well as the average operating conditions were the same. The real potential values were normalized using a constant current density corresponded to the first month in operation, j_{ref}, assumed that the ohmic overpotentials dominate within the Tafel region:

$$E_{j,\mathrm{ref}} = E_{\mathrm{therm}} + \eta'_{\mathrm{act}} + (E - E_0) \cdot \frac{j_{\mathrm{ref}}}{j}$$

where $E_{j,\mathrm{ref}}$ is the normalized potential, η'_{act} is the activation overpotential and the last term is equal to $\eta'_{\Omega,i}$,the ohmic overpotential.

The normalized cell potential increased *ca*. 100 mV for the first part of the period, between 2008 and 2012, and 100 mV, between 2012 and 2016. This normalization allowed also to represent the evolution of the activation and ohmic contributions as a function of the respective electrodes and membrane service times. The ohmic overpotential was mostly associated to the ion-exchange membranes, increasing *ca*. 100 mV during the first period, from 2008 to 2012, and *ca*. 170 mV between 2012 and 2016. The average relative error obtained between the predicted values of ohmic overpotential as a linear function of the membrane service time and the monthly ohmic overpotential was less than 3 %. For the activation overpotential related to the electrodes, it was difficult to identify a trend over time, since it remained mostly constant at *ca*. 280 mV, with the respective average relative error around 6 %. Concluding, the proposed approach enables systematic assessing of the performance of industrial chlor-alkali membrane electrolysers, which is important for the maintenance scheduling and, consequently, to bring operational and economic improvements of the process.

In the second part of the thesis, an experimental study was performed to assess the effect of the electrolyte composition and temperature on the kinetics of the chlorine evolution reaction over DSA® industrial electrodes. A parametric study was therefore performed varying: a) the sodium chloride concentration from 2.50 M to 5.20 M; b) the sodium chlorate (principal impurity) concentration from 0.0 M to 1.0 M; c) the pH from 0 to 9; and d) the temperature between 298 K and 358 K. The NaCl electrolysis was operated using a concentrated aqueous solution of NaCl; the water electrolysis should be minimized because it reduces the chlorine selectivity. For the standard operating conditions (5.0 M NaCl, 0.11 M $NaClO_3$, pH 2 and 353 K), the reversible electrode potential was equal to 1.28 V *vs.* SHE, which increases with chloride activity with a slope of -70 mV/decade of current density; the chloride activity increases with sodium concentration, which had a positive effect in the chlorine evolution. Although the E_{rev} was affected with the same factor with chloride activity, -70 mV/decade of current density, related to sodium chlorate concentration, the Tafel slope decreases with the increase of the concentration. The pH is a n important parameter for the

chlorine selectivity. If the solution had a pH below 2, the oxidation of the active sites of the DSA® electrode was inhibited and, consequently, the chlorine evolution decreases and, if pH was above 4, the Tafel slope obtained was higher than the 45 - 50 mV recorded for the remaining points, which was assigned to oxygen evolution by parasite reactions. These reactions depend directly on pH, namely the water oxidation. Finally, it was observed that, in concentrated NaCl solutions, the chloride activity had a *J*-shape increase with the temperature, which corresponds to an opposite effect of the temperature on the kinetics of the chlorine reaction. In the polarization curves, a bend was identified around 1.25 V *vs.* SHE for most of the experiments, which was related to the metal oxide transitions corresponding to the first step of the chlorine evolution mechanism, depending indirectly on the pH of the solution. This result was in agreement with the voltammograms, performed at room temperature, where it was observed a significant peak around 0.75 V *vs.* SHE, which is associated to the oxidation of the active sites on the DSA® surface, more specifically of ruthenium intermediate species.

The work described in this thesis provides relevant information about the relationship between the operating conditions of the process and the kinetics of the chlorine evolution reaction and, it can be used to maximize the selectivity of chlorine evolution. Additionally, the methodology developed based on the analysis of the cell potential and current density can be used to monitor the energy consumption in the NaCl electrolysis. This knowledge can be used to further develop tools that will support the scheduling of the maintenance operations in the industrial chlor-alkali process. This decision should, therefore, balance the maintenance costs (membranes/electrodes and working costs involved in the replacement) with the over-energy consumption and the risks of a complete failure of the membranes/electrodes.

6 RECOMMENDATIONS FOR FUTURE WORK

During this thesis, several difficulties were identified mainly related to the scarcity of scientific works that combine the electrochemical knowledge with the operational practices followed by the chlor-alkali industry. The systematic analysis of the data history of one of the electrolysers was therefore challenging, but it proved to be a promising approach for future work, especially for assisting the planning of the electrolysers maintenance. The methodology implemented in the current work allows to estimate the evolution of ohmic overpotential as a function of the service life of the cell components. Regarding the activation overpotential, the results lack precision, mainly because the related overpotentials increase is small, before reaching the exponential step, which is avoided by the industry. This work should be viewed as the beginning of a research line on the development of meaningful tools for assisting planning the maintenance actions. The following future research topics are suggested:

- Develop a computer program that implements the proposed methodology; this program will allow for a faster analysis of the electrolysers performance and thus to improving its usefulness.
- Apply the proposed methodology to electrolysers using different membranes and electrodes.
- Determine the evolution of the k-factor as a function of the service life of the membranes for each electrolyser.
- Determine the specific electricity consumption of each electrolyser, based on the estimated chlorine production for the same period of analysis.
- Obtain all costs associated with replacing membranes and recoating the electrodes.
- Obtain the evolution of electricity costs used in NaCl electrolysis.
- Calculate the interception between the evolution of electrolysis operating costs with maintenance costs and determine the optimal moment for replacement.

Another main objective of this work was to understand the effect of the operating conditions and composition of the electrolyte on the kinetics of the chlorine evolution reaction and, in turn, on the energy consumption. Even though the electrolyte used came from an industrial brine solution, the determined values for the kinetic parameters are in accordance with the literature. However, it is desirable to understand whether operating in unstable conditions, caused by unknown or unexpected reasons, can affect the deactivation of the electrodes. During this work, an attempt was made to follow this approach by adapting the laboratorial setup to operate continuously, and the accelerated ageing of the electrodes was tested for different operating conditions. However, the reaction rate never reached steady state, so it was not possible to do a full electrochemical characterization. To analyse the effect of temperature and electrolyte composition under accelerated ageing of the electrode, a new study is suggested combining the knowledge acquired from the two sets of tests described in this thesis. Here, the focus should be on studying the modifications that are occurring on the electrode surface due to changes in the oxidation state of the active species, which in turn contribute to the deactivation of the electrode, rather than the impact of the operating conditions on the kinetics of chlorine evolution. To address this research topic the following points are therefore suggested:

- Study the reaction mechanisms that contribute to the deactivation and dissolution of active species on the electrode surface.
- Obtain the electric current and the potential values as a function of the time, so that the recorded data can be used in the historical analysis method developed in the first part of this thesis.
- Obtain detailed information about the physical-chemical modifications that are occurring, by an *ex-situ* characterization (e.g., by SEM, EDS and XPS) of the anodes at different service times.